THE UNIVERSITY *of* LIVERPOOL

Speed Sensorless Induction Motor Drive Control for Electric Vehicles

Thesis submitted in accordance with the
requirements of the University of Liverpool
for the degree of Doctor of Philosophy

in

Electrical Engineering and Electronics

by

Saqib Jamshed Rind, B.Eng, M.Sc

March 2017

Speed Sensorless Induction Motor Drive Control
for Electric Vehicles

by

Saqib Jamshed Rind

To Ammi and Abbu (My Parents)

For their support, love and day & night prayers for my every success of life

I love you

Acknowledgements

I would like to express my most sincere gratitude to my supervisor Dr.Lin Jiang for his guidance, support, motivation, encouragement, useful discussions as well as competent supervision throughout my research.

I wish to express my deepest appreciation to my both brothers and their wives and specially my both sisters Samreen and Sana, for their support and encouragement during my whole PhD journey.

I am also grateful to all my friends and colleagues particulary Yaxing, Liuying, Kai and Chao in the Smart Grid Control and Renewable Energy research group at the University of Liverpool for their friendly discussions and support. Special thanks go to my friends Amit, Khurram and Tufail for their nice company, valuable discussions and moral support throughout my whole research.

Special thanks to my sponsors: Higher Education Commission (HEC) and NED University of Engineering and Technology, Pakistan. I would also like to thank, University of Liverpool for providing me partial PhD-studentship.

Finally, Special regards to my parents for their love and support throughout my entire life and also very thankful to Allah (God) for giving me the power and patience to complete this work.

Abstract

Fast diminishing fossil fuel resources, deterioration in air quality and concerns for environmental protection, continuously promote the interest in the research and development of Alternative Energy Vehicles (AEVs). Traction motor drive is an integral part and common electric propulsion system in all kinds of AEVs. It plays an utmost significant role in the development of electrified transport industry. Application of Induction Motor (IM) drive is not only limited to the domestic and industrial applications but also has an ubiquitous influence in the modern electrified transport sector. IM is characterized by a simple and rugged structure, operational reliability, low maintenance, low cost, ability to operate in a hostile environment and high dynamic performance. However, IM is one of the widely accepted choices by Electric Vehicles (EVs) manufacturer.

At present, Variable speed IM drive is almost replacing the traditional DC motor drive in a wide range of applications including EVs where a fast dynamic response is required. It became possible after the technological advancement and development in the field of power switching devices, digital signal processing and recently intelligent control systems have led to great improvements in the dynamic performance of traction drives.

Speed Sensorless control strategies offer better system's reliability and robustness and reduce the drive cost, size and maintenance requirements. Sensorless IM drives have been applied on medium and high speed applications successfully. However, instability at low speed and under different load disturbance conditions are still

a critical problem in this research field and has not been robustly achieved. Some application such as traction drives and cranes are required to maintain the desired level of torque down to low speed levels with uncertain load torque disturbance conditions. Speed and torque control is more important particularly in motor-in-wheel traction drive train configuration EVs where vehicle wheel rim is directly connected to the motor shaft to control the speed and torque.

The main purpose of this research is to improve the dynamic performance of conventional proportional-integral controller based model reference adaptive system (PI-MRAS) speed observer by using several speed profiles under different load torque disturbance conditions, which is uncertain during the whole vehicle operation apart from the vehicle own load. Since, vehicle has to face different road conditions and aerodynamic effects which continuously change the net load torque effect on the traction drive. This thesis proposes different novel methods based on the fuzzy logic control (FLC) and sliding mode control (SMC) with rotor flux MRAS. Numerous simulations and experimental tests designed with respect to the EV operation are carried out to investigate the speed estimation performance of the proposed schemes and compared with the PI-MRAS speed observer. For simulation and experimental purpose, Matlab-Simulink environment and dSPACE DS-1104 controller board are used respectively. The results presented in this thesis show great performance improvements of the proposed schemes in speed estimation & load disturbance rejection capability and provide a suitable choice of speed sensoless IM drive control for EVs with cost effectiveness.

Declaration

The author hereby declares that this thesis is a record of work carried out in the Department of Electrical Engineering and Electronics at the University of Liverpool during the period from October 2012 to March 2017. The thesis is original in content except where otherwise indicated.

Contents

List of Figures **xi**

List of Tables **xvii**

List of Notations and Abbreviations **xviii**

1 Introduction **1**
1.1 Background 1
1.2 Basic Architecture of EV 2
1.3 Classification of Traction Motors 3
1.3.1 DC Motors 5
1.3.2 AC Motors 5
1.4 Key Characteristics for Traction Motor Drive 7
1.5 Control Techniques of Induction Motor Drive 8
1.5.1 Scalar Control (V/f) Method 8
1.5.2 Vector Control Method 9
1.5.3 Direct Torque Control Method 11
1.5.4 Sensorless Control of Induction Motor Drive 12
1.6 Motivations and Objectives 14
1.7 Contribution of Research 15
1.7.1 List of Publications 17
1.8 Thesis Outline 18

2 Sensorless Control of Induction Motor- A Literature Review **22**
2.1 Introduction 22
2.2 Powertrain Configurations of EVs 24
2.3 Machine Model-Based Sensorless Control Techniques 27
2.4 MRAS for Sensorless Induction Motor Control 28
2.4.1 MRAS based on Rotor Flux Error 30
2.4.2 MRAS based on Back-EMF Error 33
2.4.3 MRAS based on Reactive Power Error 34
2.5 Other Rotor Speed Estimation Techniques 36
2.6 Estimation Through Signal Injection 38

2.7 Sensorless Control Issues at Low Speed Operation 39
2.7.1 Motor Parameter Sensitivity 39
2.7.2 Pure Integration Problem 42
2.7.3 Stator Voltage Measurement 44
2.8 Artificial Intelligence for Sensorless Motor Control 46
2.8.1 Fuzzy Logic Application in Sensorless Control 48
2.9 Conclusion 49

3 Modelling of Vehicle Dynamics, Induction Motor and MRAS Speed Estimator 51
3.1 Introduction 51
3.2 Motion and Vehicle Dynamics 52
3.3 Dynamic Modelling of the Induction Motor 55
3.3.1 Coordinate Transformation 56
3.3.2 Model in a Stationary Reference Frame 60
3.3.3 Model in a Synchronously Rotating Reference Frame 61
3.4 Modelling of Vector Control 63
3.5 Rotor Flux MRAS Modelling for Speed Estimation 67
3.5.1 Reference Model 68
3.5.2 Adaptive or Adjustable Model 71
3.5.3 Speed Adaptation Mechanism 73
3.6 Conclusion 76

4 Sensorless Induction Motor Drive Control Using Fuzzy Logic based Speed Observer 77
4.1 Introduction 77
4.2 Introduction to Fuzzy Logic System 79
4.3 Principles of Fuzzy Logic Control 80
4.3.1 Fuzzification 81
4.3.2 Fuzzy Inference System 83
4.3.3 Defuzzification 85
4.4 Proposed Fuzzy Logic based Rotor Flux-MRAS Speed Estimator . . 86
4.5 Simulation Results and Analysis 93
4.5.1 Load disturbance rejection capability of observer at different rated load torque 97
4.5.2 Quick acceleration or sudden speed change performance of observer 103
4.5.3 Observer performance during Un-smooth road condition or with time varying load disturbance 106
4.5.4 Motor speed transition from positive to negative and vice versa at different load disturbance conditions 109
4.6 Conclusion 116

5 Sensorless Induction Motor Drive Control Using Sliding Mode based Speed Observer **117**
5.1 Introduction . . . 117
5.2 Principle of Sliding Mode Control System . . . 119
5.3 Proposed Sliding Mode based Rotor Flux-MRAS Speed Estimator . 120
5.4 Simulation Results and Analysis . . . 126
5.4.1 Load disturbance rejection capability of observer at different rated load torque . . . 128
5.4.2 Quick acceleration or sudden speed change performance of observer . . . 135
5.4.3 Observer performance during Un-smooth road condition or with time varying load disturbance . . . 137
5.4.4 Motor speed transition from positive to negative and vice versa at different load disturbance conditions . . . 140
5.5 Conclusion . . . 147

6 Experimental Validation and Analysis **148**
6.1 Introduction . . . 148
6.2 The Experimental System . . . 149
6.2.1 Motor coupling system . . . 149
6.2.2 Power Electronics Drive Board . . . 151
6.2.3 DS1104 R & D controller Board and CP 1104 I/O board . . 152
6.2.4 MATLAB Simulink and Control-desk . . . 153
6.3 Experimental Results . . . 154
6.3.1 Performance of PI-MRAS Observer . . . 155
6.3.2 Performance of FLC-MRAS Observer . . . 159
6.3.3 Performance of SMC-MRAS Observer . . . 162
6.4 Conclusion . . . 164

7 Conclusion and Future Work **165**
7.1 Introduction . . . 165
7.2 Discussion and Conclusions . . . 166
7.3 Recommendations for Future Work . . . 169

References **171**

List of Figures

1.1 Basic architecture components of electric vehicle 3
1.2 Different traction motors for EVs and HEVs 1.2(a) DC traction motors 1.2(b) AC traction motors 4
1.3 Typical speed-torque characteristic curve for EVs & HEVs 8
1.4 Different rotor speed estimation techniques for sensorless control . . 13

2.1 Basic block diagram of closed loop speed sensorless control of AC electric motor drive 23
2.2 Different powertrain configurations of EVs [1]. 25
2.3 Protean Electric in-wheel motor assembly [2] 27
2.4 Machine model based closed loop motor rotor speed estimation techniques 29
2.5 Block diagram of parallel structure MRAS 30
2.6 Block diagram of rotor flux error based MRAS speed estimator . . . 31
2.7 Block diagram of back-EMF error based MRAS speed estimator . . 34
2.8 Block diagram of reactive power error based MRAS speed estimator 35
2.9 Modified block diagram of rotor flux error based MRAS speed estimator for practical immplementation 43
2.10 Fuzzy-Logic based MRAS for speed estimation 48

3.1 Acting forces on a vehicle moving along a slope surface [1] 53
3.2 Coupling effect in the three phase stator and rotor windings of motor 55
3.3 Equivalent two phase (d, q) machine model 56
3.4 Stationary frame (as, bs, cs) to (D, Q) stationary axes transformation 57
3.5 Two axes stationary frame (D, Q) to two axes synchronously rotating frame $(d - q)$ transformation 59
3.6 Dynamic machine model equivalent circuit in rotating frame $(d-q)$ 3.6(a) Machine d-axis circuit 3.6(b) Machine q-axis circuit 62
3.7 Operational principle of rotor flux oriented control 63
3.8 Types of rotor flux oriented schemes 3.8(a) Direct rotor flux oriented method 3.8(b) Indirect rotor flux oriented method 66
3.9 Block diagram of indirect vector control of induction motor drive . . 68
3.10 Block diagram of rotor flux based MRAS speed estimator for IM drive 69

3.11 Rotor flux linkage (ψ_{rD}, ψ_{rQ}) estimator based on IM's voltage model 70
3.12 Rotor flux linkage $(\hat{\psi}_{rD}, \hat{\psi}_{rQ})$ estimator based on IM's current model 72
3.13 Rotor speed estimation by using rotor flux linkage based MRAS . . 73
3.14 Equivalent of a nonlinear feedback system 74
3.15 Adaptation mechanism for rotor flux based MRAS speed estimator . 75

4.1 Basic block diagram of mamdani-type fuzzy logic control system . . 81
4.2 Representation of temperature example using [3] 4.2(a) Fuzzy sets 4.2(b) Classical Crisp sets 82
4.3 Different types of fuzzy membership functions [3] 4.3(a) Triangular function 4.3(b) Trapezoidal function 4.3(c) Gaussian function 4.3(d) Sigmoid function 83
4.4 Fuzzy inference system with If-Then rule expression for two inputs and one output 84
4.5 Conventional rotor flux PI-controller based MRAS speed estimator . 86
4.6 Block diagram of fuzzy logic controller for FLC-MRAS 88
4.7 Fuzzy logic controller input and output membership functions 4.7(a) Membership function for error ε_ω 4.7(b) Membership function for change in error $\Delta\varepsilon_\omega$ 4.7(c) Membership function for FL controller output variable $\Delta\omega_{rp}$ 90
4.8 3-D Surface view of FL controller 91
4.9 Block diagram of proposed rotor flux FLC-MRAS speed observer . 92
4.10 Fuzzy inference system modelling using Matlab. The Membership Function Editor (top left), FIS Editor (center), Rule Editor (top right), Rule Viewer (bottom left), and Surface Viewer (bottom right) [4]. . 93
4.11 Fuzzy logic controller implementation in simulink model 95
4.12 Block diagram of speed sensorless indirect vector control of induction motor traction drive by using FLC-MRAS speed estimator . . . 96
4.13 Speed estimation performance of Observer for 25% rated load disturbance rejection capability at 15 rad/sec motor speed. 4.13(a) PI-MRAS. 4.13(b) FLC-MRAS 4.13(c) Motor electromagnetic torque response T_e. 98
4.14 Absolute error of estimation speed and tracking speed at 15 rad/sec with 25% rated load disturbance at $t = 3s$. 4.14(a) Speed estimation error. 4.14(b) Speed tracking error. 99
4.15 Speed tuning signal for 25% rated load disturbance at 15 rad/sec motor speed. 100
4.16 Speed estimation performance of Observer for 60% rated load disturbance rejection capability at 15 rad/sec motor speed. 4.16(a) PI-MRAS. 4.16(b) FLC-MRAS 4.16(c) Motor electromagnetic torque response T_e. 101

4.17 Absolute error of estimation speed and tracking speed at 15 rad/sec with 60% rated load disturbance at $t = 3s$. 4.17(a) Speed estimation error. 4.17(b) Speed tracking error. 102
4.18 Speed tuning signal for 60% rated load disturbance at 15 rad/sec motor speed. 103
4.19 Speed estimation performance of Observer during quick speed change from zero speed level to 30 rad/sec motor speed. 4.19(a) PI-MRAS. 4.19(b) FLC-MRAS. 104
4.20 Absolute error of estimation speed during quick speed change at $t = 0.5s$. 105
4.21 Speed tuning signal for quick speed change of 30 rad/sec motor speed. 105
4.22 EV constant speed operation on an un-smooth road condition 106
4.23 Speed estimation performance of Observer during un-smooth road condition at 40 rad/sec motor speed. 4.23(a) PI-MRAS. 4.23(b) FLC-MRAS. 107
4.24 Absolute error of estimation speed and tracking speed during un-smooth road condition. 4.24(a) Speed estimation error. 4.24(b) Speed tracking error. 108
4.25 Speed tuning signal during un-smooth road condition. 108
4.26 The four quadrants of the torque-speed diagram for an EV [5] . . . 109
4.27 Speed estimation performance from 40 rad/s to 10 rad/s speed transition with 60% rated load disturbance. 4.27(a) PI-MRAS. 4.27(b) FLC-MRAS. 110
4.28 Absolute error of estimation speed and tracking speed during speed 40 rad/s to 10 rad/s speed transition. 4.28(a) Speed estimation error. 4.28(b) Speed tracking error. 111
4.29 Speed tuning signal during high to low positive speed transition. . . 111
4.30 Speed estimation performance from 40 rad/s to -40 rad/s speed transition with 60% rated load disturbance at $t = 3s$. 4.30(a) PI-MRAS. 4.30(b) FLC-MRAS. 112
4.31 Absolute error of estimation speed and tracking speed during +40 rad/s to -40 rad/s speed transition. 4.31(a) Speed estimation error. 4.31(b) Speed tracking error. 113
4.32 Speed tuning signal from positive to negative speed transition. . . . 113
4.33 Speed estimation performance from -40 rad/s to +40 rad/s speed transition with 60% rated load disturbance. 4.33(a) PI-MRAS. 4.33(b) FLC-MRAS. 114
4.34 Absolute error of estimation speed and tracking speed during -40 rad/s to +40 rad/s speed transition. 4.34(a) Speed estimation error. 4.34(b) Speed tracking error. 115
4.35 Speed tuning signal during negative to positive speed transition. . . 115

5.1 The sliding mode control principle 120

5.2 Block diagram of proposed rotor flux SMC-MRAS speed observer . 121
5.3 Block diagram of speed sensorless indirect vector control of induction motor traction drive by using SMC-MRAS speed estimator . . 127
5.4 Speed estimation performance of Observer for 25% rated load disturbance rejection capability at 15 rad/sec motor speed. 5.4(a) PI-MRAS. 5.4(b) SMC-MRAS 5.4(c) Motor electromagnetic torque T_e response. 129
5.5 Absolute error of estimation speed and tracking speed at 15 rad/sec with 25% rated load disturbance at $t = 3s$. 5.5(a) Speed estimation error. 5.5(b) Speed tracking error. 130
5.6 Speed tuning signal for 25% rated load disturbance at 15 rad/sec motor speed. 131
5.7 Speed estimation performance of Observer for 60% rated load disturbance rejection capability at 15 rad/sec motor speed. 5.7(a) PI-MRAS. 5.7(b) SMC-MRAS 5.7(c) Motor electromagnetic torque T_e response. 132
5.8 Absolute error of estimation speed and tracking speed at 15 rad/sec with 60% rated load disturbance at $t = 3s$. 5.8(a) Speed estimation error. 5.8(b) Speed tracking error. 133
5.9 Speed tuning signal for 60% rated load disturbance at 15 rad/sec motor speed. 134
5.10 Speed estimation performance of Observer during quick speed change from zero speed level to 30 rad/sec motor speed. 5.10(a) PI-MRAS. 5.10(b) SMC-MRAS. 135
5.11 Absolute error of estimation speed during quick speed change at $t = 0.5s$. 136
5.12 Speed tuning signal for quick speed change of 30 rad/sec motor speed. 136
5.13 Speed estimation performance of Observer during un-smooth road condition at 40 rad/sec motor speed. 5.13(a) PI-MRAS. 5.13(b) SMC-MRAS. 138
5.14 Absolute error of estimation speed and tracking speed during un-smooth road condition. 5.14(a) Speed estimation error. 5.14(b) Speed tracking error. 139
5.15 Speed tuning signal during un-smooth road condition. 139
5.16 Speed estimation performance from 40 rad/s to 10 rad/s speed transition with 60% rated load disturbance. 5.16(a) PI-MRAS. 5.16(b) SMC-MRAS. 141
5.17 Absolute error of estimation speed and tracking speed during speed 40 rad/s to 10 rad/s speed transition. 5.17(a) Speed estimation error. 5.17(b) Speed tracking error. 142
5.18 Speed tuning signal during high to low positive speed transition. . . 142

5.19 Speed estimation performance from 40 rad/s to -40 rad/s speed transition with 60% rated load disturbance at $t = 3s$. 5.19(a) PI-MRAS. 5.19(b) SMC-MRAS. 143
5.20 Absolute error of estimation speed and tracking speed during speed +40 rad/s to -40 rad/s speed transition. 5.20(a) Speed estimation error. 5.20(b) Speed tracking error. 144
5.21 Speed tuning signal from positive to negative speed transition. . . . 144
5.22 Speed estimation performance from -40 rad/s to +40 rad/s speed transition with 60% rated load disturbance at $t = 3s$. 5.22(a) PI-MRAS. 5.22(b) SMC-MRAS. 145
5.23 Absolute error of estimation speed and tracking speed during -40 rad/s to +40 rad/s speed transition. 5.23(a) Speed estimation error. 5.23(b) Speed tracking error. 146
5.24 Speed tuning signal from positive to negative speed transition. . . . 146

6.1 Schematic diagram of DSP-based electric drive experimental system [6] 149
6.2 Real time DSP-based induction motor drive experimental system . 150
6.3 Motor Coupling System showing Induction Motor, Load DC Motor and Encoder 151
6.4 Power electronic drive board with indicated key labels 152
6.5 CP1104 I/O board 153
6.6 Experimental setup of IM sensorless electric drive system 154
6.7 Different operation conditions of EV. 6.7(a) EV forward and reverse motoring operation condition. 6.7(b) EV constant speed with unsmooth road condition operation. 156
6.8 Speed regulation response of observer at 50 rad/sec motor speed with time varying load torque. 6.8(a) PI-MRAS Speed estimation response. 6.8(b) Applied load torque. 157
6.9 Speed regulation response of observer from +60 rad/sec to -60 rad/sec motor speed with specified load torque. 6.9(a) PI-MRAS speed regulation response. 6.9(b) Applied load torque. 158
6.10 PI-MRAS observer speed regulation response of staircase at 80 rad/sec reference speed. 159
6.11 Speed regulation response of observer at 60 rad/sec motor speed with time varying load torque. 6.11(a) FLC-MRAS Speed estimation response. 6.11(b) Applied load torque. 160
6.12 Speed regulation response of observer from +60 rad/sec to -60 rad/sec motor speed with specified load torque. 6.12(a) FLC-MRAS speed regulation response. 6.12(b) Applied load torque. 161
6.13 FLC-MRAS observer speed regulation response of staircase at 80 rad/sec reference speed. 162

6.14 Speed regulation response of observer from +60 rad/sec to -60 rad/sec motor speed with specified load torque. 6.14(a) SMC-MRAS speed regulation response. 6.14(b) Applied load torque. 163
6.15 SMC-MRAS observer speed regulation response of staircase at 80 rad/sec reference speed. 164

List of Tables

4.1 Linguistic rule for FLC-MRAS 89
4.2 Induction Motor Parameters & Ratings 94

List of Notations and Abbreviations

Notations

$\bar{i}_r$	Rotor current space phasor
i_{ra}, i_{rb}, i_{rc}	Rotor currents in rotor phases
$i_{r\alpha}, i_{r\beta}$	Rotor current vectors in the rotor reference frame
$\bar{i}_s$	Stator current space phasor
i_{sA}, i_{sB}, i_{sC}	Stator currents in stator phases
i_{sD}, i_{sQ}	Stator current vectors in the stator reference frame
i_{sd}, i_{sq}	Stator current vectors in the synchronous reference frame
J	Rotor inertia
K_T	Torque constant
k_1, k_2, k_3	FLC scaling factors
k_p, k_i	PI-controller Proportional and integral gains
L_m	Mutual inductance
L_s, L_{ls}	Stator self inductance and leakage inductance
L_r, L_{lr}	Rotor self inductance and leakage inductance
M	Hitting gain in SMC
p	Differential operator
P	Number of pole pairs
R_s, R_r	Stator and rotor resistances
t	Time
T	Sampling time
T_e	Electromagnetic torque
T_l	Load torque
T_r	Rotor time constant
$\bar{v}_r$	Space phasor of the rotor voltage
v_{ra}, v_{rb}, v_{rc}	Rotor voltages in rotor phases

$\bar{v_s}$	Stator voltage space phasor
v_{sA}, v_{sB}, v_{sC}	Stator voltages in stator phases
v_{sD}, v_{sQ}	Stator voltage vector in the stator reference frame
v_{sd}, v_{sq}	Stator voltage vector in the synchronous reference frame
$\bar{\psi}_r$	Space phasor of the rotor flux linkage
$\psi_{ra}, \psi_{rb}, \psi_{rc}$	Rotor flux linkages in rotor phases
ψ_{rd}, ψ_{rq}	Components of the rotor flux linkage vector
$\bar{\psi}_s$	Space phasor of the stator flux linkage
$\psi_{sA}, \psi_{sB}, \psi_{sC}$	Stator flux linkages in stator phases
ψ_{sD}, ψ_{sQ}	Stator flux linkage vector in the stator reference frame
ψ_{md}, ψ_{mq}	Components of magnetizing flux linkages
ω_e	Angular synchronous speed
ω_r	Angular rotor speed
ω_{rm}	Mechanical angular rotor speed
ω_{sl}	Angular slip speed
ε_ω	Speed tuning signal
θ_e	Rotor flux angle
θ_r	Rotor angle
θ_{sl}	Slip angle
τ_o	Torque differences
σ	Leakage coefficient
μ	Membership function value

Abbreviations

AEV	Alternative Energy Vehicle
AC	Alternating Current
AI	Artificial Intelligence
ANN	Artificial Neural Network
BLDC	Bruchless DC
BEV	Battery Electric Vehicle
CM	Current Model
DC	Direct Current
DSP	Digital Signal Processor
DTC	Direct Torque Control

EV	Electric Vehicle
ECM	Electronically Commutated Machines
EMF	Electro Motive Force
ELO	Extended Luenberger Observer
EKF	Extended Kalman Filter
ES	Expert Systems
FL	Fuzzy Logic
FLC	Fuzzy Logic Control
FIS	Fuzzy Inference System
FCEV	Fuel Cell Electric Vehicle
FNN	Fuzzy Neural Network
FSMC	Fuzzy Sliding Mode Control
GA	Genetic Algorithm
GUI	Graphic User Interface
HPF	High Pass Filter
HEV	Hybrid Electric Vehicle
IM	Induction Motor
ICE	Internal Combustion Engine
ISA	Integrated Starter Alternator
LPF	Low-Pass Filters
MRAC	Model Reference Adaptive Control
MRAS	Model Reference Adaptive Systems
MF	Membership Function
MUT	Motor under test
PI	Proportional-Integral
PMSM	Permanent Magnet Synchronous Motor
RFO	Rotor Flux Oriented
SRM	Switch Reluctance Motor
SM	Sliding Mode
SMC	Sliding Mode Control
SI	Signal Injection
VSI	Voltage Source Inverter
VM	Voltage Model
VC	Vector Control

Superscripts

$*$	Reference or command value
$\wedge$	Estimated quaintity
r	Rotor reference frame
s	Stator reference frame

Chapter 1

Introduction

1.1 Background

DETERIORATION in air quality, global warming, reduction in petroleum resources and different burning questions regarding the pollution free healthy and clean environment have focused the researcher's attention to produce the energy efficient, emission free and enhanced performance electrified transport system in the market. In developing countries, transportation sector is one of the main causes of increasing harmful exhaust emissions in the environment, especially in large cities [7, 8]. In the United States, 98% of the transportation energy comes from the fossil fuels but most of it not efficiently utilised due to the low efficiency of internal combustion engine (ICE) vehicles [9]. Automotive industry is one of the largest sources of greenhouse gas emissions today. The successful accomplishment of research in this field may prove an utmost significant step forward towards the possibility of long driving range, enhanced performance and cost competitive alternative energy vehicle (AEV).

Traction motor control is an integral part of electric propulsion system of Electric Vehicles (EVs) and Hybrid Electric Vehicles (HEVs). Performance of traction motor drive plays an important role in the evolution of AEVs and electrified trans-

port industry [7]. In the past, DC traction motors used to be the most prominent choice of most EVs and HEVs manufacturers. But both compactness in the overall traction drive train and high relative efficiency have major significance in the evolution of electrified transport industry [1, 10].

However, technological advancement and development in the field of power electronics switching devices, Digital signal processing and intelligent control systems have led to great improvements in the dynamic performance of traction drives. There are several advantages of ac traction drive over dc such as compactness, overall system robustness, less required maintenance and economic benefits [11]. These advanced controllers provide not only good steady state response but also have better and fast transient response. Apart from the industrial drive applications, induction motors (IMs) have also been adopted as a great traction motor candidate in the electrified transport industry.

Control strategies of IM drives without using any speed and position sensor mounting at the shaft of the motor have been considerable research activities in the past few years. Apart from the performance improvement of overall drive, such control strategies have the attractions of low cost , more compactness with less amount of maintenance, removing of transducer cables , reduction in electrical noises, suitability for the hostile environment including temperature, overall improved system reliability and robustness. In these sensorless strategies, the information of rotor speed estimation is extracted from the measured stator currents and voltages at the motor terminals [12, 13].

1.2 Basic Architecture of EV

Alternative energy vehicle is a multidisciplinary field and has a complex assembly that is the integration of various engineering fields [7, 14]. The basic architecture of EV comprises on four core units i.e. electrical energy storage unit, power electronic converter unit, electric motor for the propulsion purpose and transmission

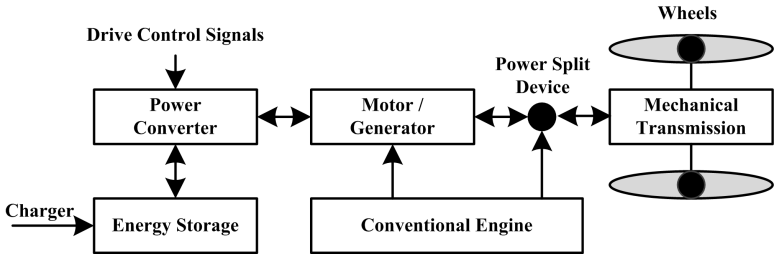

Figure 1.1: Basic architecture components of electric vehicle

drive shaft as shown in Fig 1.1 [15]. In EVs, electrical energy storage unit such as battery packs, ultra capacitors delivers the electrical energy to the power electronic converter on demand. Functions of power electronic converter unit is to convert and transfer the electrical energy according to the requirement of electric motor used for the propulsion purpose and again reverse the energy to the electrical energy storage system in case of regenerative braking mode of operation.

HEVs that have both energy sources electric motors as well as internal combustion engine, can achieve the customer's requirements and need, by facing the challenges in the design processes and managing different energy sources within the system which are mainly dependent on driving cycles, types of electric motors, battery sizing and electrical energy storage system [1]. Presently, there are four configurations of HEVs : series, parallel, series -parallel or split power and complex HEVs. These cofigurations are defined according to the way in which the propulsion power is delivered to the drive train in order to meet the load requirements during acceleration, start and different operating conditions [16, 17].

1.3 Classification of Traction Motors

Traction motor plays an utmost significant role in the development of electrified transport industry. Utilization of electric motors are not only limited to the domestic and industrial applications but also have an ubiquitous influence in the modern elec-

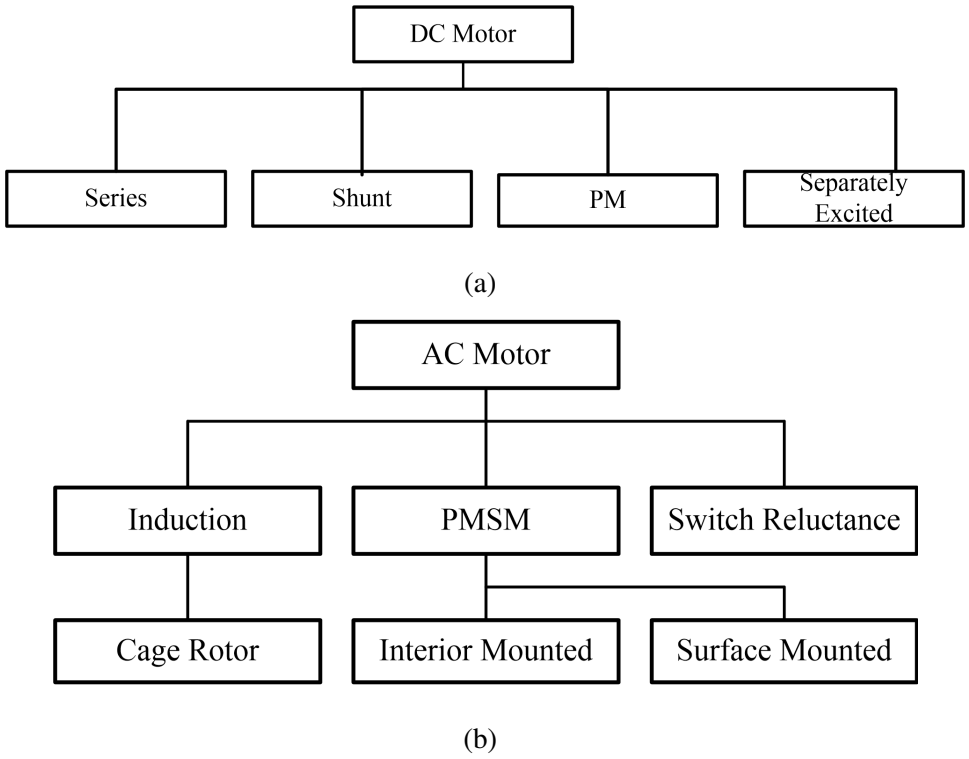

Figure 1.2: Different traction motors for EVs and HEVs 1.2(a) DC traction motors 1.2(b) AC traction motors

trified transport industry. The electric propulsion system is an integral part of EVs and HEVs [14]. Fig 1.2 illustrates different kinds of ac and dc traction motors.

There are different kinds of traction motors available in the market today but the selection of any specific motor for the electric propulsion system depends on its ruggedness, lightweight, small volume, low cost, easy and flexible electric drive control, fault tolerance capability, low acoustic noise level, better starting torque feature, high efficiency, high power density, constant torque and constant power regions over a wide speed range, fast and quick torque response, operational reliability on different driving conditions [1, 7, 14].

1.3.1 DC Motors

In the past, because of the technical and economical incentives, dc electric motors have been adopted and used to be the most prominent choice of most EVs and HEVs manufacturers [14, 18]. Simple speed control mechanism, technological maturity, relatively low cost of manufacturing as compare to other electromechanical conversion devices, better speed regulation were the main reasons to justify the substantial use of dc motors in the electrified transport industry [1, 14]. However, the use of commutators and brushes make the operation of dc motors less reliable and unsuitable for maintenance-free operation as well as high speed applications such as EVs and HEVs. In addition, electromagnetic interference due to commutator action, bulky construction, low efficiency, low reliability and also winding-excited dc motors have low specific power density [11, 19–22]. Both compactness in the overall traction drive train and high relative efficiency have major significance in the evolution of electrified transport industry [1, 14].

1.3.2 AC Motors

AC drive offers much more higher efficiency, higher power density, greater reliability, lower operating cost as well as requires less maintenance [11, 23]. AC electric motors used to be recognized into two broad classes: Synchronous Motors (SMs) and Asynchronous Motors or IMs but after the advancements in the power electronic switching devices, now a third class is also introduced that is electronically commutated machines (ECM) [12, 24–26]. ECM is usually associated with two main types: brushless DC motors (BLDC) and switch reluctance motor (SRM) [1, 12]. Machines under this category operate on the principle of DC machines but with inverter based commutations rather than the mechanical commutator. Motor design optimization, advancement in material sciences & electronics and new developed control techniques offer new motor types with high efficiency and reliability for different applications [25].

IM plays an important role not only in different kinds of domestic and industrial automation processes but also has a great deal of importance in the field of vehicle electrification. It is one of the widely accepted choice in traction motors due to its ruggedness, operational reliability, low maintenance, low cost, ability to operate in a hostile environment and high dynamic performance [1, 11, 12, 14, 20, 27]. In IMs, torque production and induction phenomena both are the function of relative angular velocity difference between rotating magnetic field and rotor speed and ultimately defined by a term slip, $s = \frac{\omega_s - \omega_r}{\omega_s} \times 100$. This slip must be smaller for the high power efficiency applications [12, 17, 28, 29].

Permanent magnet synchronous motor (PMSM) is becoming a good competitor of IMs in different applications including EVs. PMSM traction features are being applied in most of the currently available HEVs and EVs in the market including Toyota Prius (motor 60 kW, generator 42 kW), Chevy Volt (motor 110 kW, generator 55 kW), and Nissan Leaf (80 kW) [9]. In synchronous motors brushless dc motor (BLDC) is the most prominent candidate for EVs and HEVs applications [30]. The major characteristics of BLDC include high efficiency, motor compactness, simple control, low maintenance and low noise emissions [1, 11, 31]. The BLDC drives are the highest efficient in all motors available today [32, 33]. However, some disadvantages associated to the BLDC motor drive include, high cost, limited constant power range, safety matter due to very strong rare earth magnets, magnets demagnetization and poor high speed capability [1, 34].

Switch reluctance motor is getting considerable attention of researchers in the last few years for EVs and is being more highlighted as a good competitor of other machines in high dynamic performance applications [7, 11, 14, 35]. SRMs have utmost significant potential key features for electric vehicle propulsion system over IMs and PMMs including higher reliability, higher operating temperature tolerance, high speed range and suitable for gearless operation and ease of manufacturing [36]. Although, the maximum efficiency of SRMs are slightly lower than the PMSM but still maintains the efficiency over a wide speed and torque range than the other type

of motors. Due to these attractive key features, SRMs have been adopted by many automobile companies [37–39]. SRMs design and control are usually difficult and subtle due to heavy saturation of pole tips and the fringe effect of pole and slots [1]. The acoustic noise, torque ripple and vibration are the main challenges in these motors at high speed.

1.4 Key Characteristics for Traction Motor Drive

Fast and quick torque response is the most significant and main characteristic of high dynamic performance traction drive. Technological advancement and development in the field of power switching devices, Digital signal processing and intelligent control systems have led to great improvements in the dynamic performance of traction drives. Advanced controllers provide not only good steady state response but also have better and fast transient response. In general, the key characteristics required from an electrical machine for the traction applications include the following [1, 7, 14, 40, 41]:

- High torque at low speed for starting & climbing as well as high power for cruising.
- Quick and fast torque response.
- High power density & instant high power.
- High efficiency over the wide speed range with constant torque and constant power regions.
- Small size, reduced weight, lower moment of inertia and acceptable cost.
- High reliability & robustness for different vehicle operating conditions.

IM is one of the highly adopted traction motors in the present electrified transport industry. IM offers operational reliability, low cost, ruggedness, low maintenance,

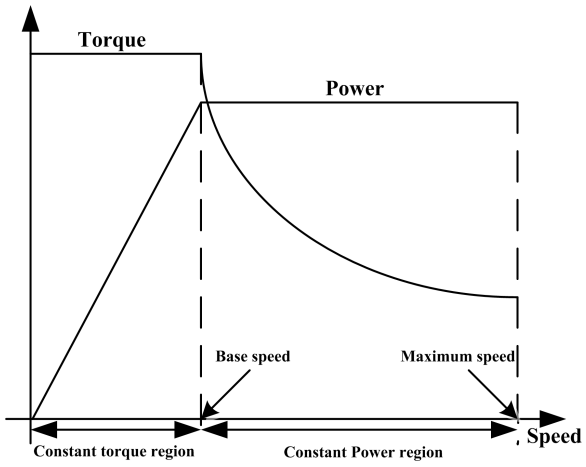

Figure 1.3: Typical speed-torque characteristic curve for EVs & HEVs

low torque ripple/noise, ability to operate in a hostile environment and high transient performance which is the most important feature in EVs and HEVs applications [1, 11, 14, 20, 27]. The constant power range of IMs can be extended 4-5 times the base speed which is generally required for the traction purpose. Fig 1.3 shows the typical speed-torque characteristic curve required for EVs and HEVs.

1.5 Control Techniques of Induction Motor Drive

1.5.1 Scalar Control (V/f) Method

Variable speed IM drive is generally classified into low performance and high performance controlled drives. Scalar control are used for low performance drives where only the magnitude and frequency of the stator voltage or current are regulated. Scalar control technique is also called volts/hertz control technique. The method is based on the control of the stator frequency. In this method the ratio between the magnitude of applied stator voltage and applied signal frequency is kept constant in order to keep the stator flux constant [13]. The objective of this method is to control the speed of motor while keeping the constant magnitude of the stator

flux. The stator flux is kept constant if $\psi = k\left(\frac{v}{f}\right)$ and the name of this method comes from this equation.

This method provides moderate level of dynamic performance and easy to implement. Therefore, this method is used for the applications where the precision in high speed is not required such as electric home appliances fans, washers, grinders and pumps etc [42]. In the past scalar controlled drives have been used widely in different industrial applications. However, the importance of this method has been reduced due to the other high performance drives. The main drawback of this scalar control is its sluggish transient response because this method disregards the inherent machine coupling. Machine's torque response is not very fast when step speed command is applied and specially during the transient the magnitude of stator flux is not maintained. Moreover, in some operating regions the system become unstable. This method is inefficient, inadequate and unsatisfactory to achieve the desired dynamic performance for EVs [1]. A detailed discussion regarding the scalar control method and some other schemes can be found in [3].

1.5.2 Vector Control Method

Vector control method is also known as, field oriented control, transvector control, orthogonal control and decoupled control method. *Professor Leonhard, Blaschke* and *Hasse* are the pioneers of VC of ac machines that has become a powerful technique worldwide today [24]. At present, high performance speed & torque control techniques are classified into two main categories Vector Control (VC) and Direct Torque Control (DTC) [3, 12]. Electric motor control for electric propulsion system is nearly implemented by VC method regardless the the traction motor type [43]. Now advanced technology assisted variable speed traction drive governs the more flexibility in control and increases the overall drive efficiency. The advent of high performance control techniques such as VC, DTC and predictive control, offering precise position and speed control and play an utmost significant role in the high dy-

namic performance of ac traction drives [44]. In the last decade, the advent of medically inspired Artificial Intelligence (AI) techniques are now also being getting more potential significance in the implementation of enhanced high performance electric drive control. These techniques include, namely fuzzy logic control (FLC), artificial neural network (ANN), genetic algorithms (GAs), and adaptive neuro-fuzzy inference system (ANFIS) [3, 24, 45].

In VC, by controlling the instantaneous positions of the voltage, current and flux linkage space vectors, the instantaneous torque and machine magnetic flux both are regulated in steady state and transient operating conditions [46]. Coordinate transformations from three phase to two phase or d-q axis are the key feature of VC method that gives the linear relationship between the control variables and motor torque [12]. This method provides better operational performance of motor over a wide speed range with very high torque at zero speed that is the most important characteristic for traction drive, fast acceleration and deceleration. The main objective of VC, is to get the same performance from an ac motor similar to that of separately excited dc motor and deals with the motor torque and flux control independently. The electro magnetic torque in dc machines is directly proportional to the field flux and armature current that explains the aim of VC for the high performance ac drive application. Electro magnetic torque in a dc machine is:

$$\begin{aligned} T_e &\propto \psi_f i_a \\ T_e &= C_t \psi_f i_a \end{aligned} \tag{1.5.1}$$

The VC method separates the current into two components to control the operation similar to dc machine, field or flux producing component i_{sd} and torque producing component i_{sq}. The electromagnetic torque is the product of d-axis flux producing current and q-axis torque producing current. If the established flux of the machine is kept constant then the quick and fast torque response can be achieved by directly controlling the q-axis current component.

There are two main variants of VC on the basis, how the flux space vector

magnitude and position are measured, direct VC scheme and indirect VC scheme [3, 12, 24]. In the direct scheme, the instantaneous position of the flux linkage space vector is determined directly by sensors, search coils or more usually by estimator or combination of both; *Blaschke* was a pioneer of this approach . In contrast indirect method uses the machine mathematical model and mainly dependent on the machine parameters. Indirect VC scheme of IM combines the calculated slip with the rotor position or speed [24]. However, this scheme is more dependent on machine parameters such as rotor time constant but still preferred than the direct scheme. Since the insertion of search coils or Hall-effect sensors for flux measurement require additional wiring, space, routine maintenance and increase the system cost. In addition the fragility of flux sensor degrades the overall robustness of the IM drive.

Performance of the VC method depends on the accurate monitored value of instantaneous flux linkage space vector magnitude and angle during the operation. However, the incorrect determination of magnitude and angle may loss the decoupling of machine torque and flux, resulting degradation in steady state and transient operation [46]. Speed oscillations, loss of input and output torque linearity relationship and reduction in the overall drive efficiency could be the major consequences of VC detuned operation [24].

1.5.3 Direct Torque Control Method

Direct torque control is another instantaneous electromagnetic torque control technique applied for high performance applications. DTC replaces the coordinate transformation concept of standard VC. The flux linkage space vectors and instantaneous electromagnetic torque both are controlled directly and independently by the optimal inverter switching mode to get the quick and fast torque response for high performance applications [47]. In DTC optimal inverter switching, both instantaneous electromagnetic torque and flux linkages are kept in the hysteresis band to get the fast torque response, low harmonic losses and low inverter switching frequency.

There are some other types of DTC including: switching table based, space vector modulation, direct self control and constant switching frequency [12, 24, 47]. DTC has following key characteristics over standard VC:

- no coordinate transformations are required, all calculations are done in stationary coordinate system [12];
- design simplicity due to absence of current control and flux regulation loops [12, 24];
- robustness against the parameters variations and overall reduced number of controllers [12, 48].

However, DTC electric drive system suffers from the low speed flux and torque estimation and control, high current and torque ripples. These torque ripples generates vibration, resulting DTC application less demanding for automotive applications. DTC operation could be considered for integrated starter alternator (ISA) applications as a motor in cranking mode. Since ISA operation time as starter is short and in the steady state, it mostly operates as an alternator. Traction drive used for BEVs or for pure EVs, propel the vehicle both in the dynamic and steady state operation. Therefore, DTC is not a preferred choice due to its torque ripples and made VC more suitable for BEVs or pure EVs [48].

1.5.4 Sensorless Control of Induction Motor Drive

Intensive research activities have been devoted to the sensorless methods in order to achieve the high performance control of electric motors. The implementation of mechanical speed sensor is not only difficult to integrate into and package within the vehicle drive train but also fragility and susceptible to the EMI and signal distortion. Electric drive with speed sensor degrades the overall motor control performance, since the corruption of the speed signal contributes disturbances into the voltage and current controllers that have tendency to unbalance the machine excitation and cause

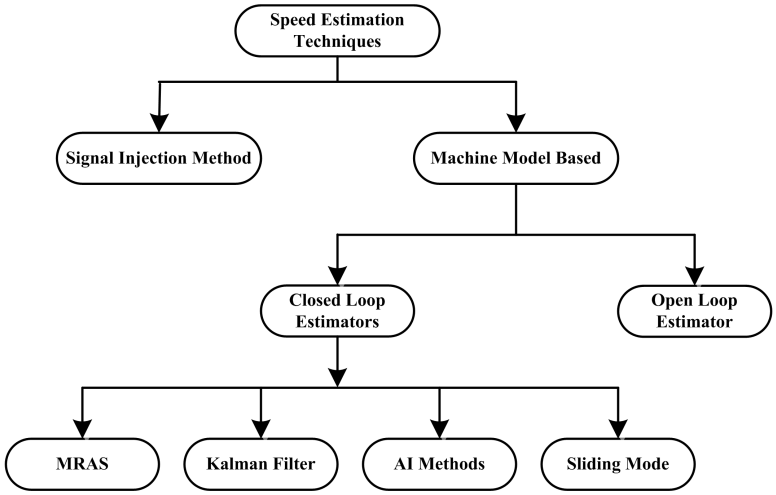

Figure 1.4: Different rotor speed estimation techniques for sensorless control

noise and vibration [43]. The elimination of speed sensor is entirely advantageous, if an adequate speed estimation algorithm is available to control the traction motor accurately according to the requirement. Advantages of such sensorless control techniques are [12, 13, 24, 46]:

- Reduce the cost of transducer and provide more compactness with less amount of maintenance.
- Increase the system noise immunity and reduce the transducer cables.
- Suitability for the hostile environment including temperature.
- Reduce the hardware complexity and increase the mechanical robustness.
- Improve the overall system reliability and robustness.

In general, these techniques are classified into two major categories; Signal Injection (SI) and estimation techniques based on machine fundamental model [12, 46]. Fig 1.4 shows different rotor speed estimation techniques for sensorless control . Over the past few years, there are several rotor speed estimation techniques and have

been implemented on the electric motor drive. Notwithstanding the advanced technology, control operation of electric drive at very low speed constitutes a persisting challenges [12, 24, 46, 49].

Traction drive for EVs, is one of the different applications of electric drive that requires fixed amount of controlled torque level down to low speed. However, huge computational efforts in rotor speed estimation and motor parameters variations during the operation are other shortcomings of sensorless control. Speed control at very low speed with different levels of torque is more important specifically motor in wheel drive train configuration of EV where motor shaft is directly connected to the wheel rim. In-wheel motors designed for the EVs are discussed as potential motor designs [50]. The comparative analysis of sensorless performance of electric drives is quite difficult, since a standard set of tests and any benchmarks has not been agreed yet. However, this benchmark issue to standardizing tests has already been addressed in [51].

1.6 Motivations and Objectives

Speed and electromagnetic torque controlling of IM drive constitutes different problems because of its non-linear dynamics, motor parameters variations during the operation and difficulty to measure electrical rotor variables. Both rotor speed and position information are important in IM controller design. Because of the sensor electrical noise problem in high performance motor control, sensorless control techniques are applied to estimate the motor rotor speed instead of the measurement from the speed encoder for high performance applications.

However, for the automobile manufacturers, the elimination of speed sensor in IM traction drive reduces the system fragility and provides not only improved performance with mechanical robustness but also provides a cost effective solution in the mass production of EVs. Speed sensorless IM drives have been applied at medium and high speed operation successfully. In spite of considerable research ef-

fort in this field, speed estimation at low speed region and in load torque disturbance condition are unsatisfactory. However, the load torque profile of vehicle is uncertain during the whole operation apart from the vehicle own load. Since, vehicle has to face different road conditions and aerodynamic effects which continuously change the net load torque effect on the traction drive. Presently, automobile companies are producing EVs and HEVs with different types of drive train configurations. Motor speed estimation is more important particularly in direct-in-wheel drive train configuration of EV where wheel rim is directly connected to traction motor to control the vehicle speed and torque. Therefore, for speed sensorless operation of the traction drive, the speed observer should be able to reject the sudden load change conditions without effecting the desired operational performance of the traction drive.

The research reported in this thesis investigates the performance of MRAS based speed sensorless IM traction motor drive by using different speed driving profiles and time varying load torques. Therefore, the main objective of this research is to design a novel speed estimator which is able to provide fast error dynamics and improved rotor speed estimation under different load torque disturbance condition and driving speed profiles for electric vehicle application

1.7 Contribution of Research

The research presented in this thesis investigates the operation of speed sensorless vector control of induction motor drive by using rotor flux MRAS observer for EV application. With respect to vehicle operation, particular attention is given on different load disturbance rejection capability of observer with different speed levels, where the conventional rotor flux observer deteriorates the performance. Different proposed rotor flux based MRAS observers are implemented and their better performance at different load disturbance conditions are shown through numerous tests. The proposed schemes have been simulated by using Matlab-Simulink platform and experimentally validated based on dSPACE DS1104 controller board. The

major contribution of the thesis can be summarized as follows:

- A novel fuzzy logic control based rotor flux model reference adaptive system (FLC-MRAS) speed observer is designed. The proposed speed observer replaces the fixed gain PI controller which is used in conventional rotor flux MRAS observer. This observer uses two differences at the same time, reference and estimated rotor fluxes as well as reference and estimated torques in order to improve the speed estimation performance. This FL scheme works in a nonlinear optimization mode. A two inputs and one output Mamdani-type FLC with triangular shape membership function. Seven different fuzzy sets are used for both inputs and one output. However, the fuzzy inference system is defined by using AND logical operator by using IF Then expression. Different simulation cases are designed with respect to the vehicle operation. All simulations are carried out by using indirect vector control induction motor drive system. In all simulation cases the performance of proposed FLC-MRAS is compared to the PI-MRAS observer. The proposed scheme shows better transient performance as well as better load torque disturbance rejection capability and found a suitable solution for speed sensorless IM drive for EVs.

- A novel sliding mode control based rotor flux model reference adaptive system (SMC-MRAS) speed observer is designed. This proposed observer also replaces the conventional rotor flux MRAS observer fixed gain PI controller. Two differences are used at the same time, reference and estimated rotor fluxes and torques for better speed estimation. This SM scheme is derived based on the Lyapunov theory to ensure the system stability as well as fast error dynamics. Switching surface or sliding surface is defined with the help of speed tuning signal in the designed SMC. However, the motion stability of state trajectories are ensured by using the Lyapunov function candidate. Different designed simulation cases with respect to the vehicle operation are performed by

using indirect vector control induction motor drive. performance of proposed SMC-MRAS is compared to the PI-MRAS observer. The proposed scheme shows much better transient performance, fast error dynamics as well as better load torque disturbance rejection capability and presents a good solution for speed sensorless IM traction drive.

- In chapter 2 a comprehensive literature review on different configurations of electric vehicles and an extensive review on rotor speed estimation techniques for robust and efficient sensorless traction drive control are highlighted. This chapter provides state of the art key global trends and tradeoff of various technologies with future trends and potential areas of research on a single platform. On the basis of this chapter, a review article has been written with highlighting the present problems and future challenges in sensorless traction drive. Article has been submitted to a Journal of Power Technologies Titled " Powertrain Configurations and Control of Traction Motors for Electric and Hybrid Electric Vehicles: A Review".

- In order to check the performance of proposed observer and compare with the PI-MRAS, different tests are designed with respect to the application in vehicle operation.

1.7.1 List of Publications

The author has published/submitted articles to international conferences and journals based on the results of research presented in this thesis. A list of publications is given below:

- Saqib.J.Rind, Y. Ren and L. Jiang, Powertrain Configurations and Control of Traction Motors for Electric and Hybrid Electric Vehicles: A Review, *Journal of Power Technologies, 2017*,(Submitted).

- Yaxing Ren, Saqib.J.Rind, Lin Jiang, Yihua Hu, and Huiqing Wen, Speed Sensorless Nonlinear Adaptive Control of Induction Motor for Electric Vehicles via a Combined Speed and Perturbation Observer, *IEEE Transaction on Mechatronics, 2016*, (Submitted 2nd revision).

- Saqib.J.Rind, Y. Ren, K. Shi, L. Jiang, and M. Tufail, Rotor flux-MRAS based speed sensorless non-linear adaptive control of induction motor drive for electric vehicles, *50th International Universities Power Engineering Conference (UPEC)*, Stoke on Trent, UK, pages 1-6, Sept 2015.

- Saqib.J.Rind, Y. Ren, and L. Jiang, MRAS based speed sensorless indirect vector control of induction motor drive for electric vehicles , *49th International Universities Power Engineering Conference (UPEC)*, Cluj-Napoca, Romania, pages 1-6, Sept 2014.

- Saqib.J.Rind, Yaxing Ren, and Lin Jiang, Traction motors and speed estimation techniques for sensorless control of electric vehicles: A review, *49th International Universities Power Engineering Conference (UPEC)*, Cluj-Napoca, Romania, pages 1-6, Sept 2014.

- Saqib.J.Rind, Y. Ren and L. Jiang, Speed Sensorless Induction Motor Traction Drive Control using Fuzzy Logic Rotor Flux Based MRAS Observer, *IET Journal of Electrical Systems and Transportation*, (In-progress).

- Saqib.J.Rind, Y. Ren and L. Jiang, Sensorless Induction Motor Drive Control using Sliding Mode Rotor Flux Based MRAS Observer for Electric Vehicles , *IET Journal of Electrical Systems and Transportation*, (In-progress).

1.8 Thesis Outline

This thesis is organised into seven chapters that are as follows.

chapter 1: Introduction

This chapter provides a general introduction of the research area and scope of this thesis. Different AC and DC electric motors used for traction purpose, Electric motor control techniques, particular attention on speed sensorless control of IM for EVs, research motivation and objectives and main contribution of the thesis are highlighted in this chapter.

chapter 2: Sensorless Control of Induction Motor- A Literature Review

This chapter presents a detailed review on machine fundamental model based rotor speed estimation techniques applied for sensorless control of IM with particular attention on MRAS based scheme due to their simplicity and easy implementation. Different issues in MRAS observer for speed estimation are discussed, specially at low speed and zero speed region and load disturbance effect on the estimation performance. Several proposed ideas and schemes in order to reduce such problems and to improve the dynamic performance of estimator are also discussed. Key characteristics of artificial intelligence and different applications in the field of variable speed drive with particular attention on the application of fuzzy logic control system in sensorless control are also discussed.

chapter 3: Modelling of Vehicle Dynamics, Induction Motor and MRAS Speed Estimator

This chapter presents about the motion and vehicle dynamic modeling and understanding of several forces acting on the vehicle during the operation and required tractive force from the traction motor to operate the vehicle. Coordinate transformations between three phase and two phase are discussed. Induction machine dynamic model in stationary and synchronously rotating reference frame are presented by using two axis theory. The machine model equations in the synchronous reference frame are used to explain the operational principle of vector control of IM drive. Finally, design of rotor flux based MRAS speed estimator rotor for speed sensorless traction drive control of IM is presented.

chapter 4: Sensorless Induction Motor Drive Control Using Fuzzy Logic based Speed Observer

This chapter proposes a novel fuzzy logic control based rotor flux model reference adaptive system speed observer. This new speed observer replaces the conventional rotor flux MRAS fixed gain PI controller. In the proposed observer, two differences are used at the same time, reference and estimated rotor fluxes and torques for improved speed estimation. Detailed design of the proposed observer is presented followed by the fuzzy logic control system fundamentals. Different simulation cases are designed in this chapter with respect to the vehicle operation such as load disturbance rejection capability, quick acceleration, un smooth road condition and different speed transition with load torque. The performance of proposed FLC-MRAS is compared to the PI-MRAS. All simulations are carried out by using indirect vector control induction motor drive system.

chapter 5: Sensorless Induction Motor Drive Control Using Sliding Mode based Speed Observer

This chapter proposes a novel sliding mode control based rotor flux model reference adaptive system speed observer. This proposed observer replaces the fixed gain PI controller of conventional rotor flux MRAS observer. The proposed observer uses two differences at the same time, reference and estimated rotor fluxes and torques in order to improve the speed estimation specifically in load torque disturbance condition. This SM scheme is derived based on the Lyapunov theory to ensure the system stability as well as fast error dynamics. Similar simulation cases are performed as mentioned in chapter 4 in this chapter and applied by using indirect vector control induction motor drive. The performance of proposed SMC-MRAS is compared to the PI-MRAS.

chapter 6: Experimental Validation and Analysis

This chapter presents a brief description of DSP-based electric-drives system, used in order to perform practical testing and the real time implementation of the proposed speed observer schemes. In this chapter the performance of proposed observers FLC-MRAS and SMS-MRAS are analyzed through experiments by using different speed profiles and load torque conditions and compared with the PI-MRAS

observer.

chapter 7: Conclusion and Future Work

Finally, the last chapter of thesis presents the summary of results with some suggestions for future work.

Chapter 2

Sensorless Control of Induction Motor- A Literature Review

2.1 Introduction

SENSORLESS control of IM drive is a vast research field and has been widely investigated in the past two decades. Such control strategies offer low cost, more compactness, less required maintenance, suitable for the hostile environment and overall more reliable and robust electric drive system [46]. Electric propulsion system is an integral part of EVs and HEVs [10], [52]. The performance of traction motor drive plays an important role in the evolution of AEVs and electrified transport industry. An IM is not only the workhorse of different kinds of domestic and industrial applications [53] but also one of the most appropriate electric motor candidates and widely accepted choice for most of the EVs and HEVs manufacturing companies [1], [15], [54].

However, the controlling of IM drive has difficulties because of its nonlinear dynamics, motor parameter variations during the operation and the unavailability of rotor currents and flux measurement [12]. Hence, a high performance controller is required for IM traction drive to achieve the fast transient response and energy

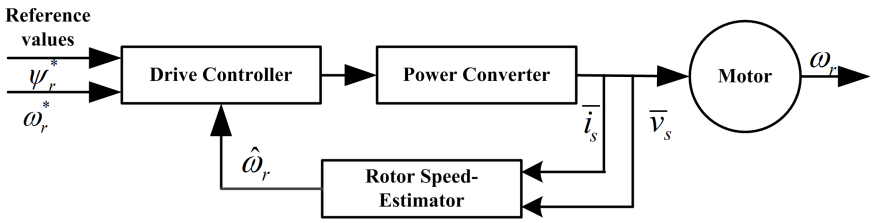

Figure 2.1: Basic block diagram of closed loop speed sensorless control of AC electric motor drive

optimization [55], [48], [56]. On the other side, due to the cost of the rotor speed and position sensor and the problem of sensor electrical noise, sensorless control which estimates the rotor speed instead of installing a speed encoder is preferred in high performance IM and EV applications [46]. The sensorless control methods for IM are possible after the rapid developments in the field of power electronics and digital signal processing [57], [58], [59].

Several rotor speed estimation methods have been proposed recently as already mentioned in chapter 1 Fig 1.4. But the main concern always arises is to which extent proposed method is successful without deteriorating the dynamic performance of drive. *Rajashekara et al.* presents a comprehensive summary of speed sensorless control techniques employed on different AC machines including IM drive [60].

Rotor speed estimation techniques based on the fundamental mathematical machine model are mainly classified into open loop and closed loop speed estimation scheme and fundamentally differ due to the absence of correction term in open loop scheme [3, 46]. These techniques use the machine dynamic equations with ignoring the space harmonics and considering the sinusoidal flux distribution using machine $d-q$ model [24]. Instantaneous values of stator currents and voltages are used in these schemes in order to extract the rotor speed information and flux linkages for sensorless control. Fig 2.1 shows the simplified block diagram of closed loop speed sensorless AC motor drive control.

Among several proposed speed estimation techniques, MRAS based methods

are more preferred due to simple implementation and less computational efforts. However, these methods fail to provide satisfactory performance at low and around zero speed operation and at different load disturbances. Machine parameter dependency during the operation is the common problems in both open loop and closed loop estimation schemes and real time parameter adaption schemes are applied to compensate the parameter variation [12, 24, 46]. In addition, inverter nonlinearity and signal distortion are the other main causes of such unsatisfactory operation of sensorless IM drive [61–63].

This chapter aims at providing a comprehensive review on the major MRAS based schemes applied for high performance control of IM drive. Other advanced AI based MRAS schemes are also discussed. The problems affecting the performance of MRAS at low speed region, load disturbance condition and different methods employed to solve such problems in the literature are presented.

2.2 Powertrain Configurations of EVs

All electric vehicle or pure electric vehicle is the vehicle uses only electric power for its propulsion system. Components arrangement of motor (M), differential (D), fixed gear (FG) and gear box (GB) make different six kinds of EV powertrain configurations as shown in Fig.2.2 [1, 64]. These configurations are similar for both in BEVs and FCEVs. Fuel cell can be either the main energy supply or secondary depending on the requirement and technology. All six drive train configurations are briefly explained below.

- In Fig.2.2(a) electric propulsion replaces the ICE of conventional vehicle drive train. The gearbox provides a set of gear ratios to modify the speed-power (torque) profile to match the load requirement. High level of gear means high torque and lower speed and vice versa. Gearbox may be replaced by an automatic transmission. The differential is a mechanical device, which is used to

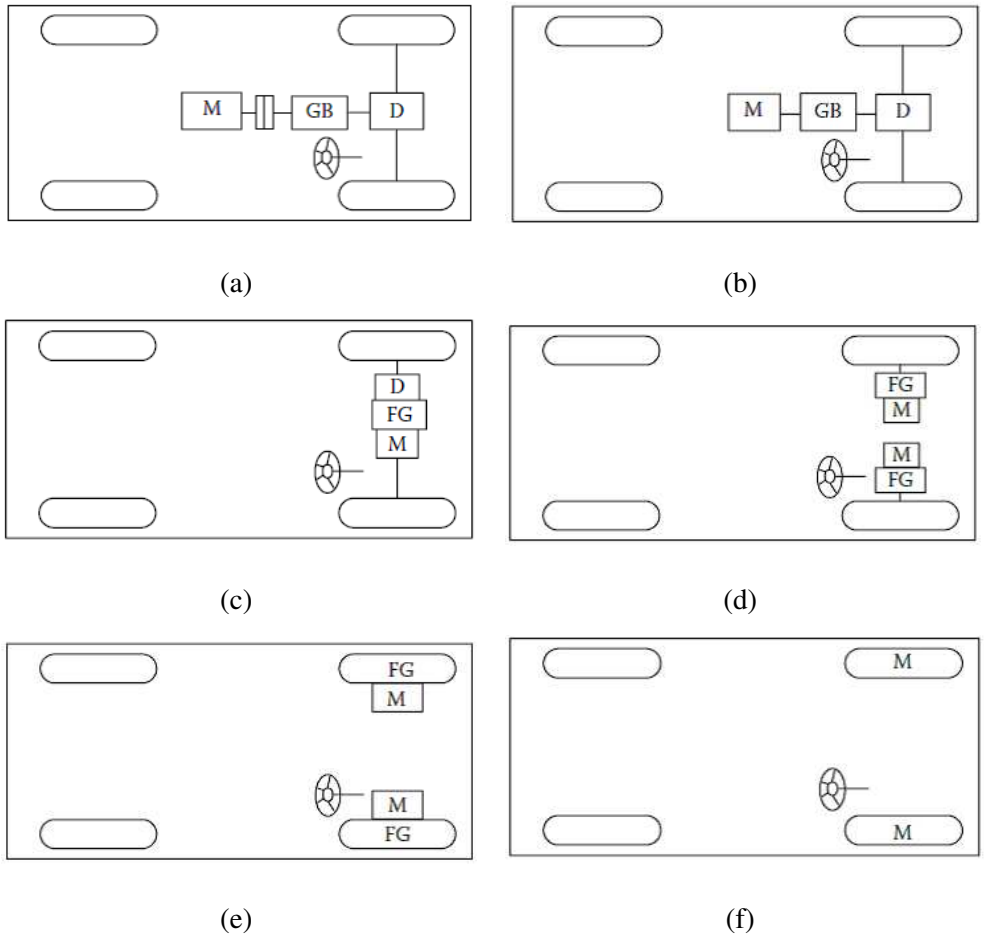

Figure 2.2: Different powertrain configurations of EVs [1].

distribute different power levels into both side wheels.

- In Fig.2.2(b) by removing the clutch and replacing the gear box with fixed gearing, not only it reduces the size and weight of the mechanical transmission, it also simplifies the drive train control. However, gear shifting is not needed and without the clutch and gear box it can not provide the desired speed and torque features.

- Fig.2.2(c) configuration is similar to the drive train in 2.2(b), electric motor, fixed gearing, and the differential can be further integrated into a single assembly while both axles point at both driving wheels. This configuration most commonly used by modern EVs.

- Fig.2.2(d) shows the dual motor configuration in which two electric motors separately drive the driving wheels through fixed gearing. These two motors are operated at different speed in the curved path and provide the differential features.

- In order to reduce the mechanical transmission path between electric motor and driving wheels, the electric motor can be placed inside the wheel as shown in Fig.2.2(e). This arrangement is also called in wheel drive configuration. Fixed planetary gearing is employed to reduce the motor speed to the desired wheel speed. Here, the advantage of planetary gearing in this configuration is to provide a high speed reduction ratio as well as an inline arrangement of input and output shafts.

- Requirement of the compact propulsion system eliminates the use of reduction gears and mechanical differential in drive line by placing a direct-drive motor at the exact location where torque is required [65]. Direct drive-in-wheel motor arrangement as shown in Fig.2.2(f) for EVs simplifies the mechanical layout. Elimination of reduction gear and mechanical differential not only reduce the number of drive line components, energy loss in transmission,

Figure 2.3: Protean Electric in-wheel motor assembly [2]

maintenance and weight but also improve the overall system reliability and efficiency [66]. This gearless wheel motor drive system is used for high torque and low speed applications [50].

In-wheel motors can be integrated into two or all of the wheels on a vehicle and could potentially use up to 96% of generated energy. Fig. 2.3 illustrates a complete assembly of the Protean In-wheel motor, integrated with its drive electronics [2]. In-wheel motors designed for the EVs are discussed as potential motor designs [50]. In this configuration the machine needs to produce the total torque directly for the wheel shaft, hence, the speed control of the traction motor represents the equivalent control of the wheel speed and hence the vehicle speed. However, this drive train configuration requires higher torque traction motor to start and accelerate the vehicle [1].

2.3 Machine Model-Based Sensorless Control Techniques

Machine model based schemes use machine dynamic equations directly to estimate the rotor speed. In open loop speed estimators, there is no speed information

feedback so that the implementation of such schemes are simpler comparatively. But noise in voltage measurement, pure integration problems and particularly machine parameter deviations constitute the major deficiencies of such schemes especially at very low or zero speed region and deteriorate the dynamic performance of drive both in steady state and transient operating mode [12, 46, 49, 67, 68]. As the stator frequency approaches to zero, rotor induced voltage also approaches to zero and finally IM variables become unobservable and lose the controllability that is the inherent limitation of these machine model based techniques [12, 46]. In general, the open loop estimators are more dependent on several parameters of the IM such as stator and rotor resistances and inductances. However, the estimation accuracy is more dependent on the accuracy of the machine parameters used in the estimator model. The variation of stator resistance has important effects on the stator flux linkage specially at low speed region and if the rotor flux linkage is obtained from the stator flux linkage then the accuracy of rotor flux linkage also affected by the stator resistance variation [24]. The accuracy of rotor flux linkage is also influenced by the schemes which use rotor time constant and vary with the change of rotor resistance. Some open loop rotor speed estimation schemes are discussed in [24, 69].

On the other hand, closed loop estimation techniques mainly differ with the open loop due to the use of an error signal between the measured and estimated quantities in order to improve the dynamic performance of drive control. However, it is possible to enhance the robustness of speed estimator against the parameter mismatch and signal noise in closed loop. Therefore, closed loop speed estimators have better accuracy as compare to the open loop schemes. Fig 2.4 shows the machine model based closed loop motor rotor speed estimation techniques.

2.4 MRAS for Sensorless Induction Motor Control

Application of MRAS based speed estimation techniques are more common in sensorless control due to their inherent simplicity, effectiveness and less computa-

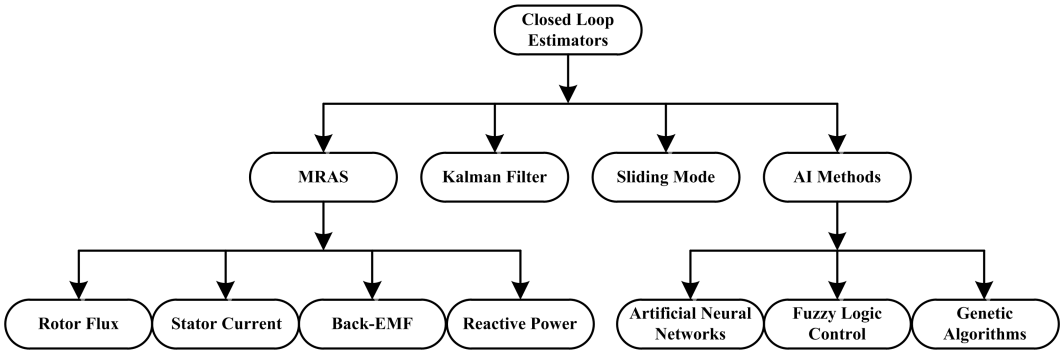

Figure 2.4: Machine model based closed loop motor rotor speed estimation techniques

tional efforts. MRAS is one of the different adaptive control techniques used for state and parameter estimation. Other techniques include, self-tuning regulators, dual control and gain scheduling [68, 70]. The fundamental idea of MRAS was proposed by Landau in the year 1979 [71]. MRAS uses two different machine models, reference model and adaptive or adjustable model in which adaptive is speed dependent model [24, 46]. An adaptation mechanism is used to minimize the error between both models to estimate the desired physical quantity. There are three different types of MRAS structure : parallel, series and series-parallel [71]. A basic parallel structure MRAS block diagram is shown in Fig 2.5.

Reference model provides the reference value of the system state variable x and equations do not include the parameter to be estimated. Whereas the adaptive model uses different set of equations with different inputs for the same estimated state variable $\hat{x}$ and include the estimated parameter in the expression. The difference between both models (error) ε passes through the adaptation mechanism usually proportional-integral controller to reduce the error. In order to minimize the error signal different set of adaptive laws have been considered such as Popov's hyperstability criterion [72], Lyapunov stability theorem [73] and recursive least square algorithm [74]. On the basis of error signal or error function used for speed estimation, MRAS further associated schemes include rotor flux, reactive power, back

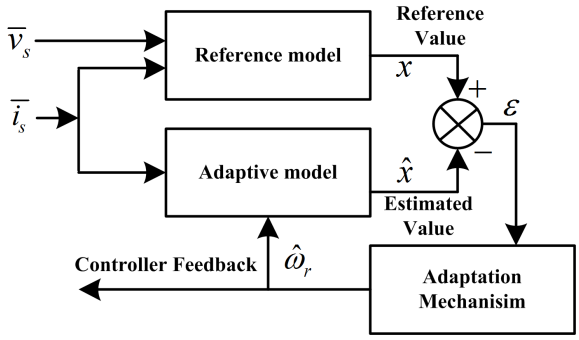

Figure 2.5: Block diagram of parallel structure MRAS

EMF and stator current based [24, 75–77].

2.4.1 MRAS based on Rotor Flux Error

The rotor flux error based MRAS for IM drive was proposed principally for the first time by Tamai et al. in 1985 [78]. Fig 2.6 shows the the basic structure of rotor flux error based MRAS speed estimator. The reference model that is also called the voltage model is independent of rotor speed and used to calculate the reference value of the rotor flux ψ_r by means of the machine terminal stator voltage and current signals. The adaptive or adjustable model that is also known as MRAS current model is rotor speed dependent and used to estimate the rotor flux $\hat{\psi}_r$. Then the speed tunning signal ε_ψ is fed to the PI controller to estimate the rotor speed $\hat{\omega}_r$. For the reference model, the stator voltage defined in the stator reference frame can be rearranged for the reference rotor fluxes as [24, 75]:

$$\psi_{rD} = \frac{L_r}{L_m}[\int (v_{sD} - R_s i_{sD})dt - \sigma L_s i_{sD}] \tag{2.4.1}$$

$$\psi_{rQ} = \frac{L_r}{L_m}[\int (v_{sQ} - R_s i_{sQ})dt - \sigma L_s i_{sQ}] \tag{2.4.2}$$

In the same way the rotor voltage in stator reference frame can be expressed for estimated rotor flux for the adaptive model as:

$$\frac{d\hat{\psi}_{rQ}}{dt} = -\frac{1}{T_r}\hat{\psi}_{rQ} + \hat{\omega}_r\hat{\psi}_{rD} + \frac{L_m}{T_r}i_{sQ} \tag{2.4.3}$$

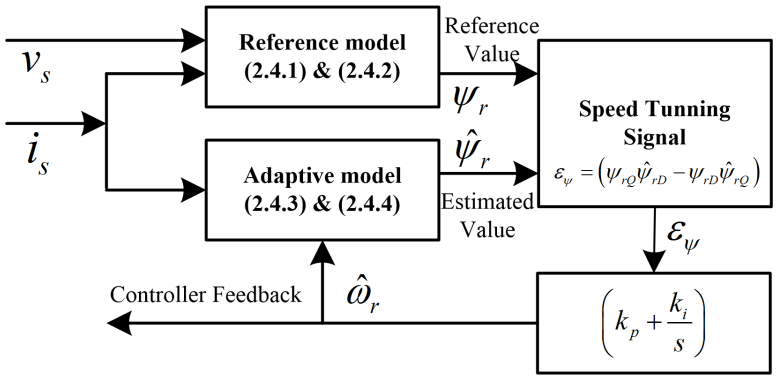

Figure 2.6: Block diagram of rotor flux error based MRAS speed estimator

$$\frac{d\hat{\psi}_{rD}}{dt} = -\frac{1}{T_r}\hat{\psi}_{rD} - \hat{\omega}_r\hat{\psi}_{rQ} + \frac{L_m}{T_r}i_{sD} \tag{2.4.4}$$

Here (2.4.1) & (2.4.2) are belong to the reference model and (2.4.3) & (2.4.4) are used for the adaptive model. The difference between reference and adaptive model rotor flux linkages are used to express the speed tunning signal as:

$$\varepsilon_\psi = \left(\psi_{rQ}\hat{\psi}_{rD} - \psi_{rD}\hat{\psi}_{rQ}\right) \tag{2.4.5}$$

This speed tunning signal passes through the PI controller that gives a stable nonlinear feedback system which was already proved by popov's hyperstability criteria. The purpose of PI controller to tune the rotor speed where the difference between two rotor flux linkage space vectors are not zero $\psi_r \neq \hat{\psi}_r$. In other word, if the estimated rotor speed is changed in such a way that the out put of the reference model and adaptive model are the same, then the estimated rotor speed $\hat{\omega_r}$ is equal to the actual speed ω_r. From the Fig. 2.6 the estimated speed can be expressed as:

$$\hat{\omega}_r = k_p\varepsilon_\psi + k_i\int \varepsilon_\psi \tag{2.4.6}$$

However, the rotor flux error based MRAS speed estimator algorithm proposed by Tamai et al. is simple but still suffers from the inaccuracy due to the inaccurate estimation of rotor time constant during the operation [79]. Moreover, an off-set error also produces and deteriorates the estimated rotor speed because of smooth

stator resistance change with temperature and it influences more specially at low speed operation region [80]. Tamai et al's idea was modified by Schauder in 1989 by using low pass filter both in reference and adaptive model to reconstruct the rotor flux and hence the rotor speed. Comparatively this idea was not very complex and more effective than the previous mentioned approach and applied by different researchers [75].

The proposed estimator is more sensitive to the motor parameter variations and makes rotor flux sensitive both from voltage and current models [51, 81]. However, machine parameter sensitivity specially stator resistance, flux pure integration problem which may cause dc drift [24], acquisition of stator voltage and current and inverter nonlinearity may limit the performance of rotor flux observer at low and around zero speed [12, 46, 82]. However, these issues may limit the performance of at or around zero speed and reduces the overall performance of electric drive. Satisfactory performance of speed estimator applied to the vector control drive above to 2Hz frequency was reported [12, 46, 75]. Better performance at zero speed reversal is possible provided that the fast transient is applied. However, a long duration operation at zero speed point is not satisfactory due to the incorrect rotor flux linkage estimation [13, 24].

In [83] discusses the rotor speed estimator based on rotor flux based MRAS which estimates the resistance and rotor resistance updating algorithm is done by the Proportional-Integrator (PI) controller. Reference [84] proposed a speed estimator for an IM drive based on the nonlinear speed estimator with the open loop rotor flux observer. However, it limits the motor load torque conditions, and less than half load is applied for low speed applications. An online rotor time constant estimator for rotor flux based MRAS IM drive is proposed by which the accurate value of the angular slip velocity can be used to calculate the correct value of rotor flux position even though the rotor time constant changes from the nominal value [85]. [86] proposes the online rotor resistance estimation and correction schemes by using rotor flux based MRAS which is independent on stator resistance variations. Recently a

discrete type rotor flux and speed estimator for high speed sensorless IM drive is presented with experimental results [87].

2.4.2 MRAS based on Back-EMF Error

The concept of back-EMF error based MRAS speed estimator was presented by Peng and Fukao in 1994. This scheme does not require any pure integration in its reference as well as adaptive model. In this scheme the back EMF is estimated and compared with the measured quantity in order to produce the speed tuning signal [82]. Then this signal passes through the PI based controller to estimate the rotor speed. The direct and quadrature axis components of back-EMF in the stationary reference frame can be expressed from the stator voltage equation of induction machine as [24]:

$$e_d = \frac{L_m}{L_r}\frac{d\psi_{rD}}{dt} = v_{sD} - R_s i_{sD} - \sigma L_s \frac{di_{sD}}{dt} \tag{2.4.7}$$

$$e_q = \frac{L_m}{L_r}\frac{d\psi_{rQ}}{dt} = v_{sQ} - R_s i_{sQ} - \sigma L_s \frac{di_{sQ}}{dt} \tag{2.4.8}$$

The above both equations (2.4.7) & (2.4.8) are used in reference model. Both components of back-EMF e_d and e_q are without integration it means there is no problem associated with drift. The corresponding equations for the adaptive model are

$$\hat{e}_d = \frac{L_m}{L_r}\frac{d\hat{\psi}_{rD}}{dt} = \frac{L_m}{L_r}\left(\frac{L_m i_{sD} - \psi_{rD} - \omega_r T_r \psi_{rQ}}{T_r}\right) \tag{2.4.9}$$

$$\hat{e}_q = \frac{L_m}{L_r}\frac{d\hat{\psi}_{rQ}}{dt} = \frac{L_m}{L_r}\left(\frac{L_m i_{sQ} - \psi_{rQ} - \omega_r T_r \psi_{rD}}{T_r}\right) \tag{2.4.10}$$

The above both equations (2.4.9) & (2.4.10) are used in the adaptive model. whereas the speed tuning signal $\varepsilon_e = (e_q \hat{e}_d - e_d \hat{e}_q)$ passes through the PI controller to estimate the rotor speed as shown in Fig. 2.7.

However, the Peng's scheme suffers from the inaccurate speed estimation due to the controller nonlinear characteristics and stator resistance dependency in the low speed operating region. Further this MRAS speed estimator shows unstable

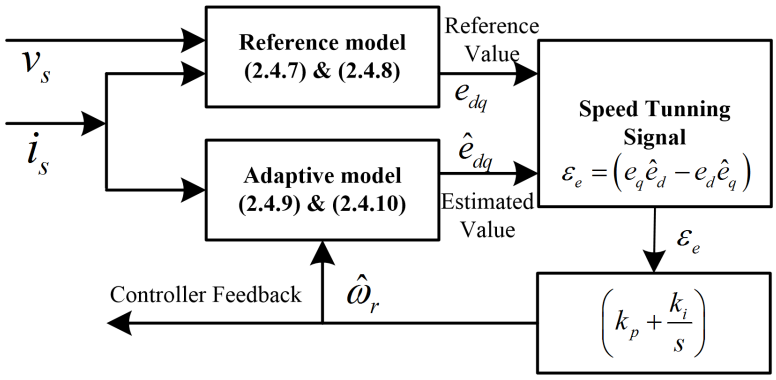

Figure 2.7: Block diagram of back-EMF error based MRAS speed estimator

dynamic performance due to the derivative form of stator current. This derivative problem is controlled by inserting the first order LPF at the output of refernce model and at the input of adaptive model. However, this scheme avoids the pure integration problem but still sensitive to the stator resistance [88] and has stability problem at low stator frequency. Moreover, it shows low noise immunity due to the stator current differentiation and unsatisfactory dynamic performance at low speed region [89].

2.4.3 MRAS based on Reactive Power Error

This reactive power error based MRAS scheme was also developed by Peng and Fukao. This scheme offers better robustness against the stator resistance variations and avoids the pure integration, resulting the accurate speed estimation at or near zero speed operation [90]. The quantity that is acquired by the cross product of back-EMF difference $\Delta\bar{e} = \bar{e} - \hat{\bar{e}}$ and the stator current space vector $\bar{i_s}$. where, $\bar{e}, \hat{\bar{e}}$ are the back-EMF space vectors in reference and adaptive models respectively.

By means of back-EMF equations, the reference model equation can be express as [24]:

$$q = \bar{e} \times \bar{i}_s = \bar{i}_s \times \left(\bar{v}_s - R_s\bar{i}_s - \sigma L_s\frac{d\bar{i}_s}{dt}\right) \tag{2.4.11}$$

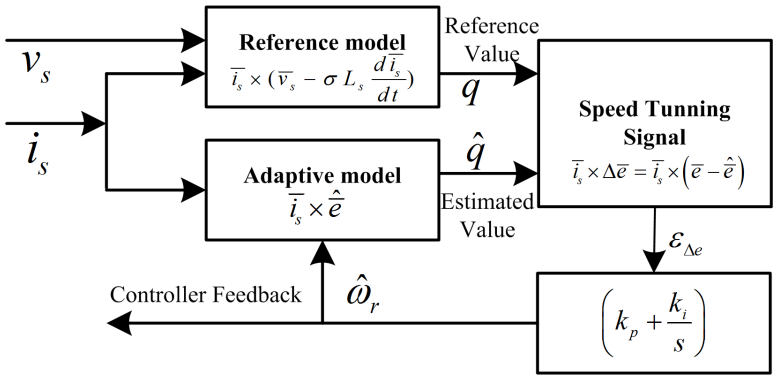

Figure 2.8: Block diagram of reactive power error based MRAS speed estimator

where q indicates the reactive power and $\bar{e}$ is the back emf vector.

$$q = \bar{i_s} \times \bar{v_s} - \sigma L_s \frac{d\bar{i_s}}{dt} \tag{2.4.12}$$

where $\bar{i}_s \times \bar{i}_s = i_{sD} i_{sQ} - i_{sQ} i_{sD} = 0$

From the above expression it is cleared there is no stator resistance term to effect the observer performance at low speed region. Similar to the previous two schemes, the stator voltage v_s can be obtained from the line voltage or in inverter fed induction motor drive, it can be reconstructed from the inverter switching states and the monitored value of the DC link voltage.

In the same way the reactive power for the adaptive model cab be expressed through the estimated back-EMF

$$\hat{q} = \hat{\bar{e}} \times i_s = i_{sD} \hat{e}_q - i_{sQ} \hat{e}_d \tag{2.4.13}$$

$$\hat{q} = \frac{L_m}{L_r} [\frac{1}{T_r} (\psi_{rD} i_{sQ} - \psi_{rQ} i_{sD}) + \omega_r (\psi_{rD} i_{sD} + \psi_{rQ} i_{sQ})] \tag{2.4.14}$$

Both equations (2.4.12) & (2.4.14) are used as a reference and adaptive model to make the final implementation of rotor speed estimator as shown in Fig. 2.8.

The MRAS based on the reactive power error is almost completely robust to the stator and rotor thermal resistance variations. Therefore, it can be considered a less machine resistance effected method than the previous two methods. It can provide

the satisfactory performance at low speed region when this method is applied on vector controlled drive [82, 89]. This speed estimator can track better actual rotor speed with the bandwidth limited by the noise, so both PI controller gains should be as large as possible. This insensitive to stator resistance variation scheme has shown the robustness for the rotor time constant T_r, when it is applied on rotor-flux-oriented vector control drive [24, 82]. Resulting, the alignment of the rotor flux could be maintained during the operation wether the incorrect rotor time constant value is used. Apart from the stator resistance insensitivity the included term $\frac{L_m}{L_r}$ does not make much effect on the performance of drive since it does not change with the temperature. Moreover, the deviation of T_r from its correct value may produce some steady state error in the estimated speed and can have significant affect at low speed.

Therefore, MRAS speed estimator based on reactive power offers robustness against the stator resistance variation which is the most important part and avoids the pure integration [24, 82]. However, it provides an instability at some operating point when passing through the regenerative mode [88, 91]. In addition, both back-EMF and reactive power quantities vanish at low speed and zero speed operation [89]. In [92] Wu et al. provides a detailed study and comparison between both back-EMF and reactive power based MRAS speed estimator. In this reference verification of the instability part of reactive power based MRAS method was reported.

2.5 Other Rotor Speed Estimation Techniques

Sliding mode control (SMC) is another widely applied scheme in electric motor control. SMC scheme is considered for less machine parameter sensitivity, external disturbances rejection, good performance against the unmodeled dynamics and has capability to provide fast transient response [24, 93, 94]. These properties are important features for a state estimation in a nonlinear plant such as speed estimation in IM drives. This characteristic makes SMC method ideal for nonlinear

control of IM drives [95]. An integral SMC has been applied for VC of IM drive with the 20% of parameter variations and stepping speed from 800 rpm to 1200 rpm [94]. Moreover, a SM flux estimator has been employed as an adaptive model in MRAS with acceleration command from 100-350 rpm and deceleration command from 350-100 rpm for the test pupose but scheme performance at zero speed was not shown [96]. Further, SM estimator has been proposed to solve the speed problem in IM drives [93–95, 97]. A detailed information is presented in [95] about the mathematical basics, design procedure and application of SMC in IM drives.

Adaptive flux observer (AFO) is also used for speed estimation in IM drive system. The structure of adaptive estimator is composed of three main unit: induction motor model, estimator's feedback gains and rotor speed adaptation mechanism. Selection of PI gains in adaptation mechanism and estimator's feedback gains in the speed estimation process [98]. An observer can be generally classified into deterministic and stochastic according to the type of representation used for the plant. Luenberger and Kalman observer are the most commonly used non-linear speed estimators. Extended Luenberger Observer (ELO) can be applied to the nonlinear time-varying deterministic systems while the Extended Kalman Filter (EKF) is applied to the nonlinear time-varying stochastic systems [12]. The advantage of both ELO and EKF is that they can combine parameter and state estimation [99].

EKF is the most widely applied non linear estimator and has been extensively used in rotor speed estimation for sensorless IM drives [100, 101]. Algorithm of EKF is suitable for the system which may have have unknown noises such as current ripple by PWM, noises by modeling error and measurement error etc. These noises are considered as disturbance in the EKF algorithm design. The EKF has advantage of considering modeling errors, inaccuracies and measurement errors in order to estimate the rotor speed over a wide speed range but not at zero speed [24]. Notwithstanding, huge computational efforts and complexity, KF has been widely applied in electric drive control system due to lower sensitivity of parameters [102]. Some drawbacks of KF are: Lack of design and tuning criteria, erroneous machine

parameters and dependency of machine model accuracy [12].

The ELO has been applied for combine rotor flux and rotor speed estimation in deterministic systems where noise is not taken into account [101]. The design of ELO is relatively flexible with less computational efforts as compare to the EKF and has capability of producing of unbiased estimations [24]. However, the joint rotor flux and speed estimation in ELO has weak observability in the low and zero speed operating region [12].

2.6 Estimation Through Signal Injection

In sensorless electric motor control these SI techniques show low machine parameter sensitivity with better low speed or zero speed performance [12]. In SI technique, a low amplitude but high frequency signal is injected to the stator windings that does not change the basic operational behavior of the machine a lot. The injected signals are modulated by the orientation of the machine asymmetries, and then processed and demodulated to get the required measurement. Such asymmetries occur more naturally in synchronous motors. Many authors have proposed different novel techniques, [103] presents speed estimation technique through SI, smooth air gap IM model combined with an MRAS. Test show the response of estimator performance through zero speed with 50 rpm step. In [104] sensorless PMSM system parameters are identified including the inverter at different operating conditions. SI based method is used first before moving on to the EMF based estimation. PM machines vary with respect to suitability for SI based techniques [12]. In [105] developed a design criteria to assist SI technique for interior PM machine using finite element analysis.

However, high frequency SI techniques are hugely complicated and their design criteria is not general and varies with the machine drive system, resulting lose the generality of technique application [13,46]. Moreover, these techniques also constitute the torque ripples and acoustic noise emissions that is not much preferable for

the EVs and HEVs applications [93].

2.7 Sensorless Control Issues at Low Speed Operation

2.7.1 Motor Parameter Sensitivity

Machine parameter variation during the operation is somewhat an important issue in speed estimation, since machine model based techniques are totally dependent on the machine mathematical model. Inaccuracy in the estimated speed is the result of motor parameter mismatch between the speed estimator and actual motor during the operation. Motor parameters vary during the operation due to the change in operating temperature, frequency and machine magnetic saturation level. Stator and rotor resistances (R_s, R_r) change with the change in operating temperature, mutual inductance L_m changes with the machine magnetic saturation level and stator and rotor leakage inductances (L_{ls}, L_{lr}) vary with the operating currents [68].

Motor internal temperature variation depends on the motor power losses during the whole operation. In these losses, stator and rotor copper losses are mainly affected when the motor operates with variable load condition, whereas, core losses are mainly affected by machine magnetic flux level. To develop a machine thermal model or implementation of temperature sensor to detect the stator and rotor resistance is not precise due to the nonlinear characteristic between the machine cooling fan flow rate and the machine speed. Moreover, the motor thermal time constant also changes with the motor speed [68, 106].

The stator resistance variation has an important effect to estimate the accurate stator flux linkages, specifically at low or around zero speed region where the stator voltage becomes very low. Low speed or zero speed estimation problems of sensorless machine model based techniques can be understood by the simplest form of

stator voltage equation that is [12]

$$v_s = R_s i_s + \frac{d\psi_s}{dt} \tag{2.7.1}$$

The rate of change in stator flux linkage ψ_s becomes zero when stator frequency approaches to zero, since stator flux linkage is the function of speed and frequency [49]. At low speed/frequency, an IM appears purely resistive at the stator terminals. It requires the stator terminal quantities when the flux linkage is determined through the integral form

$$\psi_s = \int_0^t (v_s - R_s i_s) dt \tag{2.7.2}$$

Stator flux linkage requires the integration of current and voltage, whereas signals in (2.7.2) have noise and disturbances on the measured values at low frequency, resulting reduction in accuracy. Noise and quantization appear in digital measurement while drift and offset constitute in the analog transducers [46, 49]. These effects along with imperfect integrator, reduce the performance achieved. How to implement this integrator perfectly is the main factor in order to apply these machine model techniques [12, 24, 49].

Stator resistance variation gradually dominates with temperature and this is more serious problem at low speed and this variation can be up to 50% and use of fixed value under all operating conditions is difficult [12, 46, 49]. Therefore, online parameter estimation and adaptation techniques are used to make the stable operation as well as accurate speed estimation [106, 107]. However, the incorrect rotor resistance value affects the steady state speed estimation accuracy [89, 106]. The effect of motor parameter variations on the dynamic performance of electric drive and speed estimations accuracy have been studied in different works [89, 102]. In [102]a detailed performance of the rotor flux based MRAS is presented with the machine parameter variations from 20% to 200%.

The proposed solution to overcome the problems associated with the stator resistance variation was the new developed MRAS after rotor flux based on reactive power proposed by $Peng$ and $Fukko$ as already discussed and mention in section

2.4.3. This method does not include stator resistance in the reference model, resulting no contribution in the estimation process [82]. whereas, the reactive power is determined from the cross product of back-EMF and stator current vectors. Initially, this proposed technique used to be considered a good solution of the existing problems, since neither stator resistance nor pure integrator problem in the reference model. However, this scheme provides unstable performance at some operation condition and further both back-EMF and reactive power quantities are vanished at low and zero speed region. Poor performace result was reported by $Blasco - Gimenez$ et al in [89].

Several schemes have been proposed to estimate the rotor speed with the stator resistance identification by using MRAS [88, 91, 107–109]. The MRAS speed estimator based on reactive power error, eliminates the observer sensitivity to the stator resistance and also pure integrator problem in the reference model but still the stator transient inductance effects the accuracy of speed estimation process. In order to reduce the effect of stator transient inductance in MRAS speed estimation process, $Zhen$ and Xu proposed a mutual MRAS scheme with interchangeable reference and adaptive models and the equations were derived to remove the stator transient inductance from the reference model but the stator resistance was still present [108]. The scheme was used for rotor speed estimation as well as stator resistance in a position sensorless IM drive. For the accurate rotor speed and stator resistance estimation, an online rotor time constant adaptation was incorporated with different speed command for the test purpose. However, the stator resistance and rotor speed estimation algorithms are not concurrent, resulting drive has no information of speed estimation during the resistance identification process [109].

In order to tackle these problems, $Vasic$ and $Vukosavic$ proposed a method to estimate the rotor speed and stator resistance simultaneously by using the parallel MRAS observer. In this method the conventional voltage model (VM) and current model (CM) flux observer are used as a reference and adaptive models respectively for the rotor speed estimation as also mentioned in [75]. The two observers switch

roles for the stator resistance identification and by means of two adaptation mechanisms defined by the Popov's hyperstability theory, the simultaneous rotor speed and stator resistance estimation are achieved. Moreover, the accurate rotor speed estimation was found for a short period of time at zero speed region. The incorrect value of rotor time constant has minor effect on the stator resistance estimation but has the significant affects on speed estimation.

Another rotor speed and stator resistance estimation scheme [91] applied on vector control IM drive, uses q-axis rotor flux defined in the synchronous reference frame as a tuning signal for the rotor speed estimation. This scheme uses a simple PI controller to drive q-axis rotor flux to zero so as to achieve the rotor speed. Another stator resistance identification algorithm is defined by using the difference between the d-axis rotor flux error between the VM and CM. A new stable back-EMF based MRAS for simultaneous rotor speed as well as stator resistance identification was proposed by $Rashed$ and $Stronach$ [88]. The robustness of the stator resistance estimator with the large resistance mismatch was verified both by simulation and experimentally.

2.7.2 Pure Integration Problem

Pure flux integration problem presents in the reference model of the rotor flux based MRAS has a crucial difficulty that may cause dc drift problem [24, 46, 110]. To solve this problem a Low-Pass Filter (LPF) with a low cut-off frequency typically 1-3 Hz has been proposed to replace the pure integrator [12, 13]. In rotor flux based MRAS, LPF helps to attenuate the high frequency signal component in the motor terminal voltages which make it less attractive to completely eliminate the pure integrals [75]. For practical implementation in order to avoid these problems, a LPF with the transfer function $\left(\frac{1}{s+\frac{1}{T}}\right)$ can be used instead of a pure integrator. In the reference model that already contains $\left(\frac{1}{s}\right)$ should be followed by a high pass filter $\left(\frac{s}{s+\frac{1}{T}}\right)$, since $\left(\frac{1}{s+\frac{1}{T}}\right) = \left(\frac{1}{s}\right).\left(\frac{s}{s+\frac{1}{T}}\right)$. The output of the modified reference model

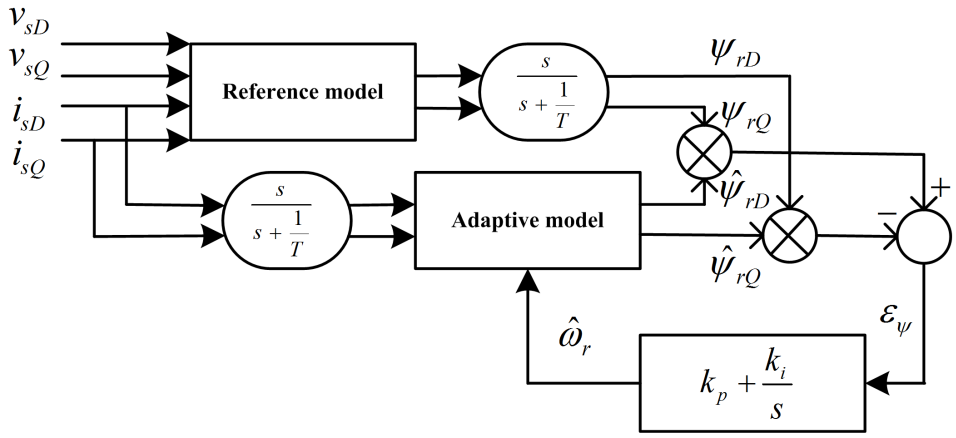

Figure 2.9: Modified block diagram of rotor flux error based MRAS speed estimator for practical immplementation

provides the modifies rotor flux linkage. In the same way the adaptive model should be adjusted to provide the corresponding modified estimated rotor flux. Therefore, a high pass filter block $\left(\frac{s}{s+\frac{1}{T}}\right)$ is placed in fron of the adaptive model. The modified rotor flux based MRAS for practical implementation is shown in Fig. 2.9.

However, a LPF behaves like an integrator only at the frequency higher than the cut-off frequency of the filter. The modification altered the mathematical structure of both reference model and adaptive model in rotor flux linkage MRAS, while maintaining the hyperstability [13, 24, 75]. In practice, the cut-off frequency of this high pass filter should be few Hz. Since the rotor speed estimation is inaccurate below the filter cut-off frequency. Moreover, implementation of this LPF introduces the gain and phase error and produces delay in the estimated speed with respect to the actual, which may affect the dynamic performance of electric drive [96, 111].

Several solutions have been proposed with the purpose of resolving the problem of pure integrator. $Karanayil$ proposed a programmable cascaded LPF (PCLPF) to remove the pure integrator problem by using a small time constant cascaded filters to attenuate the dc offset decay time. The technique proposed by $Hinkkanen-et-al$ in [112] uses the modified integrator to estimate the rotor flux having the same

frequency response as the pure integrator at steady state. In [113] $Q - Gao$ et al. proposed a nonlinear feedback integrator for drift and dc offset applied for a voltage model flux observer. This modified voltage model was applied on rotor flux based MRAS as mentioned in [75] and the proposed scheme was applied on vector control IM drive.

Another research in [110, 114] completely replace the VM by other flux linkage estimators, which reduce the scheme simplicity. Both techniques use the MRAS structure as mentioned in [75] with PI controller minimization of the cross product of flux estimates. In [110] the reference value of the rotor flux linkage MRAS estimator was generated by the state observer with current error feedback. Experimental tests were carried out with different speed commands, load torque and 50% rotor resistance mismatch. Better performance was achieved by the proposed scheme as compare to the conventional MRAS. Classical MRAS presented in [75] was applied in [89] with a closed loop flux estimator that employed a coupling controller between the VM and CM. This topology provides open loop integration of the VM with necessary feedback and no LPF is required in the VM. But as frequency approches to zero the cross product between both flux estimates also approaches to zero and speed estimation is lost.

2.7.3 Stator Voltage Measurement

Stator voltage measurement is important in MRAS based speed estimator since the state variables from the reference model such as rotor flux and back-EMF are estimated by using these voltages. Therefore, the correct measurement in voltages are required to estimate the correct state variable. The most accurate stator voltage can be taken from the machine terminals. However, it can not be implemented easily since it requires a very high sampling rate [49]. Low pass filtering the PWM waveform may resolve the problem at medium and high speed operation but not at low speed. However, the effect of filter gain and phase error cause the performance to

deteriorate. Stator voltages may be reconstructed by the inverter switching functions and the monitored DC link voltage. For the accurate voltage measurement, a model for the inverting switching devices voltage drop should be included with a thermal model that can be used to correct the value of stator resistance [24, 115].

Reference voltage can be used instead of actual voltages if inverter switching frequency is higher compare to the electrical time constant of the motor. It reduces the required number of sensors and since no voltage filtering is required to eliminate the modulation noise and no delay produces due to filtering [24]. Normally error compensation schemes must be applied, when reconstructed or reference stator voltages are used. These compensation schemes considers the voltage error caused by the effects of dead time insertion power electronic voltage drops and fluctuation in the DC link volatge.

IM drive normally driven by the voltage source inverter (VSI), which produces the series of rectangular pulses that continuously switch on and off in order to get the controllable voltage value and supply frequency, hence the resultant stator voltage may contain high frequency harmonic component. Moreover, the non-ideal characteristics of the power switching devices such as non ideal voltage transition during the device switching state on and off, unequal switching time and dead band insertion can make the nonlinear relation between the reference voltage and inverter output [115].

Another idea is to use the reference voltage from the control unit since it is harmonic component free. However, the reference voltage deviates from the actual machine terminal voltage due to inverter nonlinearities and dead time effects. Therefore,$Holtz$ and $Quan$ in [116] have modeled the invertor nonlinearities such as power devices voltage drop and the threshold voltage. As a result better stator voltage acquisition is achieved from the reference voltage of PWM inverter at low speed.

2.8 Artificial Intelligence for Sensorless Motor Control

In the last few years Artificial Intelligence (AI) based techniques are getting more attention of researchers. In the past, AI based techniques such as Artificial Neural Networks (ANNs), Fuzzy Logic Control (FLC) and Genetic Algorithms (GAs) have tackled lots of engineering problems theoretically but the practical implementation of such techniques were limited due to the unavailability of fast processing DSPs. However, the development of fast processing DSPs and advanced power electronic devices have brought the implementation of these computation intensive tools in different motion control applications.

The main objectives of these AI based techniques are to reduce the controller associated tuning efforts, enhance the robustness against the machine parameter sensitivity and by means of DSP implementation to achieve the high dynamic performance with less computational efforts [3, 24, 117]. The basic advantage of using AI techniques is to eliminate the mathematical model of machine and drive system which is dependent on lots of assumptions and parameters that are difficult to estimate during the operation [45]. In the last few years, AI based techniques are assisting and getting more attention in the field of variable speed drives and lots of technical papers have been published in the recent years. In general there are several advantages of AI based electric drive system implementation including [24, 45]:

- To improve the performance of conventional controller;
- Tuning of conventional proportional-integral (PI) controller;
- Application in the fault detection and parameter & state estimation in ac & dc drive;
- System can be easily extended and modified;
- Robust system against parameter variations;

- Electric drive efficiency optimization and in machine design optimization.

ANN mimics the human brain with the capability of generalization and learning [3]. However, expert systems and FLC based techniques are rule based and emulate the behavior of the human experience. ANN have been applied in many real world problems effectively and considered as a potential solution. One of the important key features in ANN is to learn from the experience so as to improve the operational performance of system and to adapt the changes in the environment [45, 68]. Moreover, ANN offers good capability to deal with the system uncertainties and external disturbances. A comprehensive review and the application of ANN in the field of power electronics and electric motor drive control is mentioned in [118]. In the last decade, lots of research papers have been contributed the application of ANN in the field of IM drive control. Some of the ANN supported MRAS rotor speed estimation schemes have been discussed in the literature [24, 68, 119]. ANN has also been applied for online stator and rotor resistance parameters estimation along with MRAS scheme in speed sensorless indirect vector control of IM drive [120].

GA is a stochastic search technique that mimics the mechanism of natural selection. GA is a fast and rapidly growing field in AI area. It is considered as a powerful and an effective tool to solve the optimization and different search problems. GAs are powerful, simple, derivative free, stochastic global optimization methods inspired by the laws of natural selection and genetics [45]. Several books have been published on application of AI in the field of power system and electric drive control [45, 118, 121]. Improved performance of EKF in the speed estimation of sensorless induction motor drive is presented [117]. On the basis of real coded GAs, the optimization procedure enables the noise covariance and weight matrices, on which the EKF performance critically depends, to be properly selected [117]. A comparative analysis on optimising the EKF for speed estimation of an IM using simulated annealing and GA is presented in [122].

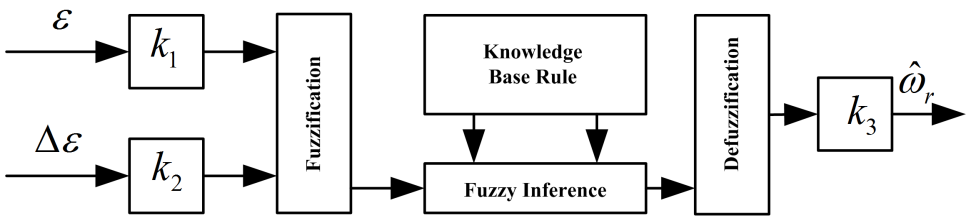

Figure 2.10: Fuzzy-Logic based MRAS for speed estimation

2.8.1 Fuzzy Logic Application in Sensorless Control

In FLC human experience and knowledge based linguistic control strategy is converted into an automatic control strategy. Therefore, there is no requirement for the mathematical model of the system to be controlled. The performance of FLCs have been found to be excellent for the systems that are imprecise, nonlinear or time varying and having unknown or uncertain parameter and structure variations. FL is considered a well established control technique and has been applied in many industrial automation processes. In the last few years some efforts have been made to utilize the FLC in speed sensorless electric drive.

A basic block diagram of FLC for the speed estimation is shown in Fig. 2.10. It has three main parts fuzzification, fuzzy inference and defuzzification. In FLC two inputs are error ε that is the difference between the reference and adaptive model and second one is the error variation $\Delta\varepsilon$ or the rate of change of error $\left(\frac{d\varepsilon}{dt}\right)$. Rotor estimated speed $\hat{\omega}_r$ is the output of FLC whereas k_1, k_2 and k_3 are the scalling factors.

In [123] a reactive power based fuzzy MRAS is applied to estimate the synchronous speed online, where the traditional PI controller is replaced by the adaptive fuzzy ones. This proposed scheme has no integrator and motor resistances, hence syncronous speed estimation is unaffected by the temperature variations. The proposed scheme was applied on sensorless IM drive with superior speed response. In [124] a high performance speed control of field oriented control (FOC) IM drive

is presented by using ANN and FLC. This MRAS scheme is used to estimate the rotor speed and rotor time constant variations. In the proposed method, FLC is incorporated with the neural controller adaptation in order to improve the robustness of generated command. Back-propagation algorithm is used in ANN controller with fuzzy controller in such a way that the output of the system tracks the reference command in order to get the accurate speed tracking in the presence of motor uncertainties and load.

In several control systems PI based controllers have been applied effectively for error minimization purpose. In [125] FLC has been used as a non-linear optimizer to minimize the speed tuning signal for the rotor speed estimation. In [126] a fuzzy self tuning identifier was proposed for vector control IM drive to estimate the rotor speed. The scheme had the similar structure as the rotor flux based MRAS as mentioned in [75]. The scheme was tested for a step speed command of 500 rpm then 500rpm to 900rpm and back to 500rpm. However, no results of low speed estimation performance was shown. In [127] fuzzy observer was proposed for rotor flux and rotor speed estimation . For the purpose of test sinusoidal reference speed was used. However, motor parameter variations and low speed performance was not presented.

2.9 Conclusion

This chapter has presented a detailed review on machine fundamental model based rotor speed estimation techniques applied for speed sensorless control of IM drive with mainly emphasis on the widely used strategy MRAS. Different issues affecting the dynamic performance of MRAS speed estimator specially at low speed and zero speed region and load disturbance effect on the estimation performance have been discussed in detail. Several proposed ideas and schemes in order to improve the dynamic performance of estimator have also been reviewed. Application of AI and offering key characteristics in the field of variable speed drive with the

application of FLC in sensorless control have also been highlighted. Notwithstanding, much efforts and progress for performance improvement, operation of MRAS sensorless drive at very low speed region and uncertain load disturbance condition are still need to be improved and investigated further.

Chapter 3

Modelling of Vehicle Dynamics, Induction Motor and MRAS Speed Estimator

3.1 Introduction

INDUCTION motor plays an important role not only in different industrial automation processes but also has a great deal of importance in the electrified transport industry due to its simple structure, ruggedness, high efficiency and low cost features. DC motor drives have almost been replaced by the IM electric drive in many high performance applications such as EVs due to the application of advanced control techniques like VC and DTC. Recent research and development in the field of power electronic devices and advanced digital signal processing have provided an economic and efficient way to implement these control techniques. Therefore a good understanding and accurate induction machine model is required to design control algorithms and observer system.

This chapter is divided into four parts. The first part presents the motion dynamics of electric vehicle and different acting forces on the vehicle during the operation.

To understand that how much total tractive force from the traction motor is required to operate the vehicle. The second part presents the mathematical model of induction machine using space vector and two-axis theory. In the third part this model is then utilized to understand the dynamic performance of the machine using vector control method. Finally, rotor speed estimation using rotor flux based MRAS strategy is investigated by using the induction machine model. This section is mainly concerned with the modelling of rotor flux MRAS speed estimator for speed sensorless IM traction drives.

3.2 Motion and Vehicle Dynamics

To determine the required tractive effort is the first step in any vehicle performance modelling. Consider a vehicle with mass M_v moving with velocity V and a slope angle α as shown in Fig 3.1. During the vehicle movement operation, there are some forces acting on a vehicle that try to stop its movement. The vehicle propulsion unit delivers the required force necessary to move the vehicle forward. This force helps the vehicle to overcome the resisting forces due to gravity, air and tire resistance [1, 128]. The acceleration of such vehicle according to the Newton's second law can be expresses as:

$$\frac{dV}{dt} = \frac{\sum F_t - \sum F_{tr}}{\delta M_v} \tag{3.2.1}$$

where δ is the mass factor, that is an effect of rotating components in the vehicle power train. The above equation can further be elaborated as:

$$M_v \frac{dV}{dt} = (F_{tf} + F_{tr}) - (F_{rf} + F_{rr} + F_w + F_g) \tag{3.2.2}$$

A Vehicle accelerates when the total tractive force from both front and rear wheels F_{tf} & F_{tr} respectively is greater than the total acting forces, front and rear wheels rolling resistance F_{rf} & F_{rr}, aerodynamic dragging resistance F_w and grading resistance F_g.

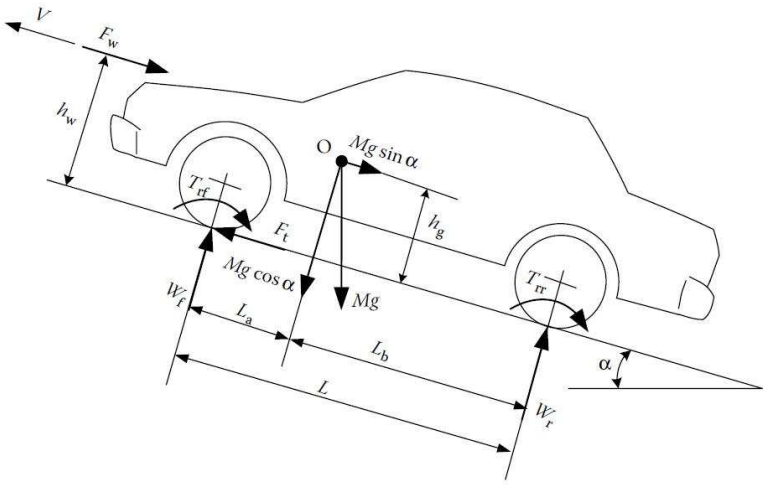

Figure 3.1: Acting forces on a vehicle moving along a slope surface [1]

Rolling resistance also called rolling drag or rolling friction, is the motion resisting force when the vehicle wheel rolls on the surface. Total rolling resistance F_r is mainly due to the friction between vehicle tyre and road surface and can be written as:

$$F_r = P f_r \cos\alpha \tag{3.2.3}$$

Rolling resistance coefficient f_r is the function of tyre type, structure, temperature, pressure and road condition. Typical value of f_r is about 0.005 for tyres developed especially for EVs. However, P is the normal load acting on the centre of the rolling wheel. In vehicle performance calculation, usually rolling resistance coefficient is considered a linear function of vehicle speed.

Aerodynamic drag force is due to the friction between vehicle body and air. The main causes of aerodynamic drag are shape drag and skin effect. The forward motion of the vehicle has two different air pressure zones. The high air pressure zone that is the front area of the vehicle and second the air zone behind the vehicle which can not be filled instantaneously left by the vehicle forward motion is low air pressure zone. Due to these two zones of pressures, the resulting force on the vehicle which opposes the motion is shape drag. Aerodynamic drag force is a function of air

density ρ, frontal area A_f, vehicle velocity V, wind speed V_w and can be expressed as:

$$F_w = \frac{1}{2}\rho A_f C_D (V + V_w)^2 \tag{3.2.4}$$

The drag coefficient C_D depends on the shape of the vehicle and can be reduced by good vehicle design. V_w is the direction of wind speed with respect to the vehicles moving direction, which has positive sign when the vehicle moves in the opposite direction and negative sign in case of the same direction movement.

Finally, the hill climbing force produced by its weight that always directed downwards and can be written as:

$$F_g = M_v g \sin\alpha \tag{3.2.5}$$

Vehicle total tractive effort in case of four wheel drive is

$$F_t = F_{tf} + F_{tr} \tag{3.2.6}$$

Required maximum tractive force for the rear-wheel and front wheel driven vehicle is respectively

$$F_{t_{\max}} = \frac{\mu M_v g \cos\alpha [L_a + f_r(h_g - r_d)]}{L + \mu h_g} \tag{3.2.7}$$

$$F_{t_{\max}} = \frac{\mu M_v g \cos\alpha [L_b + f_r(h_g - r_d)]}{L + \mu h_g} \tag{3.2.8}$$

Where μ is the coefficient of road adhesion also known as frictional coefficient and r_d is effective radius of tire. For the vehicle stable operation, the maximum tractive force transferred from the vehicle power plant to driven wheels should not exceed this value otherwise wheels will spin and cause to vehicle instability [1].

Through the gearbox and drive train of the vehicle, the reference speed and load torque on motor can be transferred from the vehicle side as

$$\omega_r^* = \frac{30 i_g i_o V_{ref}}{\pi r_d} \tag{3.2.9}$$

$$T_l = \frac{r_d}{i_g i_o \eta_t} (F_r + F_w + M_v g \sin\alpha) \tag{3.2.10}$$

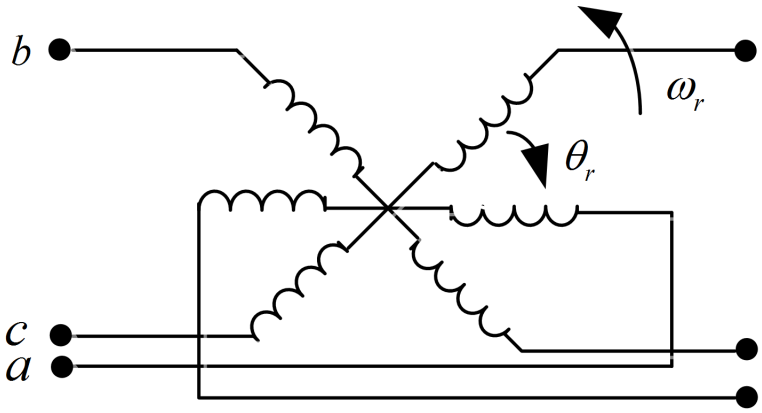

Figure 3.2: Coupling effect in the three phase stator and rotor windings of motor

where V_{ref} is the reference speed of vehicle given by driver, i_g & i_o are the gear ratios of transmission and final drive, r_d is effective radius of tire, η_t is the efficiency of the final drive line and T_l load torque.

3.3 Dynamic Modelling of the Induction Motor

Under steady state operating conditions, IM equivalent circuit model is used to determine the motor quantities such as motor torque, stator current and power factor while running from the balanced sinusoidal supply. But in order to analyze the transient as well as steady state performance of the machine with any type of supply, a dynamic model of machine is defined based on two axis theory. In this analysis machine three phase variables are described by an equivalent two phase phase representation which simplifies the machine equations. In the dynamic machine model or $d-q$ model, electrical variables can be chosen such as fluxes, currents and combination of both [24].

The high performance electric motor control, such as vector control or field oriented control is based on machine (d, q) model. Therefore, a good understanding of the machine (d, q) model is very important to understand such methods. The dy-

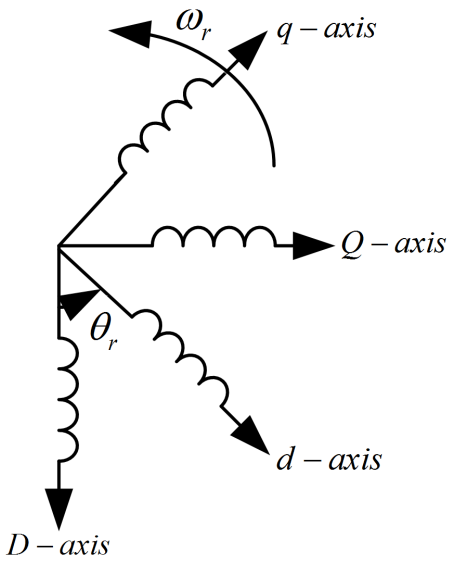

Figure 3.3: Equivalent two phase (d, q) machine model

namic performance of the AC machines are somewhat complex since the three phase of the rotor windings rotate with respect to the three phase of the stator windings as shown in Fig. 3.2. It represents like a transformer with rotating secondary windings, where a coupling coefficient between the three phase stator and rotor windings continually changes when the rotor position angle θ_r changes. Motor model described by a set of different equation with time varying mutual inductances is considered a complex model. A three phase machine model can be represented by its equivalent two phase model as shown in Fig. 3.3, where D and Q represent the stator direct and quadrature axes, while d and q represent the rotor or rotating direct and quadrature axes.

3.3.1 Coordinate Transformation

Consider a symmetrical three phase induction motor with the stationary as, bs and cs axes that are 120^0 angle apart to each other as shown in Fig. 3.4. The aim of these axes transformation is to transform the three phase stationary reference frame

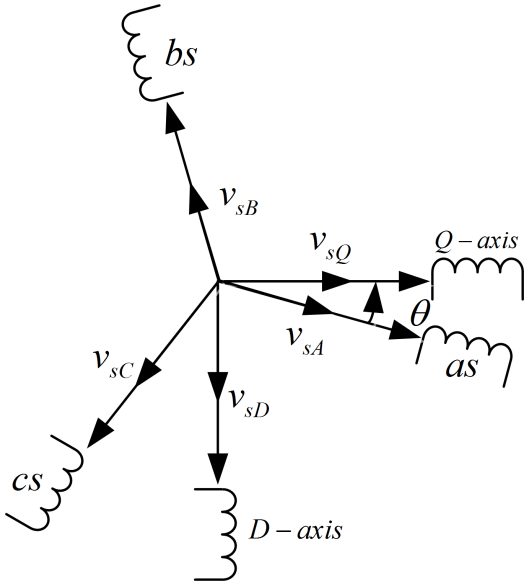

Figure 3.4: Stationary frame (as, bs, cs) to (D, Q) stationary axes transformation

variables (as, bs, cs) into two phase stationary reference frame (D, Q) variables and then transform to synchronously rotating reference frame (d, q) variables and vice versa. Assume that the stationary reference frame (D, Q) is oriented with the angle θ as shown in Fig. 3.4. The two phase stator voltages defined into the stationary reference frame v_{sD} and v_{sQ} can be resolved into three phase stationary components v_{sA},v_{sB} and v_{sC} and can be represented in the matrix form as:

$$\begin{bmatrix} v_{sA} \\ v_{sB} \\ v_{sC} \end{bmatrix} = \begin{bmatrix} \cos\theta & \sin\theta & 1 \\ \cos(\theta - 120^0) & \sin(\theta - 120^0) & 1 \\ \cos(\theta + 120^0) & \sin(\theta + 120^0) & 1 \end{bmatrix} \begin{bmatrix} v_{sQ} \\ v_{sD} \\ v_{s0} \end{bmatrix} \tag{3.3.1}$$

The corresponding inverse relation from three phase stationary v_{sA},v_{sB} and v_{sC} to two phase stationary v_{sD} and v_{sQ} can be expressed as:

$$\begin{bmatrix} v_{sQ} \\ v_{sD} \\ v_{s0} \end{bmatrix} = \frac{2}{3} \begin{bmatrix} \cos\theta & \cos(\theta - 120^0) & \cos(\theta + 120^0) \\ \sin & \sin(\theta - 120^0) & \sin(\theta + 120^0) \\ \frac{1}{2} & \frac{1}{2} & \frac{1}{2} \end{bmatrix} \begin{bmatrix} v_{sA} \\ v_{sB} \\ v_{sC} \end{bmatrix} \tag{3.3.2}$$

where v_{s0} is a zero sequence component, which may or may not be present. The current and flux linkages can be transformed in the similar manner. For convenience, to set $\theta = 0$ so that the Q axis is aligned to the as axis. Ignoring the zero sequence component, then the transformation relation between two phase to three phase stationary can be written as:

$$v_{sA} = v_{sQ} \tag{3.3.3}$$

$$v_{sB} = -\frac{1}{2}v_{sQ} - \frac{\sqrt{3}}{2}v_{sD} \tag{3.3.4}$$

$$v_{sC} = -\frac{1}{2}v_{sQ} + \frac{\sqrt{3}}{2}v_{sD} \tag{3.3.5}$$

Inverse relation can be written as:

$$v_{sD} = -\frac{1}{\sqrt{3}}v_{sB} + \frac{1}{\sqrt{3}}v_{sC} \tag{3.3.6}$$

$$v_{sQ} = \frac{2}{3}v_{sA} - \frac{1}{3}v_{sB} - \frac{1}{3}v_{sC} = v_{sA} \tag{3.3.7}$$

Both above v_{sA},v_{sB} and v_{sC} to two phase stationary v_{sD} and v_{sQ} and vice versa transformation can be expressed in matrix form as:

$$\begin{bmatrix} v_{sA} \\ v_{sB} \\ v_{sC} \end{bmatrix} = \begin{bmatrix} 1 & 0 \\ -\frac{1}{2} & -\frac{\sqrt{3}}{2} \\ -\frac{1}{2} & \frac{\sqrt{3}}{2} \end{bmatrix} \begin{bmatrix} v_{sQ} \\ v_{sD} \end{bmatrix} \tag{3.3.8}$$

$$\begin{bmatrix} v_{sQ} \\ v_{sD} \end{bmatrix} = \begin{bmatrix} \frac{2}{3} & -\frac{1}{3} & -\frac{1}{3} \\ 0 & -\frac{1}{\sqrt{3}} & \frac{1}{\sqrt{3}} \end{bmatrix} \begin{bmatrix} v_{sA} \\ v_{sB} \\ v_{sC} \end{bmatrix} \tag{3.3.9}$$

Fig. 3.5 shows the relationship between the synchronously rotating $d-q$ axes, which rotate with the synchronous speed ω_e with respect to the stationary axes $D-Q$ with angle $\theta_e = \omega_e t$. The stator voltages present in the two phase stationary reference frame $D-Q$ to two phase synchronously rotating reference frame $d-q$ can be written as:

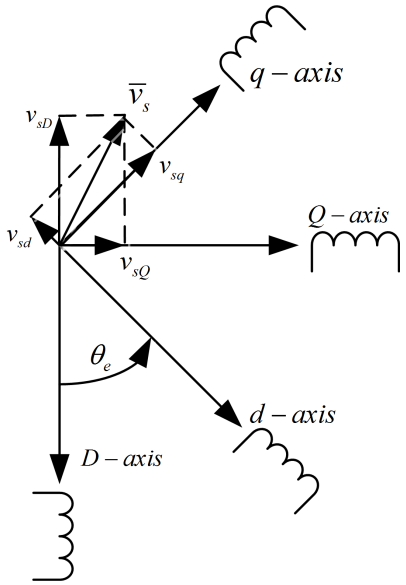

Figure 3.5: Two axes stationary frame (D, Q) to two axes synchronously rotating frame $(d - q)$ transformation

$$v_{sd} = v_{sQ} \sin\theta_e + v_{sD} \cos\theta_e \tag{3.3.10}$$

$$v_{sq} = v_{sQ} \cos\theta_e - v_{sD} \sin\theta_e \tag{3.3.11}$$

In the same way two phase synchronously rotating reference frame $d - q$ to $D - Q$ relation will be

$$v_{sD} = -v_{sq} \sin\theta_e + v_{sd} \cos\theta_e \tag{3.3.12}$$

$$v_{sQ} = v_{sq} \cos\theta_e + v_{sd} \sin\theta_e \tag{3.3.13}$$

The stator space vector $\bar{v_s}$ has corresponding components (v_{sD}, v_{sQ}) defined into the stationary frame whereas components defined into the rotating reference frame are (v_{sd}, v_{sq}). Note that the vector magnitude v_m both are equal in the stationary reference frame and rotating reference frame.

$$|v_m| = \sqrt{(v_{sD})^2 + (v_{sQ})^2} = \sqrt{(v_{sd})^2 + (v_{sq})^2} \tag{3.3.14}$$

3.3.2 Model in a Stationary Reference Frame

In order to drive the expressions for stator and rotor voltage equations, it is assumed that the machine is balanced, the magnetics are linear, sinusoidal mmf in the airgap and the iron and stray losses are neglected [43]. The induction motor model defined in the stationary reference frame can be expressed by the following stator and rotor voltage equations [3]:

$$v_{sD} = R_s i_{sD} + \frac{d\psi_{sD}}{dt} \tag{3.3.15}$$

and stator Q axis voltage component

$$v_{sQ} = R_s i_{sQ} + \frac{d\psi_{sQ}}{dt} \tag{3.3.16}$$

Rotor voltage components in (D, Q) axes will be

$$v_{rD} = 0 = R_r i_{rD} + \frac{d\psi_{rD}}{dt} + \omega_r \psi_{rQ} \tag{3.3.17}$$

$$v_{rQ} = 0 = R_r i_{rQ} + \frac{d\psi_{rQ}}{dt} - \omega_r \psi_{rD} \tag{3.3.18}$$

Both components (D, Q) of rotor voltages are zero in case of squirrel cage type rotor three phase induction motor. In the stationary frame these components will be time varying when the sinusoidal inputs are applied.

The electromagnetic torque equations can also be expressed in the corresponding variables defined in the stationary reference frame as:

$$T_e = \frac{3}{2}\left(\frac{P}{2}\right)(\psi_{sD} i_{sQ} - \psi_{sQ} i_{sD}) \tag{3.3.19}$$

$$T_e = \frac{3}{2}\left(\frac{P}{2}\right) L_m (i_{sQ} i_{rD} - i_{sD} i_{rQ}) \tag{3.3.20}$$

$$T_e = \frac{3}{2}\left(\frac{P}{2}\right)(\psi_{rD} i_{rQ} - \psi_{rQ} i_{rD}) \tag{3.3.21}$$

3.3.3 Model in a Synchronously Rotating Reference Frame

In order to present the induction motor model defined in the synchronously rotating reference, the stator and rotor voltage variables are converted from stationary reference frame $(D-Q)$ to rotating reference frame $(d-q)$. The stator voltage components in $(d-q)$ can be written as [24]:

$$v_{sd} = R_s i_{sd} + \frac{d\psi_{sd}}{dt} - \omega_e \psi_{sq} \tag{3.3.22}$$

$$v_{sq} = R_s i_{sq} + \frac{d\psi_{sq}}{dt} + \omega_e \psi_{sd} \tag{3.3.23}$$

All the variables mentioned in equations (3.3.22) and (3.3.23) are defined in rotating frame. The last term in both equation are speed emf or rotational emf due to the rotation of the axes.

The rotor actually moves at speed ω_r, the $(d-q)$ axes frame fixed on the rotor move at a speed $\omega_e - \omega_r$ relative to the synchronously rotating reference frame. However, the rotor voltage equations can be defined in the rotating reference frame as:

$$v_{rd} = R_r i_{rd} + \frac{d\psi_{rd}}{dt} - (\omega_e - \omega_r)\psi_{rq} \tag{3.3.24}$$

$$v_{rq} = R_r i_{rq} + \frac{d\psi_{rq}}{dt} + (\omega_e - \omega_r)\psi_{rd} \tag{3.3.25}$$

where ω_e is the excitation frequency (i.e the electrical frequency) and ω_r is the rotor mechanical angular speed. The advantage of this model defined in the rotating reference frame that all the sinusoidal variables appear as dc quantities in the synchronous frame. Fig.3.6 shows the dynamic model of IM defined in the rotating reference frame and satisfy the equations (3.3.22),(3.3.23),(3.3.24) and (3.3.25).

The stator, rotor and magnetizing flux linkages in terms of stator and rotor currents cab be written as:

$$\psi_{sq} = L_{ls} i_{sq} + L_m (i_{sq} + i_{rq}) \tag{3.3.26}$$

$$\psi_{rq} = L_{lr} i_{rq} + L_m (i_{sq} + i_{rq}) \tag{3.3.27}$$

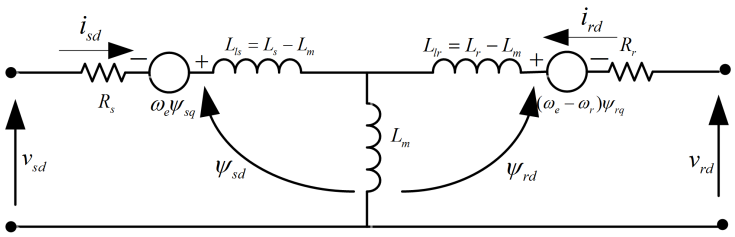

(a)

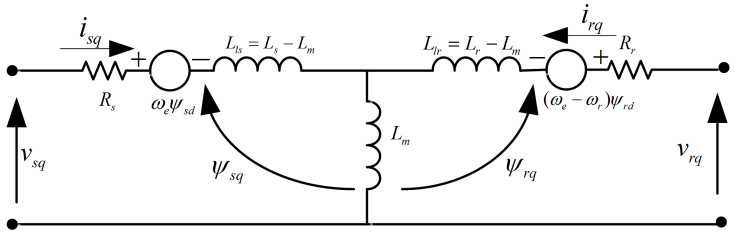

(b)

Figure 3.6: Dynamic machine model equivalent circuit in rotating frame $(d-q)$ 3.6(a) Machine d-axis circuit 3.6(b) Machine q-axis circuit

$$\psi_{mq} = L_m(i_{sq} + i_{rq}) \tag{3.3.28}$$

$$\psi_{sd} = L_{ls}i_{sd} + L_m(i_{sd} + i_{rd}) \tag{3.3.29}$$

$$\psi_{rd} = L_{lr}i_{rd} + L_m(i_{sd} + i_{rd}) \tag{3.3.30}$$

$$\psi_{md} = L_m(i_{sd} + i_{rd}) \tag{3.3.31}$$

Several electromagnetic torque equations can be expressed as:

$$T_e = \frac{3}{2}\left(\frac{P}{2}\right)(\psi_{sd}i_{sq} - \psi_{sq}i_{sd}) \tag{3.3.32}$$

$$T_e = \frac{3}{2}\left(\frac{P}{2}\right)L_m\,(i_{sq}i_{rd} - i_{sd}i_{rq}) \tag{3.3.33}$$

$$T_e = \frac{3}{2}\left(\frac{P}{2}\right)(\psi_{rd}i_{rq} - \psi_{rq}i_{rd}) \tag{3.3.34}$$

$$T_e = \frac{3}{2}P\frac{L_m}{L_r}(\psi_{rd}i_{sq} - \psi_{rq}i_{sd}) \tag{3.3.35}$$

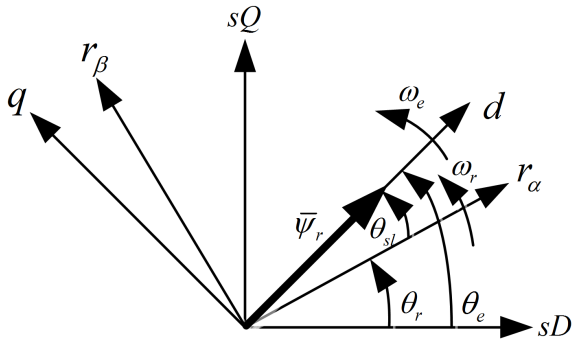

Figure 3.7: Operational principle of rotor flux oriented control

The motor electromagnetic torque T_e related to motor electrical speed ω_r can be written as:

$$T_e = T_l + J\frac{d\omega_{rm}}{dt} = T_l + \frac{2}{P}J\frac{d\omega_r}{dt} \tag{3.3.36}$$

where ω_{rm} rotor mechanical speed, T_l is the load torque, J is the rotor inertia.

3.4 Modelling of Vector Control

The main aim of vector control or field oriented control is to get the same performance from an induction motor similar to that of separately excited dc motor and deals with the motor torque and flux control independently. It is now well established control method in all ac electric motors to provide the performance and control characteristics similar to the armature controlled dc machines [68]. In order to achieve this by orienting the synchronous frame axes in such a way that the d-axis is aligned with the rotor flux space vector $\bar{\psi}_r$ as shown in Fig. 3.7. On the basis of this operation, this control technique is also called rotor flux oriented technique. This flux oriented control scheme can be understood by the mathematical model of the squirrel-cage IM defined in the $(d-q)$ synchronous rotating reference frame. For the purpose of simplification $p = \frac{d}{dt}$ and $\omega_{sl} = (\omega_e - \omega_r)$ are used. IM stator

and rotor voltage equations in synchronous frame can be expressed as:

$$v_{sd} = R_s i_{sd} + p\psi_{sd} - \omega_e \psi_{sq} \tag{3.4.1}$$

$$v_{sq} = R_s i_{sq} + p\psi_{sq} + \omega_e \psi_{sd} \tag{3.4.2}$$

$$0 = R_r i_{rd} + p\psi_{rd} - \omega_{sl} \psi_{rq} \tag{3.4.3}$$

$$0 = R_r i_{rq} + p\psi_{rq} + \omega_{sl} \psi_{rd} \tag{3.4.4}$$

where the components of the rotor flux linkages can be written as:

$$\psi_{rd} = L_m i_{sd} + L_r i_{rd} \tag{3.4.5}$$

$$\psi_{rq} = L_m i_{sq} + L_r i_{rq} \tag{3.4.6}$$

In rotor flux oriented condition, rotor flux has only d-axis component and q-axis component becomes zero, since rotor flux space vector $\bar{\psi}_r$ is aligned on the d-axis of the synchronous frame. therefore, the rotor flux components can be expressed as:

$$\begin{aligned} \bar{\psi}_r &= \psi_{rd} \\ \psi_{rq} = 0, p\psi_{rq} &= 0 \end{aligned} \tag{3.4.7}$$

By substituting the rotor flux oriented condition $\psi_{rq} = 0, p\psi_{rq} = 0$ into stator voltage equations (3.4.3) and (3.4.4) and rotor flux linkage equation (3.4.6):

$$R_r i_{rd} + p\psi_{rd} = 0 \tag{3.4.8}$$

$$R_r i_{rq} + \omega_{sl} \psi_{rd} = 0 \tag{3.4.9}$$

$$L_m i_{sq} + L_r i_{rq} = 0 \tag{3.4.10}$$

Rotor current from (3.4.10) can be expressed as:

$$i_{rq} = -\frac{L_m}{L_r} i_{sq} \tag{3.4.11}$$

By substituting (3.4.11) into (3.4.9) then the expression for the slip frequency command ω_{sl} can be written as:

$$\omega_{sl} = \frac{L_m}{T_r \psi_{rd}} i_{sq} \tag{3.4.12}$$

Rotor d axis current component from (3.4.8):

$$i_{rd} = -\frac{1}{R_r} p\psi_{rd} \tag{3.4.13}$$

By substituting the rotor current from (3.4.13) into (3.4.5) will present the rotor flux dynamics as:

$$T_r p\psi_{rd} + \psi_{rd} = L_m i_{sd} \tag{3.4.14}$$

Derivative terms will be zero under steady state condition

$$p\psi_{rd} = 0 \tag{3.4.15}$$

Putting (3.4.15) into (3.4.13) and (3.4.14) yields:

$$i_{rd} = 0 \tag{3.4.16}$$

$$\psi_{rd} = L_m i_{sd} \tag{3.4.17}$$

(3.4.17) shows that the rotor flux can be directly controlled through the d-axis stator current. By substituting (3.4.17) into (3.4.12) in order to get the expression for angular slip frequency ω_{sl}:

$$\omega_{sl} = \omega_e - \omega_r = \frac{1}{T_r}\frac{i_{sq}}{i_{sd}} \tag{3.4.18}$$

This angular slip frequency ω_{sl} can also be calculated from the reference values of both d-axis and q-axis stator components and can be expressed as [24]:

$$\omega_{sl} = \frac{1}{T_r}\frac{i^*_{sq}}{i^*_{sd}} \tag{3.4.19}$$

The slip relation shows that the particular ratio between the q axis stator current to the d axis stator current maintains the FOC for rotor flux orientation [43]. From the Fig. 3.7 rotor flux angle θ_e can be written as:

$$\theta_e = \theta_r + \theta_{sl} \tag{3.4.20}$$

$$\theta_e = \theta_r + \int \frac{1}{T_r}\frac{i^*_{sq}}{i^*_{sd}} dt \tag{3.4.21}$$

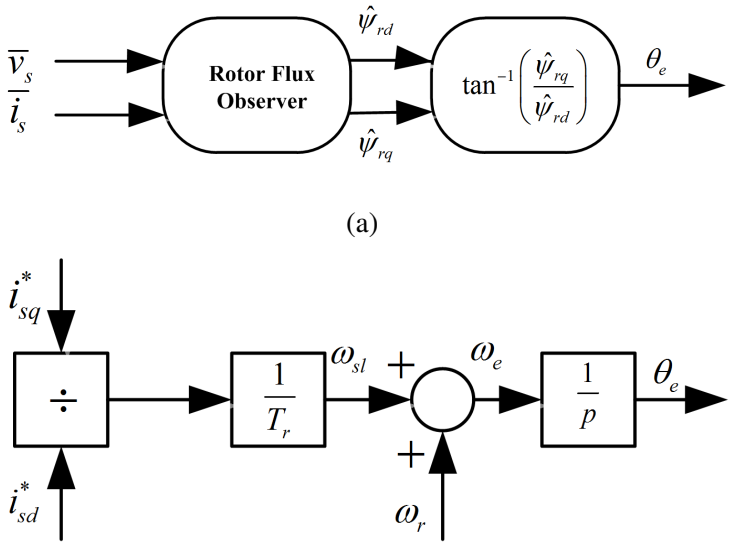

Figure 3.8: Types of rotor flux oriented schemes 3.8(a) Direct rotor flux oriented method 3.8(b) Indirect rotor flux oriented method

Under rotor flux oriented condition the electromagnetic torque expression will represent the analogous of DC machine by substituting (3.4.7) condition into (3.3.35) and can be expressed as:

$$T_e = \frac{3}{2}P\frac{L_m}{L_r}(\psi_{rd}i_{sq}) \tag{3.4.22}$$

It can be simplified to the dc machine torque expression as:

$$T_e = K_T\psi_{rd}i_{sq} \tag{3.4.23}$$

where K_T is the torque constant which becomes

$$K_T = \frac{3}{2}P\frac{L_m}{L_r} \tag{3.4.24}$$

Both equations (3.4.17) and (3.4.23) are similar to the separately excited DC machine in which both stator current components i_{sd} and i_{sq} are the analogous of field current and armature current respectively. Under FOC the IM control is completely decoupled in which both the d axis and q axis interactions are eliminated. Machine flux and torque can be controlled separately by independent controlling of the d-axis

and q-axis stator current space vectors in the synchronous frame respectively. In order to achieve fast and quick machine torque, usually rotor flux is kept constant by a constant value of i_{sd} and machine torque is controlled directly by adjusting the i_{sq} value.

Better performance of the vector control method depends on the accurate knowledge of the rotor flux angle θ_e that is used for the transformation. This is the angle that represents the rotor flux space vector $\bar{\psi}_r$ position with respect to the D-axis stationary reference frame. There are two main methods to determine this rotor flux angle: Direct and indirect method.

Direct vector control method relies on the direct measurement of the rotor flux position as shown in Fig. 3.8(a). In the past it was measured by fixing flux sensors in the air gap such as search coils and Hall-effect sensors. Presently, flux observers or estimators are used for this purpose in which the rotor flux position is estimated through the monitored stator current and voltages.

In the indirect field oriented method, by means of machine mathematical model slip ω_{sl} is calculated and then rotor position is added to determine the rotor flux position θ_e as shown in Fig. 3.8(b). This method is more preferred than the direct because it is simple and does not need any flux sensor or flux observer. However, this method is highly sensitive to the rotor time constant T_r variations which may contribute to reduce the dynamic performance of IM drive. The Block diagram of indirect vector control is illustrated in Fig. 3.9.

3.5 Rotor Flux MRAS Modelling for Speed Estimation

The model reference adaptive system based speed estimation strategies are the most successful in adaptive control due to simplicity and less computational efforts. The design of rotor flux linkage based MRAS speed estimator for the IM drives com-

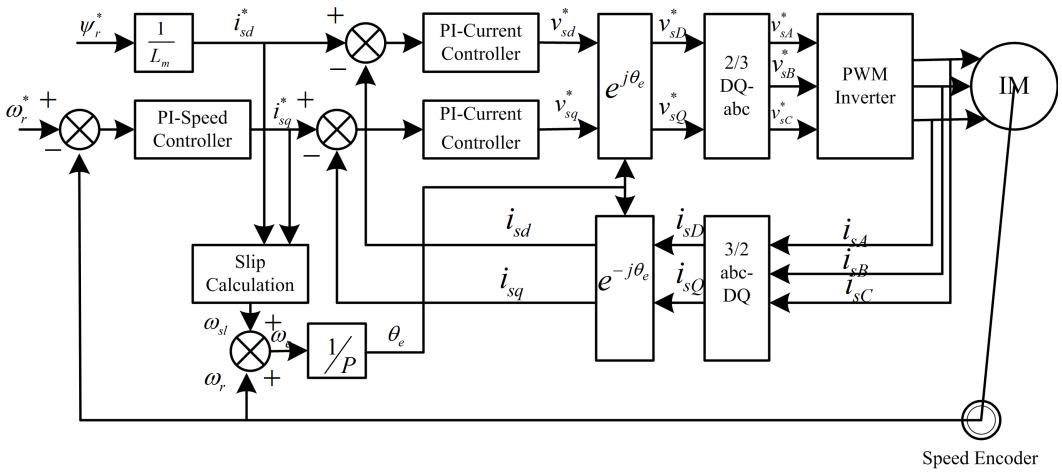

Figure 3.9: Block diagram of indirect vector control of induction motor drive

prises of two independent rotor flux estimator models. The first model is known as a reference model (voltage model), which is independent of rotor speed. whereas, the second model is adaptive or adjustable model (current model), which is rotor speed dependent. The reference values of the rotor flux (ψ_{rD}, ψ_{rQ}) are compared with the estimated rotor flux values $(\hat{\psi}_{rD}, \hat{\psi}_{rQ})$ as shown in Fig. 3.10. The speed tuning signal ε_ω is fed to the PI-controller to estimate the rotor speed $\hat{\omega}_r$ which is used to adjust the adaptive model. This process continues till the generated error from the both models becomes zero [24]. The following section presents the modeling of rotor flux based MRAS speed estimator using the $d-q$ model of induction machine.

3.5.1 Reference Model

In the reference or voltage model, machine terminal voltage or current are sensed in order to calculate the reference values of rotor flux. The stator voltage equation defined into the stator reference frame can be expressed as:

$$v_s^s = R_s i_s^s + \frac{d\psi_s^s}{dt} \tag{3.5.1}$$

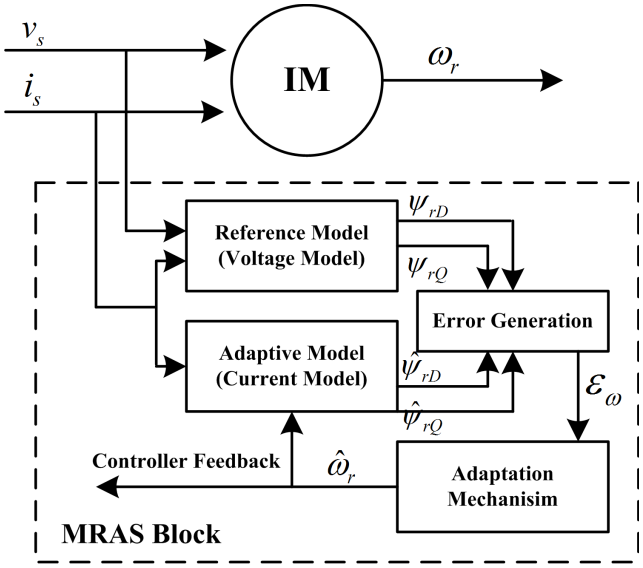

Figure 3.10: Block diagram of rotor flux based MRAS speed estimator for IM drive

Superscript s indicates that the variables are defined into the stator reference frame. The above (3.5.1) stator voltage equation can be written in $(D-Q)$ components:

$$\begin{aligned} v_{sD} &= R_s i_{sD} + \tfrac{d\psi_{sD}}{dt} \\ v_{sQ} &= R_s i_{sQ} + \tfrac{d\psi_{sQ}}{dt} \end{aligned} \tag{3.5.2}$$

The $(D-Q)$ components of the stator flux linkages can be expressed as:

$$\begin{aligned} \psi_{sD} &= L_s i_{sD} + L_m i_{rD} \\ \psi_{sQ} &= L_s i_{sQ} + L_m i_{rQ} \end{aligned} \tag{3.5.3}$$

In the same way the $(D-Q)$ components of the rotor flux linkages can be expressed as:

$$\begin{aligned} \psi_{rD} &= L_r i_{rD} + L_m i_{sD} \\ \psi_{rQ} &= L_r i_{rQ} + L_m i_{sQ} \end{aligned} \tag{3.5.4}$$

By substituting the $(D-Q)$ components of the stator flux linkages (3.5.3) into the (3.5.2), the expressions for the $(D-Q)$ components of the stator voltage will be:

$$\begin{aligned} v_{sD} &= R_s i_{sD} + L_s p i_{sD} + L_m p i_{rD} \\ v_{sQ} &= R_s i_{sQ} + L_s p i_{sQ} + L_m p i_{rQ} \end{aligned} \tag{3.5.5}$$

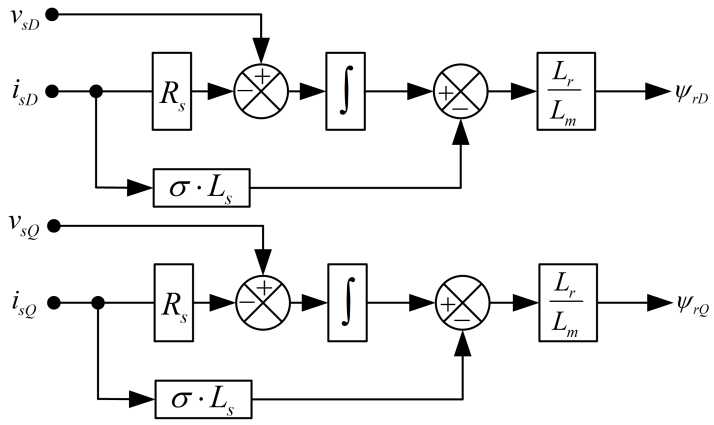

Figure 3.11: Rotor flux linkage (ψ_{rD}, ψ_{rQ}) estimator based on IM's voltage model

Here p indicates the differential operator. By substituting the $(D-Q)$ components of rotor current from (3.5.4) into the (3.5.5), the voltage expression can be written as:

$$\begin{aligned} v_{sD} &= R_s i_{sD} + \sigma L_s p i_{sD} + \tfrac{L_m}{L_r} p\psi_{rD} \\ v_{sQ} &= R_s i_{sQ} + \sigma L_s p i_{sQ} + \tfrac{L_m}{L_r} p\psi_{rQ} \end{aligned} \tag{3.5.6}$$

where σ is a leakage coefficient of inductances

$$\sigma = 1 - \frac{L_m^2}{L_s L_r}$$

The reference model can be formulated by rearranging the (3.5.6) to generate the reference rotor flux components. Fig. 3.11 shows the rotor flux linkage which is normally expressed by the VM that represents the voltage equations. The reference rotor flux components can be obtained from the monitored stator voltage and current and can be expressed by using $(D-Q)$ representation as [24, 75]:

$$\begin{aligned} p\psi_{rD} &= \tfrac{L_r}{L_m}\left(v_{sD} - R_s i_{sD} - \sigma L_s p i_{sD}\right) \\ p\psi_{rQ} &= \tfrac{L_r}{L_m}\left(v_{sQ} - R_s i_{sQ} - \sigma L_s p i_{sQ}\right) \end{aligned} \tag{3.5.7}$$

3.5.2 Adaptive or Adjustable Model

The adaptive model is usually expressed by the current model where the rotor voltage equation presents in terms of rotor speed and rotor current defined into the stator reference frame as:

$$v_r^s = R_r i_r^s + \frac{d\psi_r^s}{dt} - j\omega_r \psi_r^s \tag{3.5.8}$$

The rotor voltage equation (3.5.8) can be written in $(D-Q)$ components as:

$$\begin{aligned} v_{rD} &= R_r i_{rD} + \tfrac{d\psi_{rD}}{dt} + \omega_r \psi_{rQ} \\ v_{rQ} &= R_r i_{rQ} + \tfrac{d\psi_{rQ}}{dt} - \omega_r \psi_{rD} \end{aligned} \tag{3.5.9}$$

By substituting the $(D-Q)$ rotor flux components from (3.5.4) into the (3.5.9), the rotor voltage can be written in the same coordinate as:

$$\begin{aligned} 0 &= \tfrac{1}{T_r}\psi_{rD} - \tfrac{L_m}{T_r} i_{sD} + p\psi_{rD} + \omega_r \psi_{rQ} \\ 0 &= \tfrac{1}{T_r}\psi_{rQ} - \tfrac{L_m}{T_r} i_{sQ} + p\psi_{rQ} - \omega_r \psi_{rD} \end{aligned} \tag{3.5.10}$$

The estimated rotor flux components expressed in terms of stator current and estimated rotor speed $\hat{\omega}_r$ can be written from (3.5.10) as [24, 75]:

$$\begin{aligned} p\hat{\psi}_{rD} &= \tfrac{L_m}{T_r} i_{sD} - \tfrac{1}{T_r}\hat{\psi}_{rD} - \hat{\omega}_r \hat{\psi}_{rQ} \\ p\hat{\psi}_{rQ} &= \tfrac{L_m}{T_r} i_{sQ} - \tfrac{1}{T_r}\hat{\psi}_{rQ} + \hat{\omega}_r \hat{\psi}_{rD} \end{aligned} \tag{3.5.11}$$

where $T_r = \frac{L_r}{R_r}$ is rotor time constant. This model can provide the estimated rotor flux only from the stator currents (i_{sD}, i_{sQ}) components if only the speed signal is available. These equations are defined as a current model in the rotor flux linkage estimation process, which was originally formulated by $Blaschke$ and also called the $Blaschke$ equation [3]. Fig. 3.12 shows the rotor flux estimator based on the IM's current model of MRAS. If the estimated speed signal is correct, then the both flux values from the reference model (ψ_{rD}, ψ_{rQ}) should be equal to the flux values from the adaptive model $(\hat{\psi}_{rD}, \hat{\psi}_{rQ})$, that is $\psi_{rD} = \hat{\psi}_{rD}$ and $\psi_{rQ} = \hat{\psi}_{rQ}$. In order to tune the speed $\hat{\omega}_r$ an adaptation mechanism is used with a PI-controller which tries to make the speed tuning signal to zero [3].

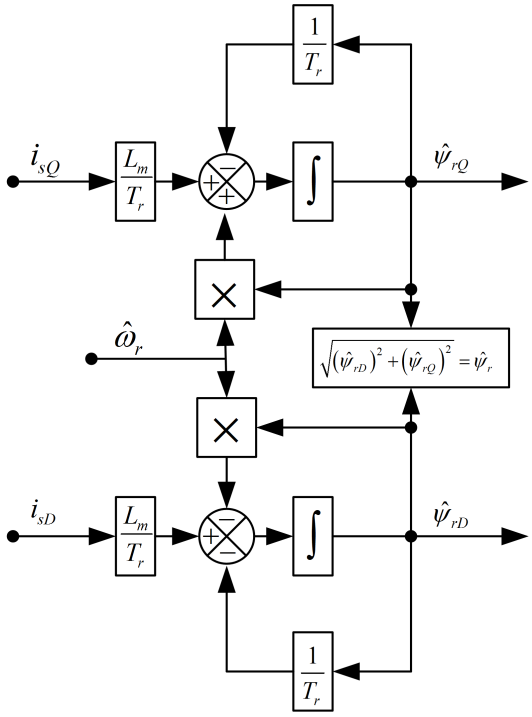

Figure 3.12: Rotor flux linkage $(\hat{\psi}_{rD}, \hat{\psi}_{rQ})$ estimator based on IM's current model

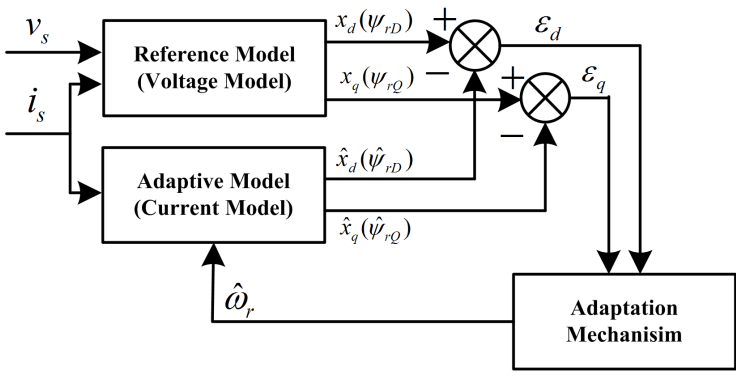

Figure 3.13: Rotor speed estimation by using rotor flux linkage based MRAS

Flux estimation through this model requires the speed encoder, but the advantage is that the driver operation can be extended down to zero speed. However, the performance of the driver is affected by the machine parameter variations. In particular, the variation in rotor resistance, which may be more than 50% and becomes dominant by the temperature variation. Compensation of this parameter is difficult since it is not accessible. The voltage model flux-linkage estimation is better at high speed region while the current model estimation can be made at any speed [3, 24].

3.5.3 Speed Adaptation Mechanism

The state variables estimated in the rotor flux based MRAS are (ψ_{rD}, ψ_{rQ}) components from the reference model and $(\hat{\psi}_{rD}, \hat{\psi}_{rQ})$ from the adaptive or adjustable model based on the motor's current model. In the MRAS based estimator, rotor speed is estimated on the difference between the state variables from the reference model and adaptive model, where the difference is essentially the error. This error is fed to the appropriate adaptation mechanism to generate the estimated speed and adjust the adaptive model until the generated error becomes to zero. Fig. 3.13 shows the block diagram of rotor flux linkage based MRAS speed estimation.

In order to design an appropriate adaptation mechanism for MRAS, hypersta-

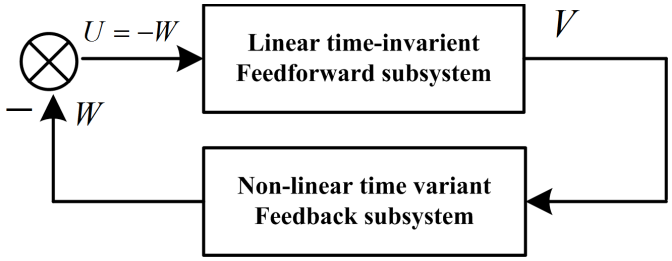

Figure 3.14: Equivalent of a nonlinear feedback system

bility theory is one of the main approaches employed for this purpose. The MRAS speed estimator can be represented by a nonlinear feedback system comprising on two different blocks one linear time invariant feedforward and nonlinear time variant feedback subsystem as shown in Fig. 3.14 [24]. The input of the linear feedforward subsystem is U, which contains the stator current and voltages while the output is V which is the speed tuning signal or generalized error and can be represented here $V = [\varepsilon_d, \varepsilon_q]^T$. The output of the nonlinear time variant feedback subsystem is W and $W = -U$. The MRAS adaptation mechanism is designed based on Popov's hyperstability theory in which the transfer function matrix of the linear feedforward subsystems must be strictly positive real and the nonlinear time variant feedback subsystem satisfies the popov's integral in equality $\int V^T W dt \geq 0, \forall t \geq 0$ [75]. Detailed description of hyperstability is quite complicated and beyond the scope of this work. The detailed procedure of MRAS design using hyperstability can be found in $Landau$ [71]. However, a brief description of adaptation mechanism is presented in the following section.

The MRAS adaptation mechanism design using this concept ensures the overall stability of the system and convergence of the estimated speed to the desired value with suitable dynamics [75]. In order to obtain the adaptation mechanism the transfer function $F(S)$ of the linear time invariant feedforward subsystem must be obtained. One proof uses the state variable error equation $\frac{dV}{dt} = AV - W$, which may be obtained by subtracting the state variable equation of adjustable model (ro-

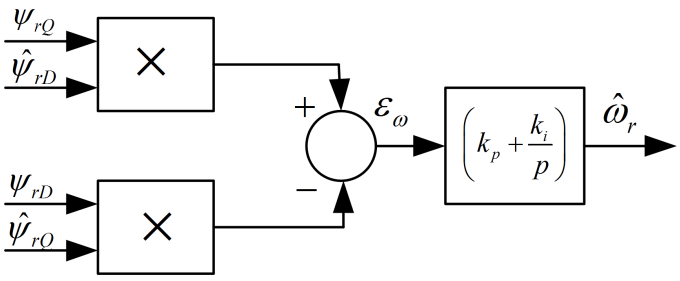

Figure 3.15: Adaptation mechanism for rotor flux based MRAS speed estimator

tor model) from the state variable equation of the reference model (stator model). Both stator and rotor models are the stator and rotor voltage equations defined into the stationary reference frame in two-axis components. The transfer matrix of the linear time invariant feedforward path subsystem is $F(s) = [sI - A]^{-1}$ where I is the identity matrix and A is the state matrix and can be expressed as:

$$A = \begin{bmatrix} -\frac{1}{T_r} & -\omega_r \\ \omega_r & -\frac{1}{T_r} \end{bmatrix}$$

It follows from the derivation of the error state equation that $W = [\hat{\omega}_r - \omega_r]\,[-\hat{x}_q \hat{x}_d]^T$ where $(\hat{x}_d, \hat{x}_q)$ are the estimated states from the adaptive model. Therefore, the W is substituted into the popov's integral inequality and it can be shown that the inequality can be satisfied by letting $\hat{\omega}_r = \left(k_p + \frac{k_i}{p}\right)\varepsilon_\omega$ with appropriate speed tuning signal that is $\varepsilon_\omega = \psi_{rQ}\hat{\psi}_{rD} - \psi_{rD}\hat{\psi}_{rQ}$ for rotor flux based MRAS. Here, $\frac{1}{p}$ is the integrator. The speed tuning signal is minimized by the PI-controller which generates the estimated rotor speed as shown in Fig. 3.15. If the rotor speed is changed in the adaptive model in such a way that the difference between both the reference model and adaptive model is zero then the estimated rotor speed is equal to the actual motor speed. The speed tuning signal actuates the rotor speed estimation algorithm and PI controller makes this error converge to zero.

3.6 Conclusion

This chapter has presented the motion and vehicle dynamic modelling, which provides the understanding of different acting forces on the vehicle during the operation and required tractive force from the traction motor to operate the vehicle. Coordinate transformations from three phase to two phase and between different reference frames have also been discussed. Induction machine dynamic model in stationary and synchronously rotating reference frame has been presented by using two axis theory. The machine model equations in the synchronous reference frame are used to explain the operational principle of vector control of IM drive. Finally, rotor speed estimation for speed sensorless traction drive control of IM using MRAS strategy has been presented. Design of reference model, adaptive model and adaptation mechanism of rotor flux based MRAS by using machine equations have been presented.

Chapter 4

Sensorless Induction Motor Drive Control Using Fuzzy Logic based Speed Observer

4.1 Introduction

APPLICATION of Fuzzy logic control (FLC) has shown fast growth and different developments in the past two decades. FLC has been successfully applied in different fields of industrial control applications in order to solve the problem of control, estimation, identification and optimization issues. Different FLC techniques have also been applied successfully in the filed of IM drive control to solve the problem of optimization. However, there are more other applications of FLC, where it has been applied due to simple and rapid implementation and operational performance improvements. Different applications and proven advantages of using FLC in industrial sector as well as in domestic applications have shown the revolution in this field and believed to be continued.

FLC strategies have been adopted in variable speed drive including IM drive control for system performance improvements. Replacement of conventional speed

or position controller by FL system for performance improvement is not the only task but FL system has also been applied for different tasks in variable speed drive control. One of the major advantages in FLC applications is saving the development and implementation times, since in FL system there is no explicit need for finding and developing a suitable mathematical model as required in classical controllers [45].

PI based controllers are hugely used in different industrial control system applications. Its simple structure can produce a satisfactory performance over a wide range of operation. Therefore, most of the adaptation mechanism in MRAS speed observer already discussed in the literature are based on fixed gain linear PI controller to generate the estimated speed. However, during the motor operation, continuous change in motor parameters due to temperature variations, uncertain load disturbances, and further non-linearities presented in the inverter, PI-based controller may not be able to produce the required satisfactory performance [129]. In order to avoid such problems, adaptive control strategies are applied to enhance the performance of controller where PI gains are varied with the current operating conditions. Researchers more attention need to be required to study other types of observer adaptation mechanism to minimize the speed tuning signal and to improve the speed estimation performance.

This chapter presents a novel rotor flux based FLC-MRAS speed observer. This proposed speed observer uses two differences at the same time, the first difference is in between reference and estimated rotor fluxes as already mentioned in the conventional rotor flux MRAS and second is in between reference and estimated electromagnetic torques. In the proposed observer, a fixed gain linear PI-controller is replaced by a two inputs and one output Mamdani-type FL controller to minimize the speed tuning signal. However, torque differences are used to enhance the performance of observer under load disturbance condition as well as better speed estimation under transient mode. The proposed rotor flux FLC-MRAS provides better load disturbance rejection capability and improved speed estimation over PI-MRAS ob-

server. The performance of new FLC-MRAS and PI-MRAS observes is compared through the detailed simulation tests. Different speed and load torque profiles are used with respect to the application of EV for the purpose of simulation tests.

4.2 Introduction to Fuzzy Logic System

Fuzzy logic control is another field of artificial intelligence. History of FLC and its different applications are more recent than the expert systems (ES). After the development of boolean logic, ES principles were formulated on the basis of boolean logic theory. It has been emphasised that human thinking does not always follow the yes/no logic. But this thinking is often qualitative, imprecise, uncertain or fuzzy in nature. The concept of fuzzy logic first came in July 1964 and published in 1965 by computer scientist Lofti A. Zadeh (University of California, Berkeley) [3]. In the beginning, fuzzy logic theory had to face many criticism from the professional and scientific community. But gradually (from the 90s) with the support of many researchers across the world, FL has captured the imagination of scientific community and finally emerged entirely a new field of AI.

The application importance of this new theory was due to the fact that advanced control systems are very complicated which makes the relevant mathematics accessible only by experts. Control system needs an accurate model of the process that needs to be controlled. Such models could be deterministic considering the perfect model or stochastic including different system uncertainties and noises. However, system mathematical models are rarely accurate and different uncertainties and nonlinearities often influence the operation of the system. Further it is not always possible to model these all disturbances which influence the behaviour of system. These features make system accurate operation more difficult and an expensive task. In order to avoid these problems, a new theory which does not depend on the mathematical model of the system was needed. In case of FL, system mathematical model is not necessary however an experienced engineers may be able to control the sys-

tem process on the basis of physical characteristic familiarity and their practical experience. FLC provides ability to extract operational knowledge from the experts by means of normal linguistics and support human decision making. In general, the aim of FLC is to set the outputs from the given control inputs in a non-linear system, without using system mathematical model equations but by using the linguistic system operational control rules [45].

FL systems have been applied in many areas of control theory. The main key feature of FLC is that such control offer robustness against system uncertainties and can control the nonlinear system. FL has contributed in the areas where conventional complicated scheme has field such as the contribution in the field of space technology where overcome problems used to considered impossible. In the beginning 1990s, different US companies have started using FL systems in the aerospace industry applications including rotor transmission, servo control, missile warning, automated manufacturing and navigation systems [130]. FL has been successfully applied in system modelling, process control, estimation, identification, software (medical diagnosis and securities), systems (train, cranes, automotive, traffic control and elevator), Consumer products, military science and stock market prediction, etc [3]. However, a lack of design technique is a significant drawback of FLC. Since there is no clear method of controller design.

4.3 Principles of Fuzzy Logic Control

The most commonly applied FLC system is mamdani-type which comprises of the following three main parts: fuzzification, fuzzy infereance system and defuzzification as shown in Fig. 4.1.

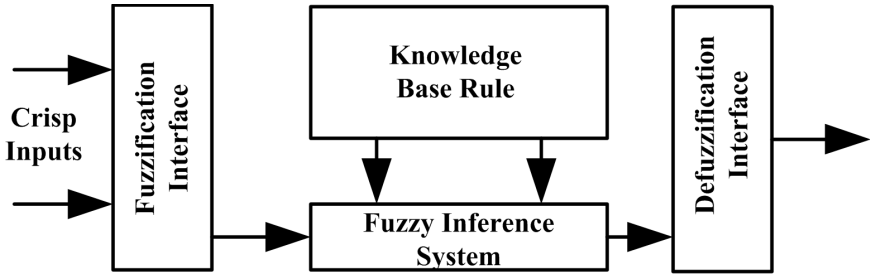

Figure 4.1: Basic block diagram of mamdani-type fuzzy logic control system

4.3.1 Fuzzification

FLC is originally based on the linguistic variables, so the first step in FLC is to map all the input variables into fuzzy sets and to assign membership values for each input to these different sets. This first step is known as fuzzification, where each point from the input space which is also called the universe of discourse, is assigned a membership value μ between zero and one. Zero for no membership and one for full membership of the given input fuzzy set. Fig. 4.2 shows the representation of temperature variation using 4.2(a) fuzzy sets 4.2(b) crisp set for cold, mild and hot by using triangular and straight line membership function respectively. The universe of discourse comprises of different temperature from 20 degrees to 90 degrees Fahrenheit.

Membership function (MF) is a curve that defines the value of μ or degree of membership between 0 and 1 for specific mapped input fuzzy set. The fuzzy sets given in Fig.4.2 can have more subdivision such as very cold, medium cold, medium hot and very hot etc for the more precise information about the input fuzzy variables. For fuzzy sets cold and hot, temperature less 40 and more 80 have MF value 1 whereas more than 40 and less than 80 have MF value less than 1. More coverage of the universe of discourse would include overlapping between the different input fuzzy sets to make more rules for better system controlling.

There are different types of MF; some are smooth such as Gaussian and sigmoid

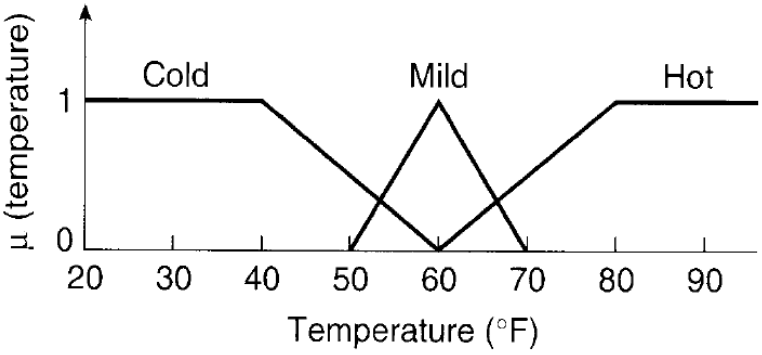

(a)

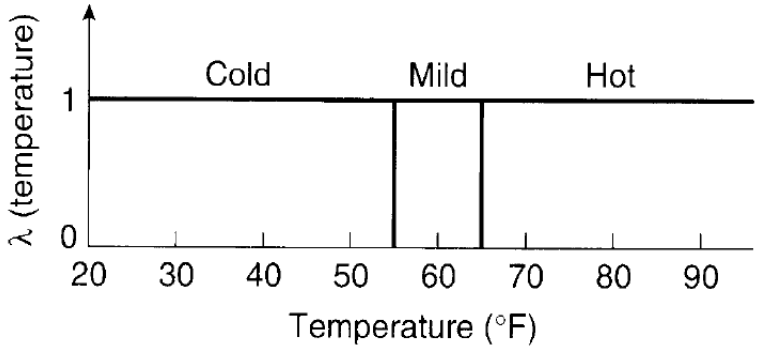

(b)

Figure 4.2: Representation of temperature example using [3] 4.2(a) Fuzzy sets 4.2(b) Classical Crisp sets

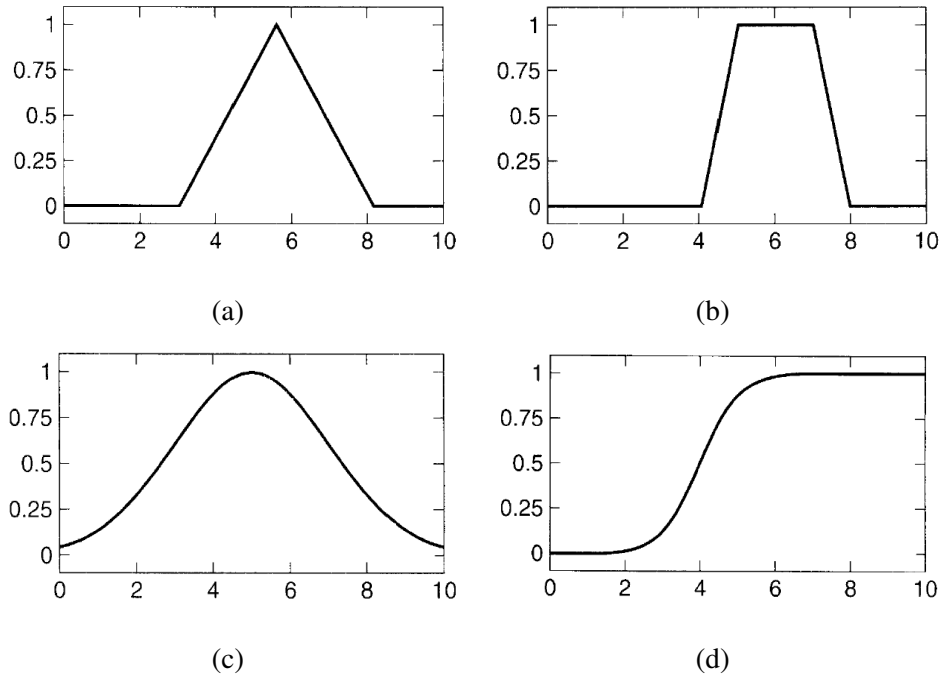

Figure 4.3: Different types of fuzzy membership functions [3] 4.3(a) Triangular function 4.3(b) Trapezoidal function 4.3(c) Gaussian function 4.3(d) Sigmoid function

and others are non-smooth or linear type like triangular and trapezoidal as shown in Fig. 4.3. Some other types of MF are two sided Gaussian, generalized bell, difference sigmoid, product sigmoid, polynomial-Z, polynomial-Pi and polynomial-S. Moreover, apart from these MF, any arbitrary MF can be produced by the expert. The choice of specific shape of MF is not very unique and it depends on the experience of control system designer. However, the most commonly used MF are triangular and trapezoidal due to their linear characteristics and more than enough to solve most of the problems.

4.3.2 Fuzzy Inference System

The main purpose of fuzzy inference system is to connect the fuzzified inputs to the output fuzzy set through defined lingustic rules as shown in Fig. 4.4. This

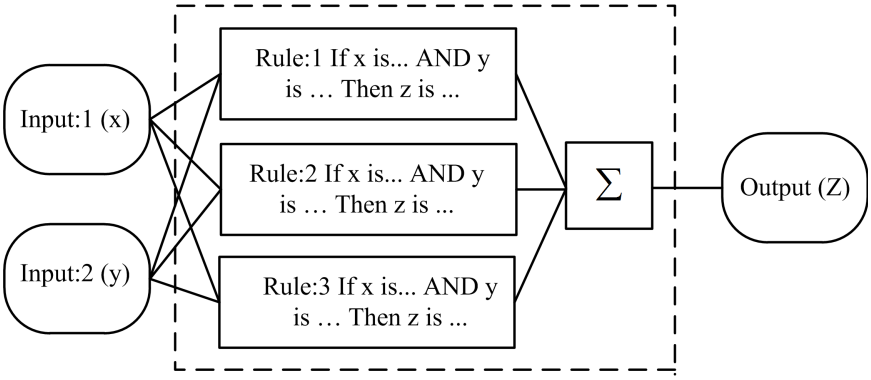

Figure 4.4: Fuzzy inference system with If-Then rule expression for two inputs and one output

mapping process or fuzzy inference process comprises on the five following steps:

- Step:1 To convert the input variables into fuzzy sets or fuzzification
- step:2 Implementation of the fuzzy logic operator such as AND, OR and NOT in the IF antecedent part of the rule
- Step:3 Define antecedent to the conclusion part after THEN expression
- Step:4 Aggregation of the consequents across the rule
- Step:5 Defuzzification

This linguistic rule can be defined by If-Then expression such as if first input fuzzy set (x) is A_i and/or second input fuzzy set (y) is B_i then output fuzzy set (z) is C_i whereas A_i, B_i and C_i are the values of MF of inputs and output respectively. Boolean logic properties are also valid for FLC systems and any logical operation such as OR, AND and NOT can be performed on fuzzy sets (x) and (y) with specific shape of MF.

The union of two fuzzy sets A and B with the universe of discourse X is equivalent to the OR boolean logic operation. The union of $(A \cup B)$ is also a fuzzy set of X universe of discourse with a MF value given as

$$\mu_{(A \cup B)}(x) \equiv \max[\mu_A(x), \mu_B(x)] \tag{4.3.1}$$

The intersection of two fuzzy sets A and B with the universe of discourse X is equivalent to the AND boolean logic operation. The MF value of intersection of $(A \cap B)$ with X universe of discourse can be written as

$$\mu_{(A \cap B)}(x) \equiv \min[\mu_A(x), \mu_B(x)] \tag{4.3.2}$$

The complement or negation of fuzzy set A with a universe of discourse X is equivalent to the NOT operation in boolean logic. The MF value can be represented as

$$\mu_{\bar{A}}(x) \equiv 1 - \mu_A(x) \tag{4.3.3}$$

In the step three of fuzzy inference process is implication of method. There are two main methods, Mamdani type and Sugeno or Takagi-Sugeno Kang method. Mamdani type is the most commonly used method FLC system. The output value of MF in each rule is a singleton spike that multiplies to the respective degree of fulfillment to generate the fuzzy output of each rule. These MFs are further aggregated to produce the total fuzzy output in the system.

4.3.3 Defuzzification

The last step of FLC system or fuzzy inference process is the defuzzification process in which the final fuzzy output after aggregation is transformed back to the real value. The conversion of this fuzzy output to the crisp output is called defuzzification. There are different defuzzification methods such as: maximum, mean of maxima, centre of area or centre of gravity.

Scaling factors are used at the input and output of FLC in order to normalize and de-normalize the controller input and output. These scaling factors can be tuned off-line by using any optimization technique such as genetic algorithms. These parameters can be constant after tuning process during the normal operation of controller. In order to enhance the operational robustness of the system, these parameters can be tunned on-line. In adaptive fuzzy controller, these scaling factors are tuned on-line.

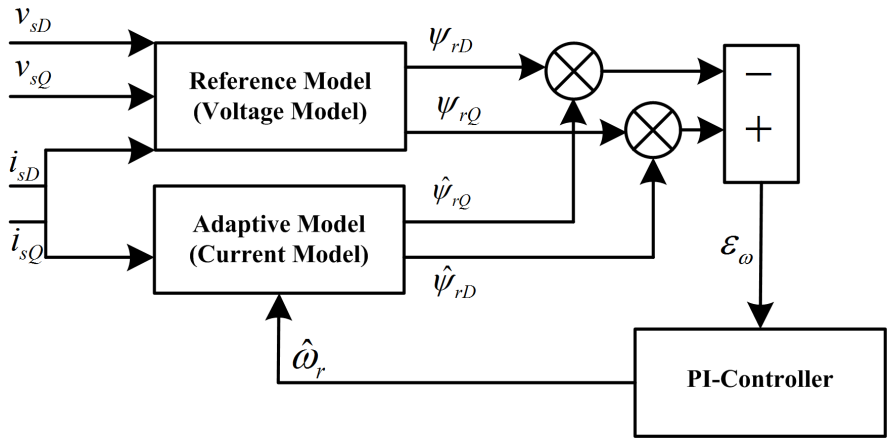

Figure 4.5: Conventional rotor flux PI-controller based MRAS speed estimator

4.4 Proposed Fuzzy Logic based Rotor Flux-MRAS Speed Estimator

In the proposed rotor flux FLC-MRAS speed observer, two differences are used at the same time. The first is between rotor fluxes, which is the difference between reference value of rotor fluxes (ψ_{rD}, ψ_{rQ}) from voltage model and estimated value of rotor fluxes ($\hat{\psi}_{rD}, \hat{\psi}_{rQ}$) from current model as mentioned in Fig.4.5 of conventional PI-controller based rotor flux MRAS observer. In contrast, in the proposed method, at the same time the second difference is carried between reference electromagnetic torque T_e and estimated value of electromagnetic torque $\hat{T}_e$ by means of reference and estimated values of rotor fluxes in order to improve the speed estimation of observer specifically in transient region of operation [131].

The reference value of the rotor flux components expressed in the stationary reference frame are generated from the monitored stator voltage and current components. The reference rotor flux components obtained from the reference or voltage

model can be written as

$$\begin{aligned} p\psi_{rD} &= \frac{L_r}{L_m}\left(v_{sD} - R_s i_{sD} - \sigma L_s p i_{sD}\right) \\ p\psi_{rQ} &= \frac{L_r}{L_m}\left(v_{sQ} - R_s i_{sQ} - \sigma L_s p i_{sQ}\right) \end{aligned} \tag{4.4.1}$$

The adaptive model or adjustable model is usually expressed by the current model where the rotor voltage equation presents in terms of rotor speed and rotor current defined into the stator reference frame. The estimated rotor flux components expressed in terms of stator current and estimated rotor speed ($\hat{\omega_r}$) can be written as

$$\begin{aligned} p\hat{\psi}_{rD} &= \frac{L_m}{T_r} i_{sD} - \frac{1}{T_r}\hat{\psi}_{rD} - \hat{\omega}_r \hat{\psi}_{rQ} \\ p\hat{\psi}_{rQ} &= \frac{L_m}{T_r} i_{sQ} - \frac{1}{T_r}\hat{\psi}_{rQ} + \hat{\omega}_r \hat{\psi}_{rD} \end{aligned} \tag{4.4.2}$$

The adaptation mechanism generates the rotor estimated speed in such a way in order to minimize the error between reference and estimated rotor fluxes. This error or speed tuning signal can be expressed as

$$\varepsilon_\omega = \psi_{rQ}\hat{\psi}_{rD} - \psi_{rD}\hat{\psi}_{rQ} \tag{4.4.3}$$

In the conventional rotor flux MRAS, this error or speed tuning signal is minimized through the PI-controller in order to generate the rotor estimated speed. However, in the proposed method, PI controller is replaced with a fuzzy logic controller to solve the problem of optimization. In MRAS speed observer, the mechanism of the rotor speed estimation is considered as a problem of optimization.

The proposed FLC is a Mamdani-type with two inputs and one output. In two inputs, one is speed tuning signal ε_ω and the second input is the rate of change in speed tuning signal $\Delta\varepsilon_\omega$. This rate of change in speed tuning signal can be expressed as

$$\Delta\varepsilon_\omega(k) = \varepsilon_\omega(k) - \varepsilon_\omega(k-1) \tag{4.4.4}$$

The above expression can be written in the z-domain as

$$\Delta\varepsilon_\omega(z) = \frac{(z-1)}{z}\varepsilon_\omega(z) \tag{4.4.5}$$

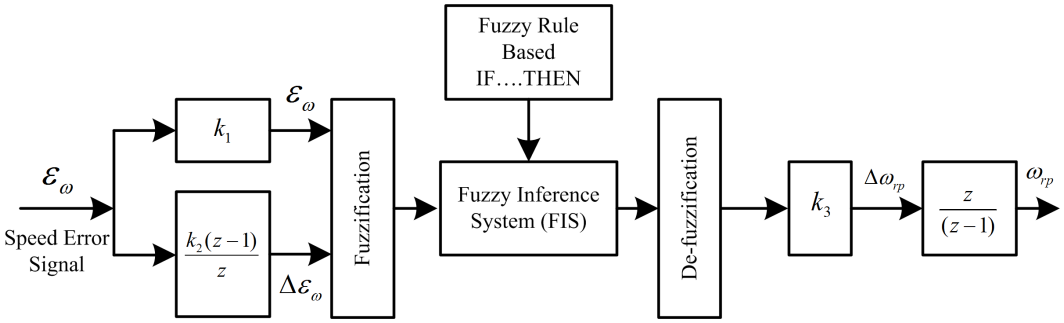

Figure 4.6: Block diagram of fuzzy logic controller for FLC-MRAS

These both inputs error ε_ω and change in error $\Delta\varepsilon_\omega$ are multiplied by two scaling factors k_1 and k_2 respectively. The output of the FL controller after de-fuzification process is further multiplied by a third scaling factor k_3. This third scaling factor is used to generate the rate of change in pre-stage estimated rotor speed $\Delta\omega_{rp}$. In the end, a discrete integration is used to get the value of pre-stage estimated rotor speed ω_{rp}. However, the structure of the implemented FLC controller is shown in Fig.4.6. The pre-stage estimated rotor speed can be written as

$$\omega_{rp}(k) = \omega_{rp}(k-1) + \Delta\omega_{rp}(k) \tag{4.4.6}$$

The z-domain of the above expression can be written as

$$\omega_{rp}(z) = \left(\frac{z}{z-1}\right)\Delta\omega_{rp}(z) \tag{4.4.7}$$

The choice of scaling factors k_1,k_2 and k_3 has huge influence in the performance of FL controller. Here, on the basis of trial and error these scaling factors are tuned for the optimal performance of controller. All variables both inputs and output in the FLC have seven defined membership functions. Each variable has following seven fuzzy sets: NB= Negative Big, NM= Negative Medium, NS= Negative Small, ZE= Zero, PS= Positive Small, PM= Positive Medium, PB= Positive Big. The universe of the discourse is defined between -0.1 and 0.1 with triangular functions as shown in Fig. 4.7. As already discussed before that the choice of specific membership

Table 4.1: Linguistic rule for FLC-MRAS

CHANGE IN ERROR ($\Delta\varepsilon_\omega$)	ERROR (ε_ω)							
		NB	NM	NS	ZE	PS	PM	PB
	NB	NB	NM	NM	NS	NS	NS	ZE
	NM	NM	NM	NS	NS	NS	ZE	PS
	NS	NM	NM	NS	NS	ZE	PS	PM
	ZE	NB	NM	NS	ZE	PS	PM	PM
	PS	NS	NS	ZE	PS	PS	PM	PM
	PM	NS	ZE	PS	PS	PS	PM	PM
	PB	ZE	PS	PS	PM	PM	PB	PB

function is not unique and in most of the cases triangular membership functions can solve the problems so that it is used in the presented FL controller.

Table 4.1 shows the used fuzzy rule base with 49 rules [129]. This FLC is modeled with the help of Matlab Simulink Fuzzy logic tool box. Implementation of this fuzzy logic tool box will be explained in the next section. 3-D surface view shows the relationship that how the variation in input variables effect the output variable. This surface view is shown in Fig. 4.8.

Finally the second loop in which torque differences are used at the same time to improve the speed estimation performance of observer. According to the motor motion equation

$$T_e - T_l = J\frac{d\omega_r}{dt} + f\omega_r \tag{4.4.8}$$

The electromagnetic torque can be expressed as

$$T_e = \frac{PL_m}{L_r}(i_{sQ}\psi_{rD} - i_{sD}\psi_{rQ}) \tag{4.4.9}$$

In case of unknown load torque and viscous coefficient f then (4.4.8) can be written as

$$T_e - T = J\frac{d\omega_r}{dt} \tag{4.4.10}$$

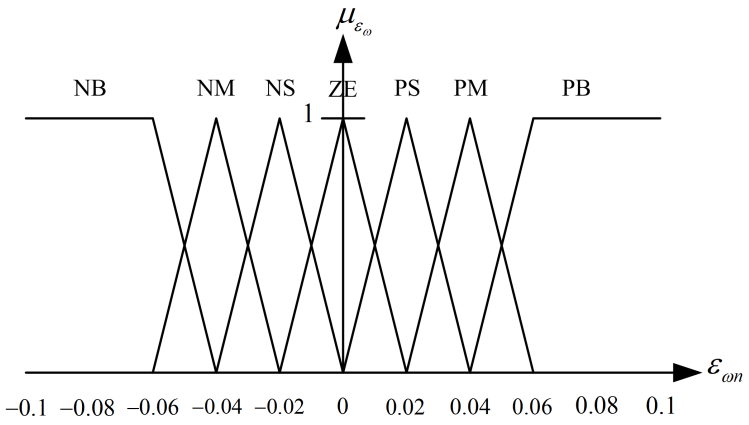

(a)

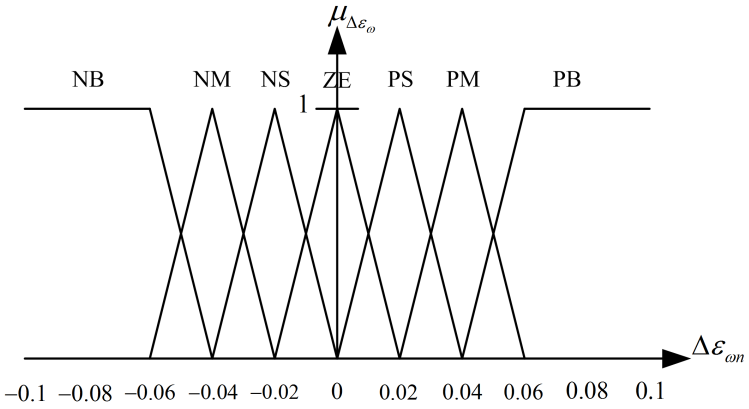

(b)

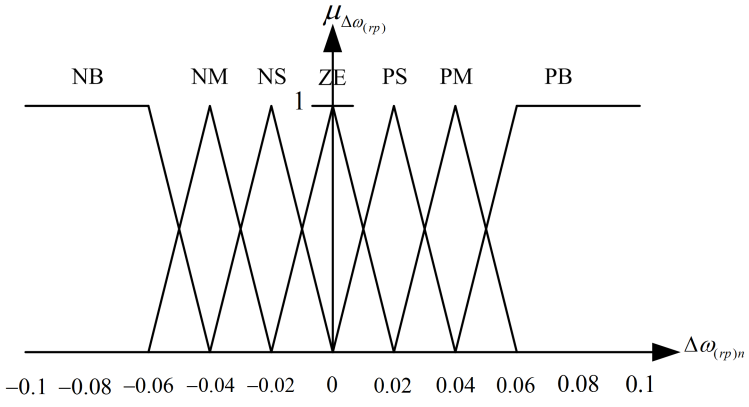

(c)

Figure 4.7: Fuzzy logic controller input and output membership functions 4.7(a) Membership function for error ε_ω 4.7(b) Membership function for change in error $\Delta\varepsilon_\omega$ 4.7(c) Membership function for FL controller output variable $\Delta\omega_{rp}$

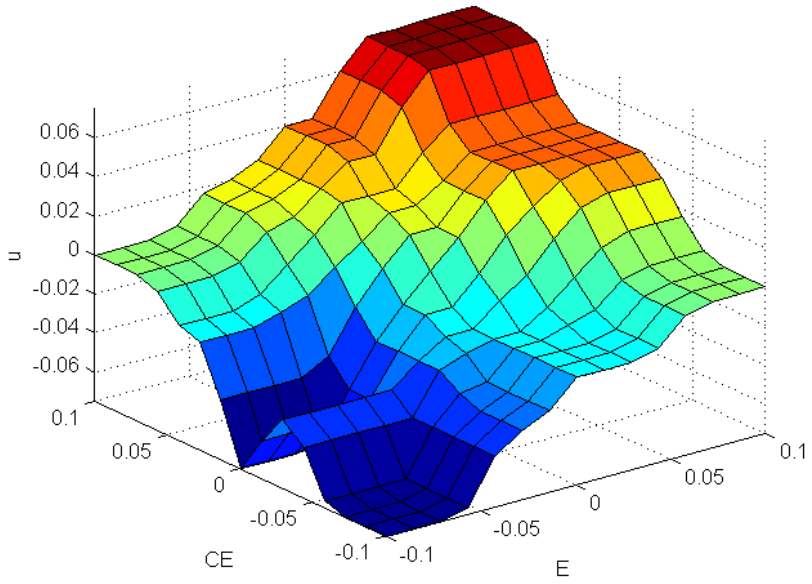

Figure 4.8: 3-D Surface view of FL controller

where, $T = T_l + f\omega_r$

With the help of reference fluxes (ψ_{rD}, ψ_{rQ}), the reference electromagnetic torque can be written as

$$T_e = \frac{PL_m}{L_r}(i_{sQ}\psi_{rD} - i_{sD}\psi_{rQ}) \tag{4.4.11}$$

The estimated electromagnetic torque can be written with the help of estimated rotor fluxes ($\hat{\psi}_{rD}, \hat{\psi}_{rQ}$)

$$\hat{T}_e = \frac{PL_m}{L_r}(i_{sQ}\hat{\psi}_{rD} - i_{sD}\hat{\psi}_{rQ}) \tag{4.4.12}$$

It is well understood that the motion expression in (4.4.8) explains the mechanical dynamics part of the motor. This equations reveals that the variation in a load torque results in the variation of motor speed and this change will continue until the steady state condition appears or electromagnetic torque becomes equal to the load torque.

On the basis of same principle, a variation in an estimated torque results in the

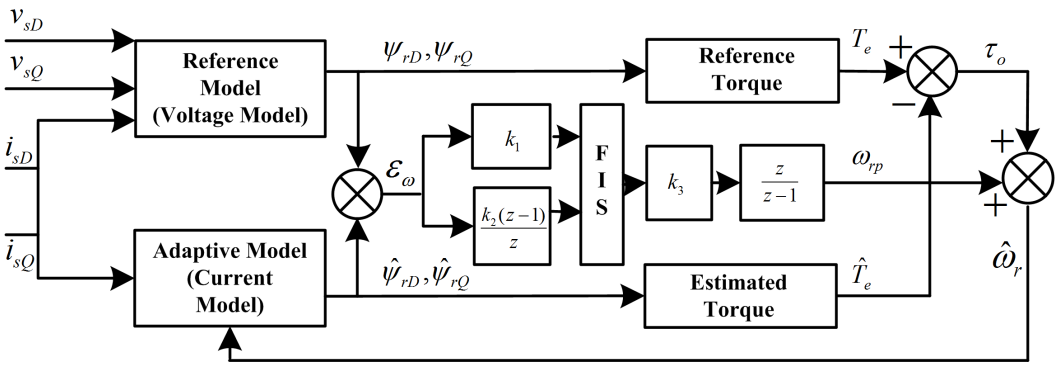

Figure 4.9: Block diagram of proposed rotor flux FLC-MRAS speed observer

variation of estimated speed of motor and this change will continue until the steady state condition appears or estimated torque becomes equal to the motor electromagnetic torque. With the help of motor mechanical equation (4.4.8), the electromagnetic torque and the motor speed can be expressed in their estimated form as

$$\hat{T}_e - T_l = J\frac{d\hat{\omega}_r}{dt} + f\hat{\omega}_r \tag{4.4.13}$$

By subtracting the (4.4.13) from (4.4.8), the following expression can be obtained

$$\tau_o = T_e - \hat{T}_e = J\frac{d(\omega_r - \hat{\omega}_r)}{dt} + f(\omega_r - \hat{\omega}_r) \tag{4.4.14}$$

Finally, rotor estimated speed expression can be written as

$$\hat{\omega}_r = \omega_{rp} + \tau_o \tag{4.4.15}$$

The expression in (4.4.14) explains the purpose of utilization of this torque loop, since the difference between both torques estimated and reference appears when the rate of change in estimated speed appears from the reference speed under transient or load disturbance condition. In order to improve the observer speed estimation performance under load disturbance or robustness against the load variation, this torque difference is added in the conventional rotor flux loop. The basic block diagram of proposed rotor flux FLC-MRAS is shown in Fig. 4.9.

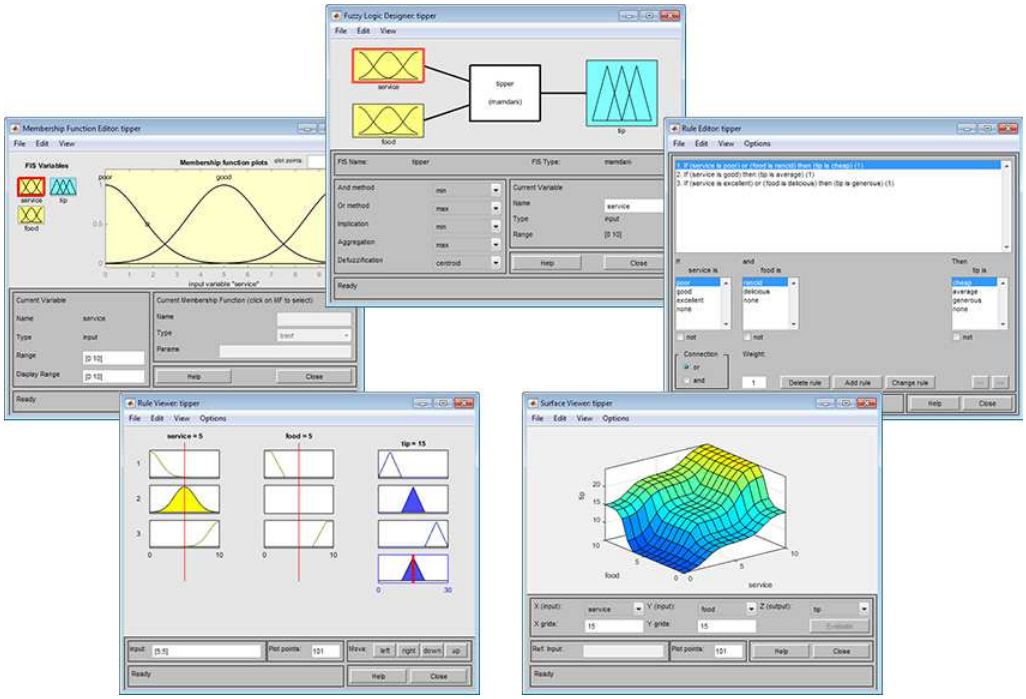

Figure 4.10: Fuzzy inference system modelling using Matlab. The Membership Function Editor (top left), FIS Editor (center), Rule Editor (top right), Rule Viewer (bottom left), and Surface Viewer (bottom right) [4].

4.5 Simulation Results and Analysis

Fuzzy logic tool box in Matlab provides the user friendly environment for user to model a fuzzy logic system. FLC system can be developed either by using the graphic user interface (GUI) as shown in Fig. 4.10 or command line functions. In Matlab there are five GUI tools provided to develop the model and edit the FLC. These are fuzzy inference system (FIS) editor, membership function editor, rule editor, rule viewer and surface viewer as shown in Fig. 4.10. These all tools are dynamically interconnected to each other and change in one will effect the others.

The FIS editor is the main GUI tool that gives the general information about the Fuzzy system. By means of this editor number and names of inputs and outputs are defined. This tool box supports Mamdani and Sugeno inference methods. MF editor is used to define the shape of MF such as triangular or trapezoidal and range of the

Table 4.2: Induction Motor Parameters & Ratings

Motor Parameters & Ratings	Values
Stator Resistance (R_s)	0.1607 Ω
Rotor Resistance (R_r)	0.1690 Ω
Stator Self Inductance (L_s)	6.017 mH
Rotor Self Inductance (L_r)	5.403 mH
Magnetizing Inductance (L_m)	5.325 mH
Rotor Inertia (J)	0.000145 kgm^2
No of Poles (P)	4
Rated Power	200 W
Rated Speed	3621 rpm

MF or universe of discourse. Rule editor is used for editing the fuzzy system rule. Through rule editor any fuzzy logic operation can be selected such as AND, OR and NOT and any rule can be changed, deleted or added according to the requirement. The proposed FL controller is Mamdani type with two inputs speed error and change in speed error and one out put change in speed. Controller uses triangular shape membership function with universe of discourse between -0.1 and 0.1. Both inputs and one output of the controller have seven different fuzzy sets for the operation control. However, the AND logical operator is used to define the IF Then expression in fuzzy inference system. Surface viewer generates the 3D view and shows the relation between input variables and output variable. Both rule viewer and surface viewer are the read only tools and are used to understand the characteristics of FIS [4].

In order to analyse and compare the operational performance of both PI-MRAS and FLC-MRAS, different simulation tests are carried out by using different speed and torque profiles usually required in EV operation. Different speed levels and percentages of rated load torque are used to examine the operational performance of both observers. An indirect vector control method is implemented to control the

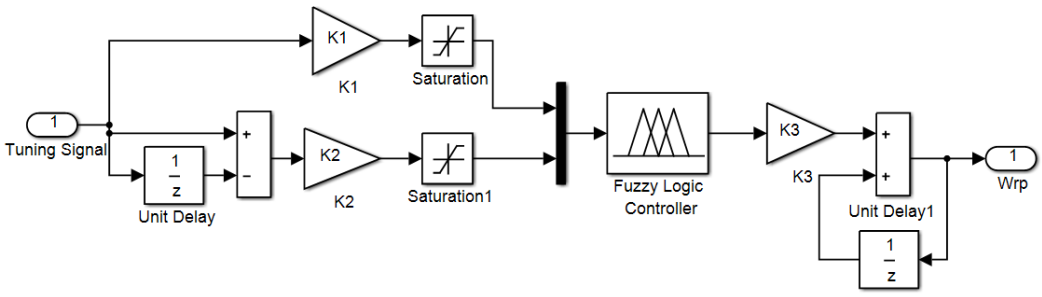

Figure 4.11: Fuzzy logic controller implementation in simulink model

operation of IM drive in all simulations.

In this section, satisfactory speed estimation performance of proposed FLC-MRAS observer structure is verified through different simulation tests. For this purpose, a 4-pole and 200 watt induction machine is used, whereas the detail of induction machine parameters are given in Table 4.2. Induction machine is modelled using two axis theory or $d-q$ axis theory as discussed in chapter 3. The mechanical rotor speed of induction motor is taken from the given expression

$$T_e - T_l = J\frac{d\omega_{rm}}{dt} \tag{4.5.1}$$

where the relationship between rotor mechanical speed ω_{rm} and its related electrical speed ω_r is given by:

$$\omega_{rm} = \left(\frac{2}{P}\right)\omega_r \tag{4.5.2}$$

The speed sensorless indirect vector control method based-IM drive system is developed with the help of simulink library blocks in Matlab-Simulink environment. Induction machine $d-q$ model is directly fed through the reference voltages, therefore, an ideal inverter operation as well as pulse width modulator are considered in all simulations. In both PI-MRAS and FLC-MRAS, reference model is solved using pure integration and there is no drift and initial condition issues are considered in the simulations. It should be noted that in order to compare the operational performance difference between both observers, the PI controller gains used in the vector

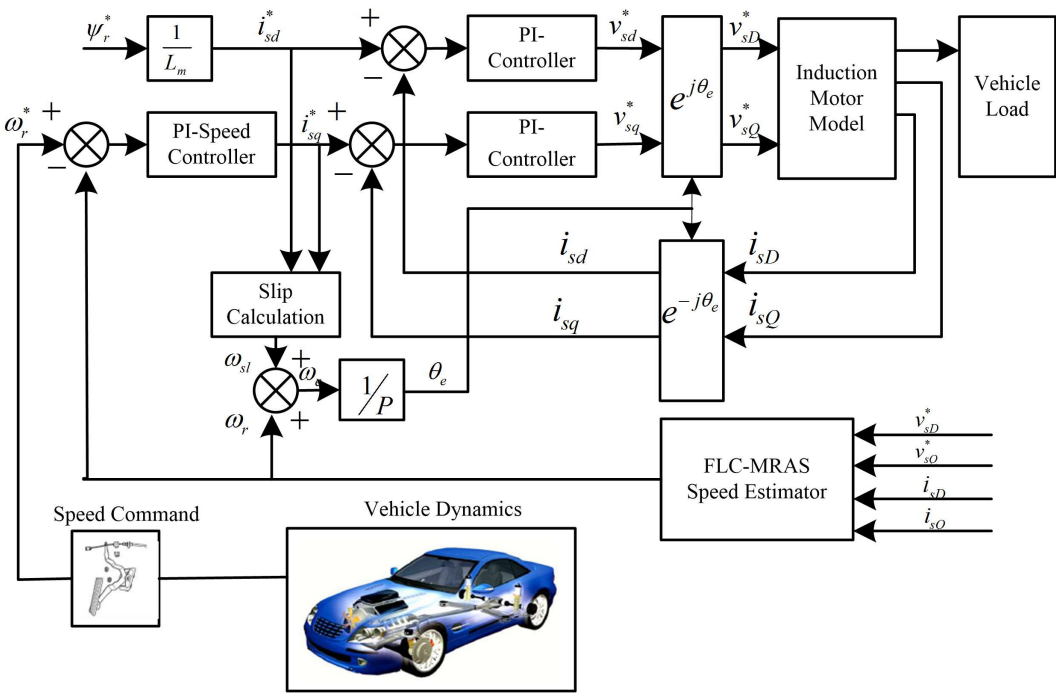

Figure 4.12: Block diagram of speed sensorless indirect vector control of induction motor traction drive by using FLC-MRAS speed estimator

control blocks are the same during all simulations. The proposed FLC-MRAS is implemented on Matlab-Simulink by using fuzzy logic tool box. Fig. 4.11 shows the implementation of FL controller in simulink model. Fig. 4.12 illustrates the basic block diagram of FLC-MRAS speed sensorless indirect vector control of induction motor traction drive.

In order to understand the operational performance effectiveness of the proposed speed observer compare to the PI-based MRAS, different tests are designed with respect to the observer application specifically in EV operation. Since in the vehicle operation it is important to follow the speed limits, avoid collisions and to start, accelerate, decelerate and stop when it is required. In the vehicle operation there are two main controls in order to adjust the speed operation, the first one is accelerator, which controls the driving torque, and the brake, which adjusts the load torque. Vehicle safely operation is impossible without these two controls, and driver has to

maintain a required speed operation in spite of the changes in the load, such as an uphill, downhill or strong wind conditions. In all these tests, observer speed regulation response, speed tracking error, speed estimation error, convergence of speed tuning signal under different load conditions etc are considered for performance comparison. The following tests are presented in this section.

4.5.1 Load disturbance rejection capability of observer at different rated load torque

The basic aim of this test is to check the load disturbance rejection capability of the proposed speed observer. For this purpose, different values of rated load torque are applied at different speed levels during the motor operation. Ideally observer speed estimation and motor speed should not have any effect of the applied load disturbance but practically should be as minimum as possible. It is intuitively obvious that the operation of traction drive is not like used in different home appliances or used for specific industrial applications with desired speed level and defined load conditions. Traction drive is operated both in forward and reverse motoring and braking regions with different levels of speed as well as load torque.

However, the applied load torque profile is the most important operational parameter which is uncertain during the whole operation apart from the vehicle own load. Since, vehicle has to face different road conditions and aerodynamic effects which continuously change the net load torque effect on the traction drive. Therefore, for sensorless operation of the traction drive, the speed observer should be able to reject the sudden load change conditions without effecting the desired operational performance of the traction drive.

Load disturbance rejection capability of observer at 15 rad/sec motor speed with applied 25% rated load disturbance:

Indirect vector control induction motor is operated at reference speed 15 rad/sec. In order to check the observer performance, 25% rated step load torque is applied

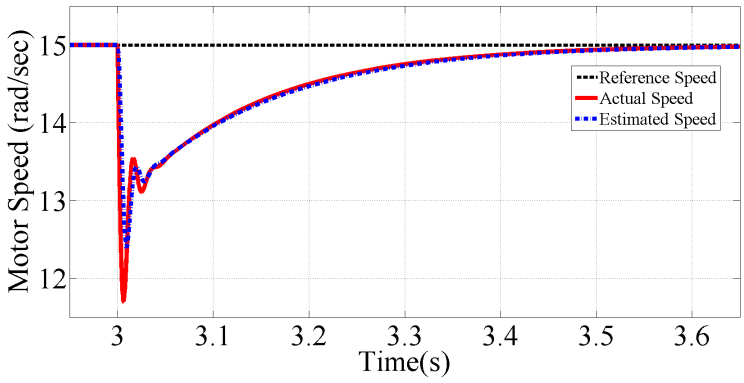

(a)

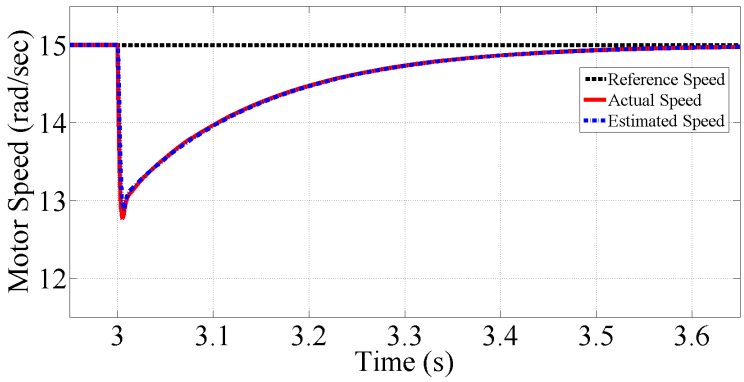

(b)

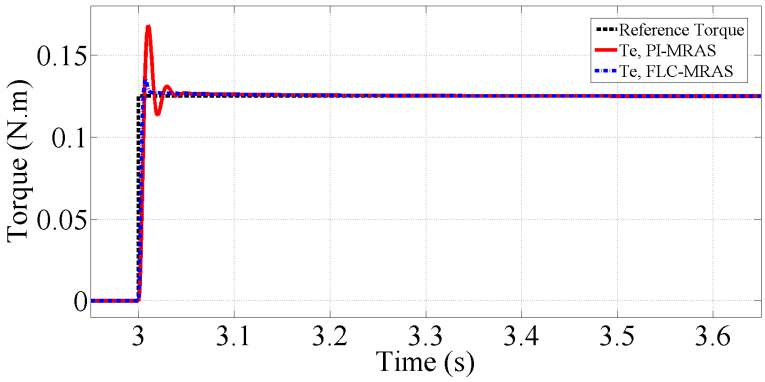

(c)

Figure 4.13: Speed estimation performance of Observer for 25% rated load disturbance rejection capability at 15 rad/sec motor speed. 4.13(a) PI-MRAS. 4.13(b) FLC-MRAS 4.13(c) Motor electromagnetic torque response T_e.

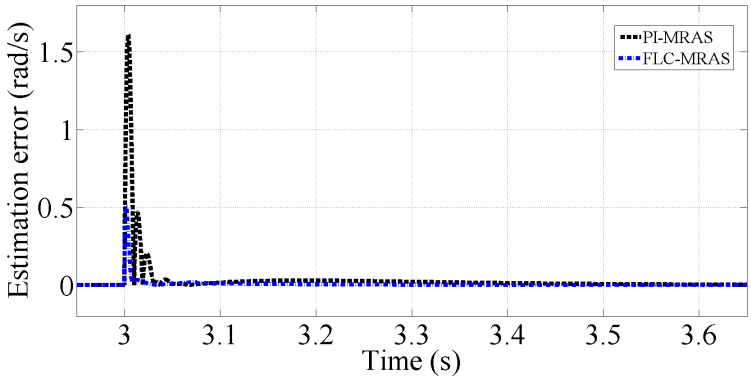

(a)

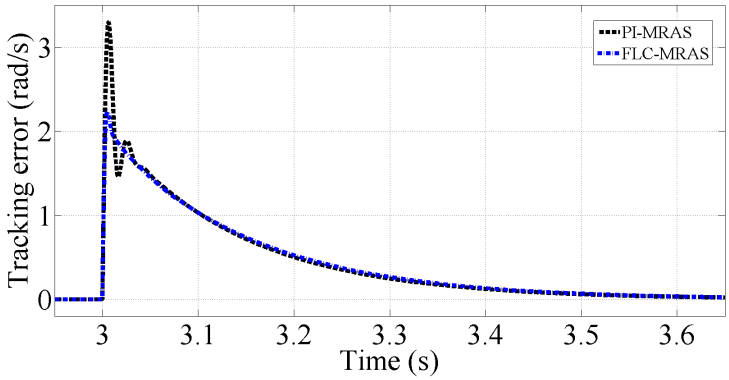

(b)

Figure 4.14: Absolute error of estimation speed and tracking speed at 15 rad/sec with 25% rated load disturbance at $t = 3s$. 4.14(a) Speed estimation error. 4.14(b) Speed tracking error.

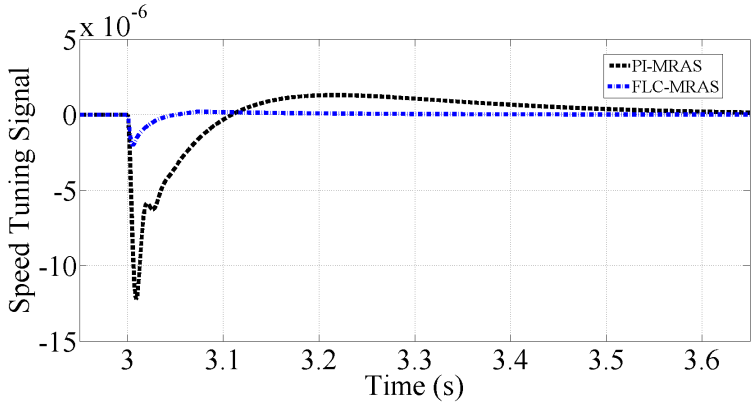

Figure 4.15: Speed tuning signal for 25% rated load disturbance at 15 rad/sec motor speed.

at $t = 3s$. Speed observer performance is measured in terms of speed regulation response, speed estimation error which is the difference between motor actual speed and observer estimated speed, speed tracking error which is the difference between reference or command speed and motor actual speed and speed tuning signal. In case of PI-MRAS 22% and 5.98% tracking error and estimations error are obtained respectively while in case of FLC-MRAS 14.85% and 1.09% tracking error and estimations error are achieved respectively. However, the relative tracking and estimation errors are 7.15% and 4.89% respectively. Simulation results present the superiority of the proposed FLC-MRAS as compare to PI-MRAS. The transient response or dynamic response of the proposed scheme is faster than the conventional PI based scheme. The minimum speed tuning or error signal is achieved in the proposed scheme with fast convergence to zero in the transient state. Fig.4.13 shows the speed and motor torque response by using both FLC-MRAS and PI-MRAS schemes. Whereas, Fig.4.14 shows the speed estimation error as well as speed tracking error and Fig.4.15 illustrates the speed tuning signal.

Load disturbance rejection capability of observer at 15 rad/sec motor speed with applied 60% rated load disturbance:

The similar observer load disturbance rejection capability test is performed at 15 rad/sec motor speed with applied 60% rated load torque disturbance at $t = 3s$.

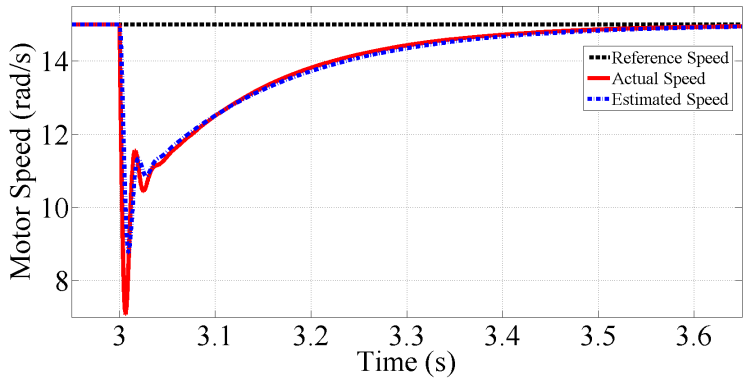

(a)

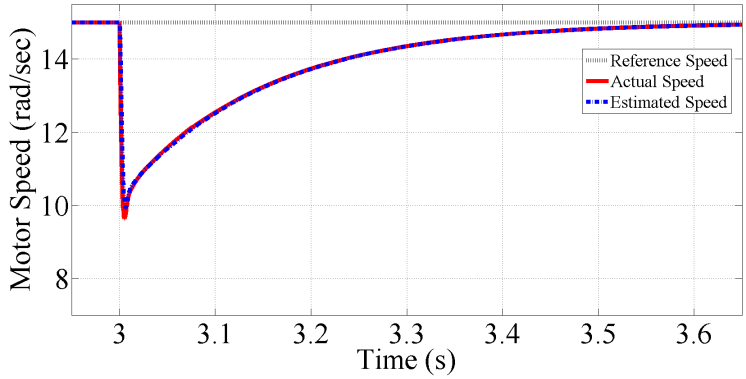

(b)

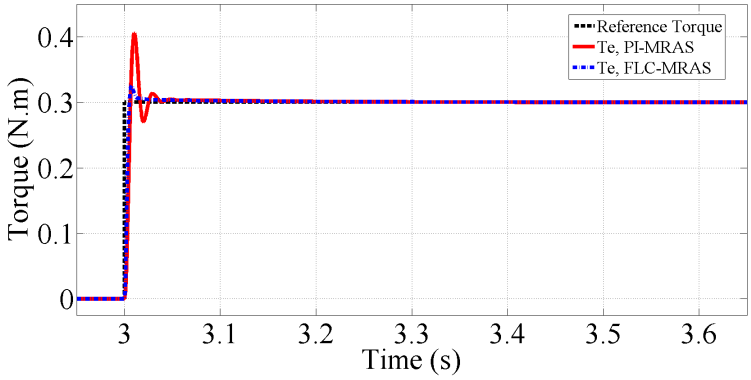

(c)

Figure 4.16: Speed estimation performance of Observer for 60% rated load disturbance rejection capability at 15 rad/sec motor speed. 4.16(a) PI-MRAS. 4.16(b) FLC-MRAS 4.16(c) Motor electromagnetic torque response T_e.

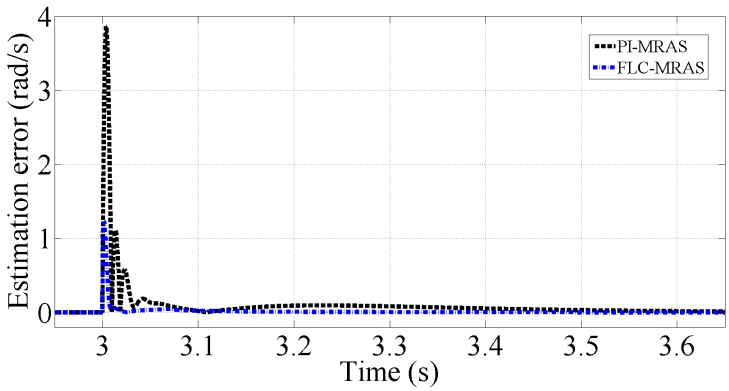

(a)

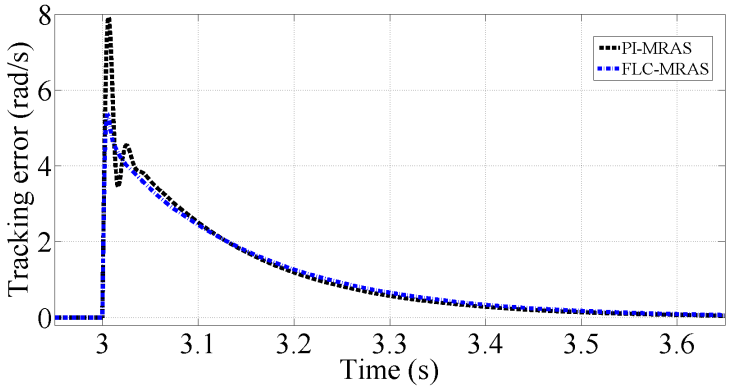

(b)

Figure 4.17: Absolute error of estimation speed and tracking speed at 15 rad/sec with 60% rated load disturbance at $t = 3s$. 4.17(a) Speed estimation error. 4.17(b) Speed tracking error.

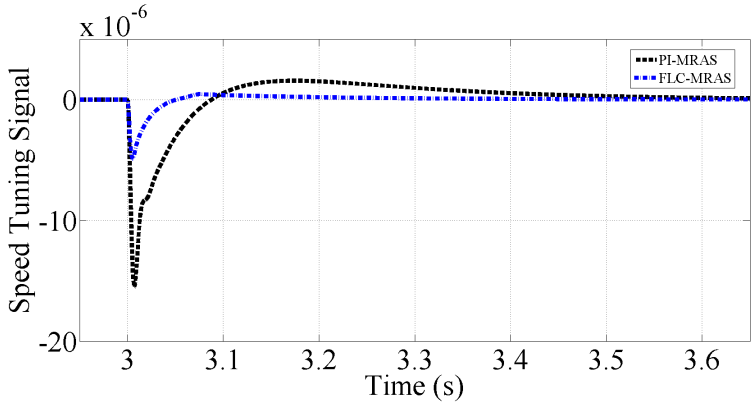

Figure 4.18: Speed tuning signal for 60% rated load disturbance at 15 rad/sec motor speed.

At higher applied rated load torque, slightly higher speed estimation and tracking error are achieved but still better performance over to PI based scheme is obtained. In case of PI-MRAS 52.79% and 24.98% tracking error and estimations error are obtained respectively when the load disturbance is applied at $t = 3s$ while in case of FLC-MRAS 35.45% and 3.27% tracking error and estimations error are achieved respectively. However, the relative tracking and estimation errors are 17.34% and 21.71% respectively. Fig.4.16, Fig.4.17 and Fig.4.18 illustrate the speed regulation response, speed estimation & tracking error and speed tuning signal at 15 rad/sec motor speed with applied 60% rated load disturbance.

4.5.2 Quick acceleration or sudden speed change performance of observer

The basic aim of this test is to check the performance of speed observer under quick acceleration and quick speed change condition. Normally this performance is required from the vehicle at cruising operation and in start operation with quick speed change. The motor should respond to the reference speed as quickly as possible and in the same way the accurate speed estimation through the observer.

For this purpose a quick speed change is applied in the command speed from

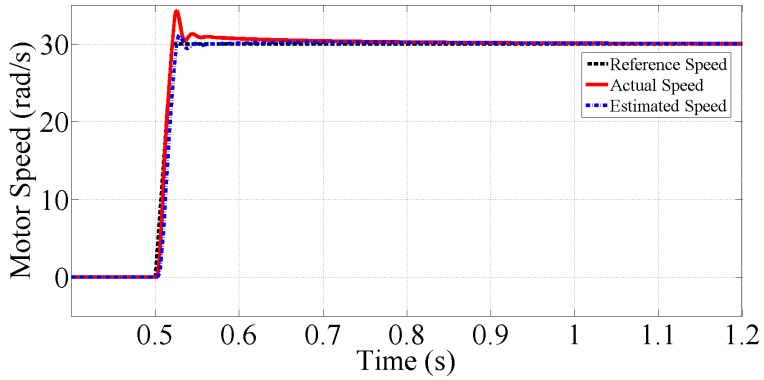

(a)

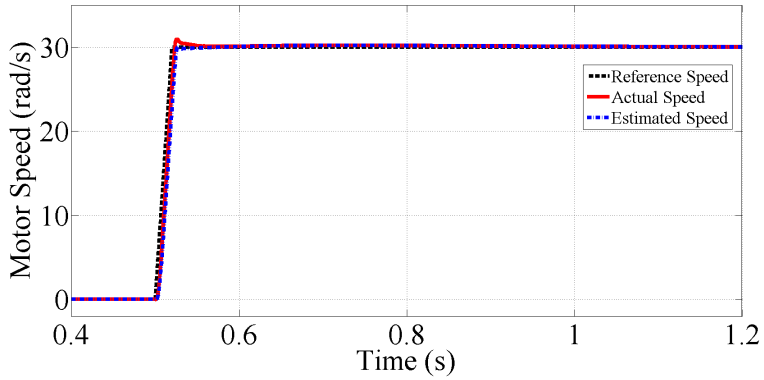

(b)

Figure 4.19: Speed estimation performance of Observer during quick speed change from zero speed level to 30 rad/sec motor speed. 4.19(a) PI-MRAS. 4.19(b) FLC-MRAS.

zero to 30 rad/sec at $t = 0.5s$. It is noticeable that the motor actual speed is less deviated from the reference speed and provides fast transient response with less speed estimation error in the proposed FLC-MRAS over PI-MRAS. Fig.4.19 and Fig.4.20 show the observer speed regulation response and speed estimation error whereas Fig.4.21 illustrates the optimal obtained speed tuning or error signal during the sudden speed change operation.

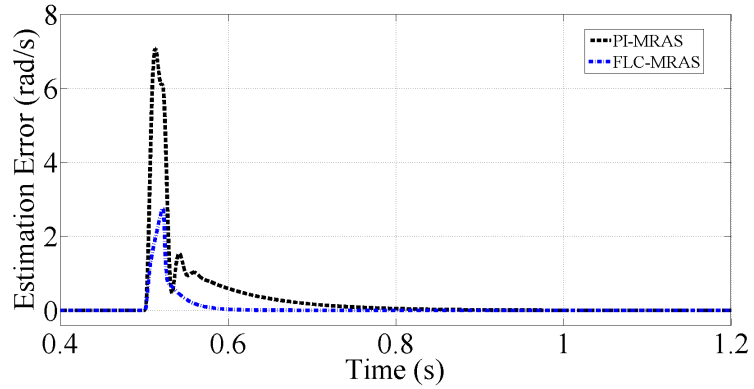

(a)

Figure 4.20: Absolute error of estimation speed during quick speed change at $t = 0.5s$.

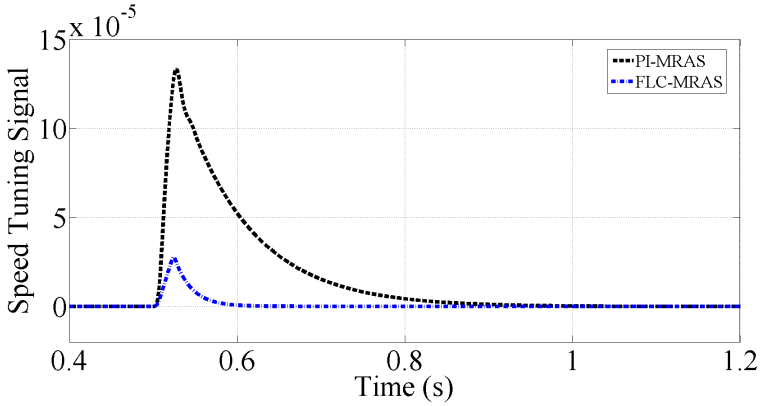

Figure 4.21: Speed tuning signal for quick speed change of 30 rad/sec motor speed.

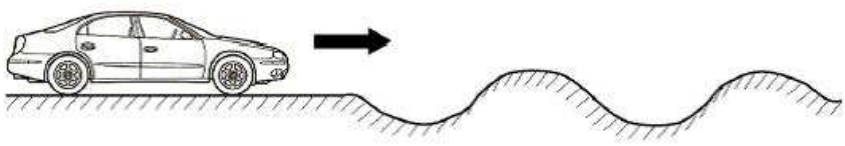

Figure 4.22: EV constant speed operation on an un-smooth road condition

4.5.3 Observer performance during Un-smooth road condition or with time varying load disturbance

The aim of this test is to check the performance of observer under time varying load condition. It is intuitively obvious that during the whole motoring operation or different driving conditions, it is quite impossible for traction drive to face a fixed kind of load torque. So that the observer should be able to provide a satisfactory performance during time varying load condition. Fig. 4.22 illustrates the operation of EV from constant speed to un-smooth road condition for this test.

In this test the performance of proposed observer is measured with applied reference speed 40 rad/sec at 20% rated load torque. In order to generate the un-smooth road condition, a sawtooth shape from 20% to 50% rated load torque is applied between $t = 2.5s$ and $t = 4s$. With respect to vehicle operation, this applied load torque provides first linearly increase and then sudden reduction in between 20% and 50% rated load condition. It is noticeable that the performance of both observer are similar in steady state before $t = 2.5s$ but during the transient region, speed regulation performance of proposed FLC-MRAS is much better and less effected with time varying load torque condition than PI-MRAS as shown in Fig.4.23. Whereas, Fig.4.24 and Fig.4.25 illustrate absolute value of speed estimation and tracking error and speed tuning signal during Un-smooth road condition.

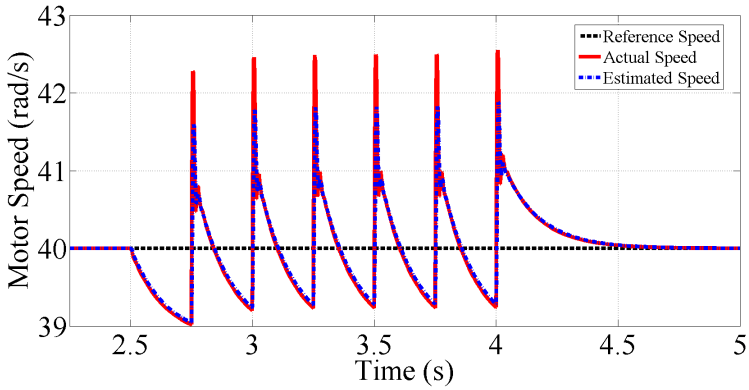

(a)

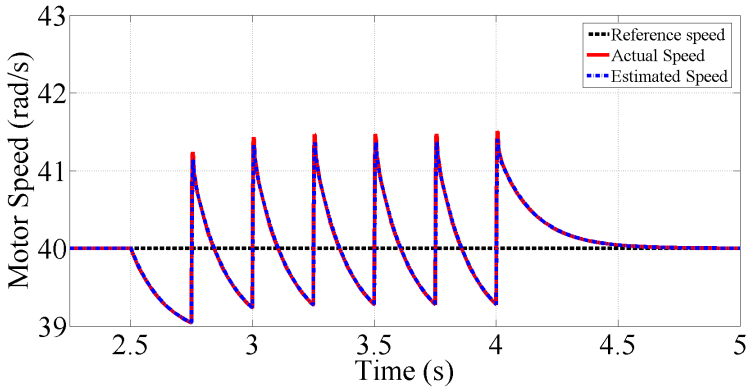

(b)

Figure 4.23: Speed estimation performance of Observer during un-smooth road condition at 40 rad/sec motor speed. 4.23(a) PI-MRAS. 4.23(b) FLC-MRAS.

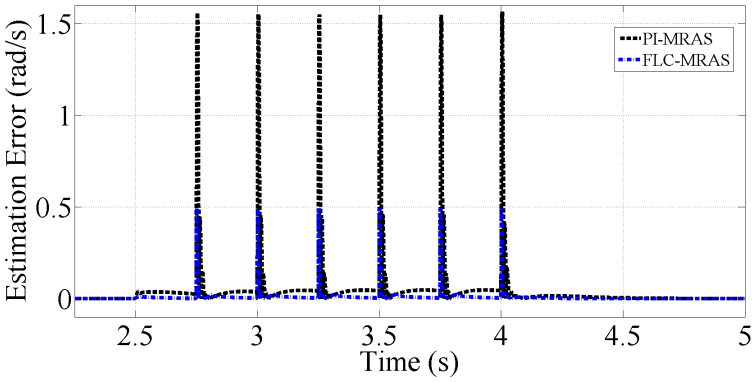

(a)

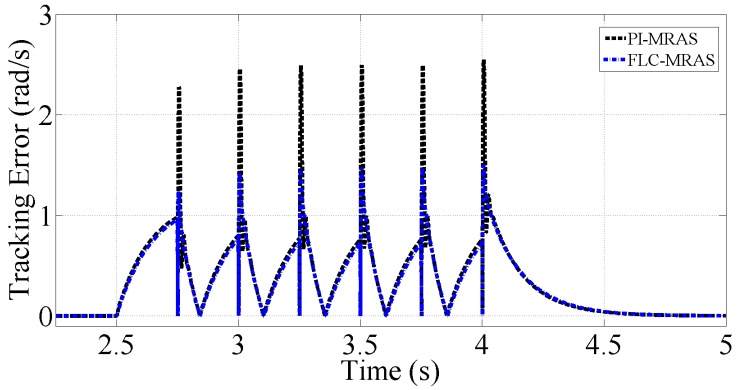

(b)

Figure 4.24: Absolute error of estimation speed and tracking speed during un-smooth road condition. 4.24(a) Speed estimation error. 4.24(b) Speed tracking error.

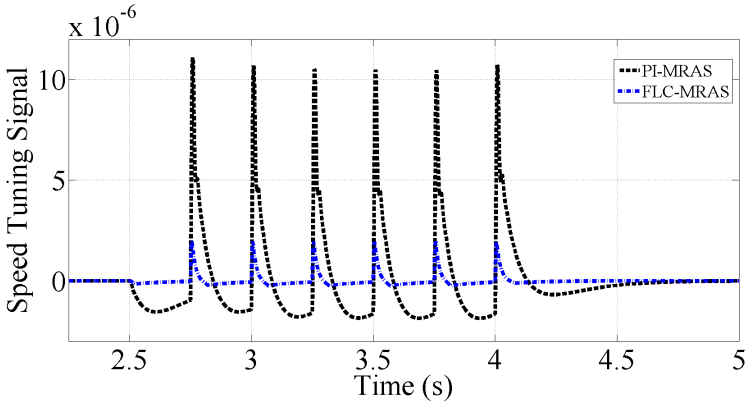

Figure 4.25: Speed tuning signal during un-smooth road condition.

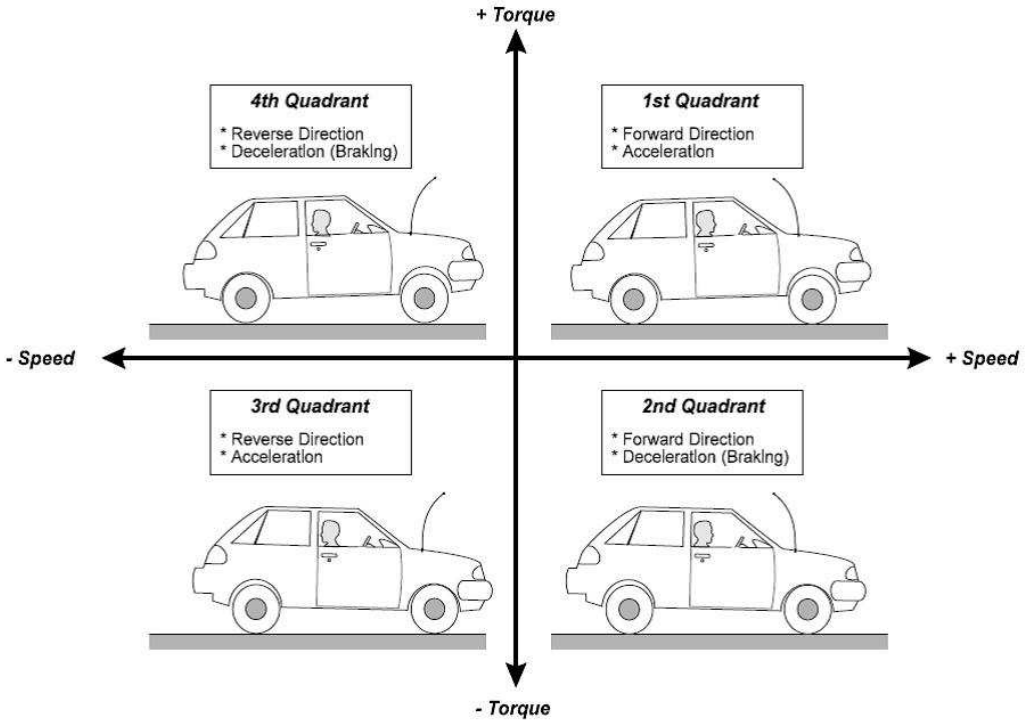

Figure 4.26: The four quadrants of the torque-speed diagram for an EV [5]

4.5.4 Motor speed transition from positive to negative and vice versa at different load disturbance conditions

The basic aim of this test is to check the operational performance of speed observer when different speed change appears under certain load torque conditions. In case of vehicle operation, such speed change could happen in any quadrant of the following mode of operation as Fig. 4.26 illustration shows. Energy flow direction between traction motor and vehicle wheels in any quadrant of operation depends on the sign of traction motor power which is the product of torque and motor speed. Energy is transferred from the prime mover (traction motor) to the mechanical load (vehicle wheels) when power is positive which means both motor torque and speed have the same sign either positive in case of forward motoring and negative in case of reverse motoring. whilst, power sign negative indicates that both motor torque

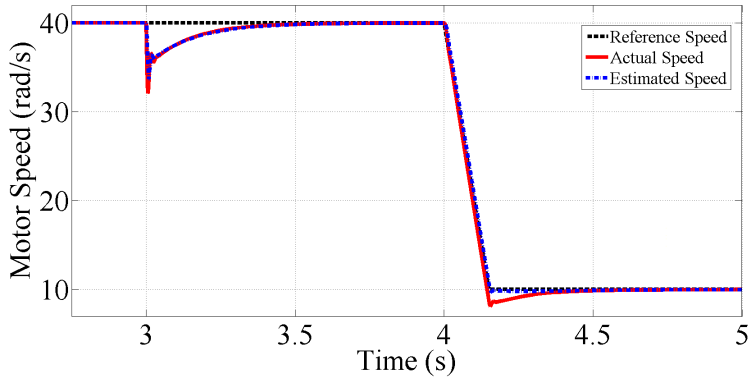

(a)

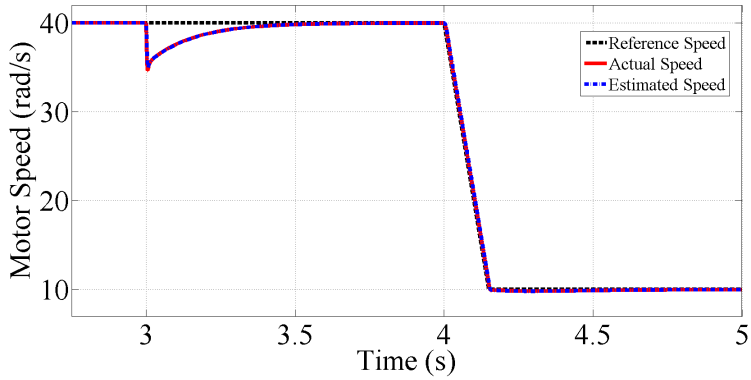

(b)

Figure 4.27: Speed estimation performance from 40 rad/s to 10 rad/s speed transition with 60% rated load disturbance. 4.27(a) PI-MRAS. 4.27(b) FLC-MRAS.

and speed have different sign and traction motor is being operated either in forward braking or reverse braking. In this case energy is transferred from the wheels back to the prime mover or traction motor. In some kinds of electrical traction drives this energy can be transferred back into the power supply system, which is called regenerative braking. In this section different reference speed change are used with 60% rated load torque. In all cases improved speed regulation response with minimal speed estimation, tracking error and tuning signal are obtained.

Motor speed transition from high to low positive speed with 60% rated load disturbance:

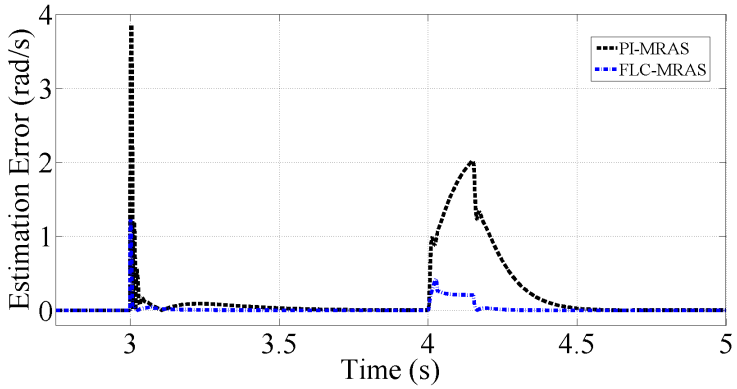

(a)

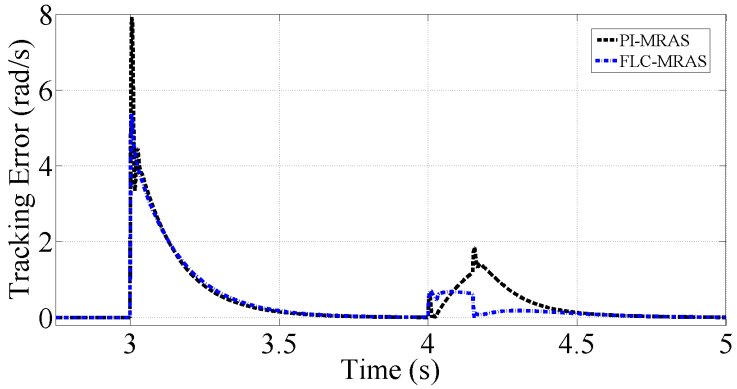

(b)

Figure 4.28: Absolute error of estimation speed and tracking speed during speed 40 rad/s to 10 rad/s speed transition. 4.28(a) Speed estimation error. 4.28(b) Speed tracking error.

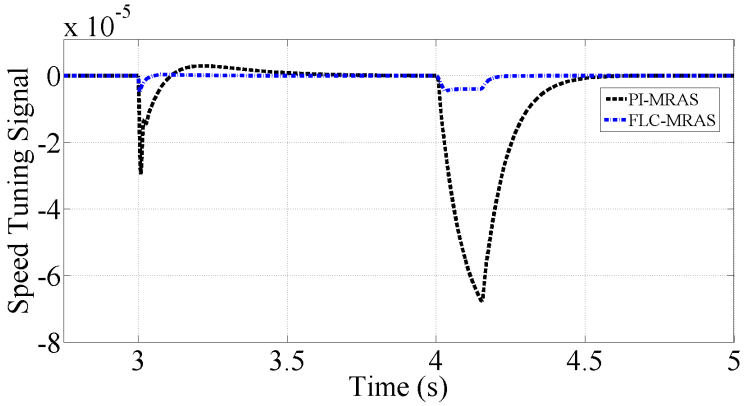

Figure 4.29: Speed tuning signal during high to low positive speed transition.

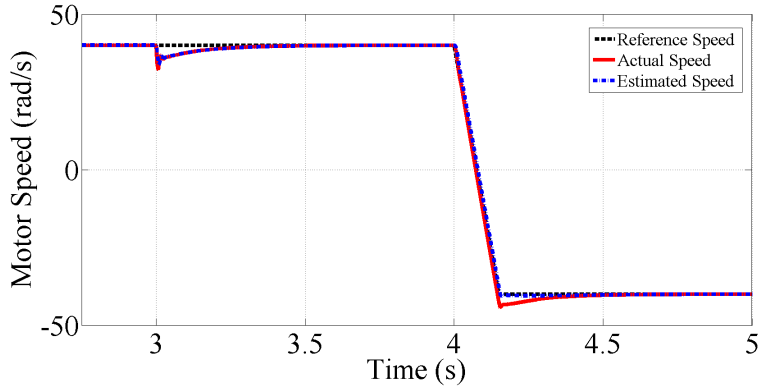

(a)

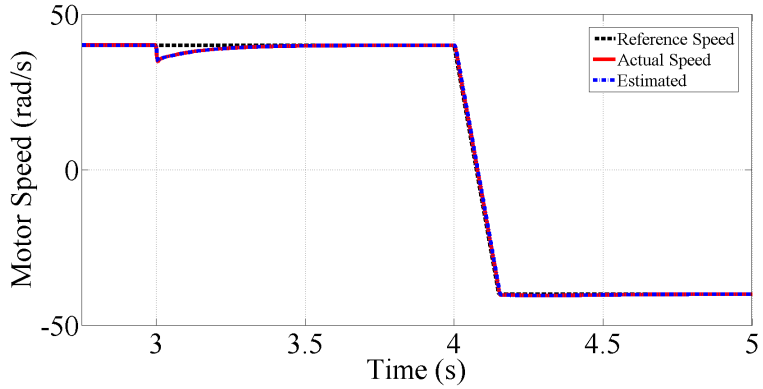

(b)

Figure 4.30: Speed estimation performance from 40 rad/s to -40 rad/s speed transition with 60% rated load disturbance at $t = 3s$. 4.30(a) PI-MRAS. 4.30(b) FLC-MRAS.

In this case a reference speed is applied from 40 rad/sec to drop down 10 rad/sec with 60% rated load torque applied at $t = 3s$. Fig.4.27, Fig.4.28 and Fig.4.29 illustrate motor speed regulation, speed estimation & tracking errors and speed tuning signal respectively under speed transition from high to low positive speed with 60% rated load disturbance.

Motor speed transition from positive to negative with 60% rated load disturbance at $t = 3s$

For this case a reference speed is applied from 50 rad/sec to -50 rad/sec with 60%

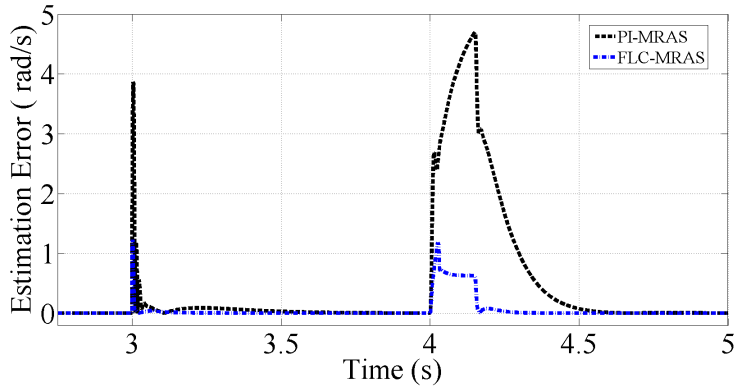

(a)

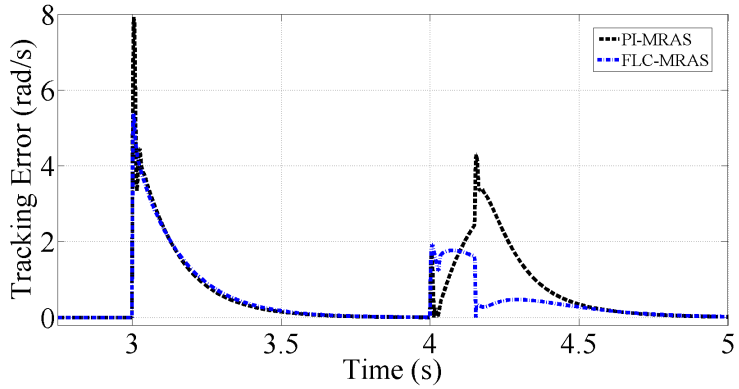

(b)

Figure 4.31: Absolute error of estimation speed and tracking speed during +40 rad/s to -40 rad/s speed transition. 4.31(a) Speed estimation error. 4.31(b) Speed tracking error.

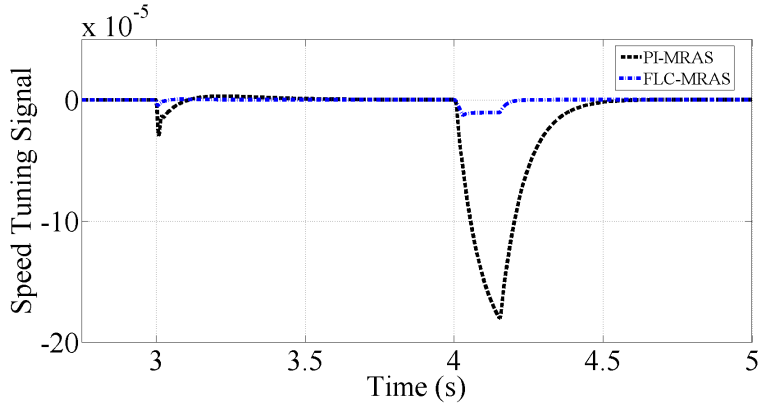

Figure 4.32: Speed tuning signal from positive to negative speed transition.

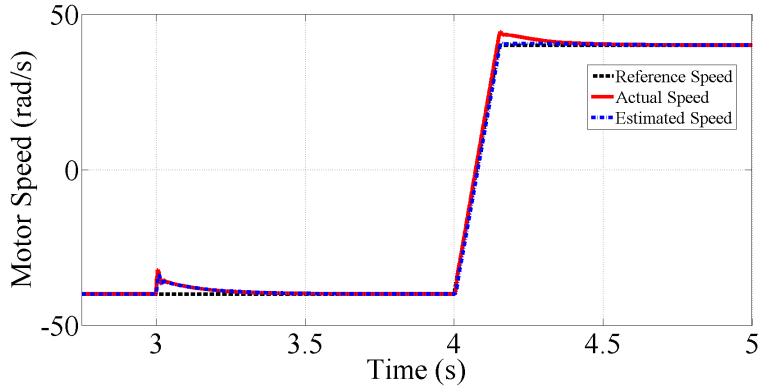

(a)

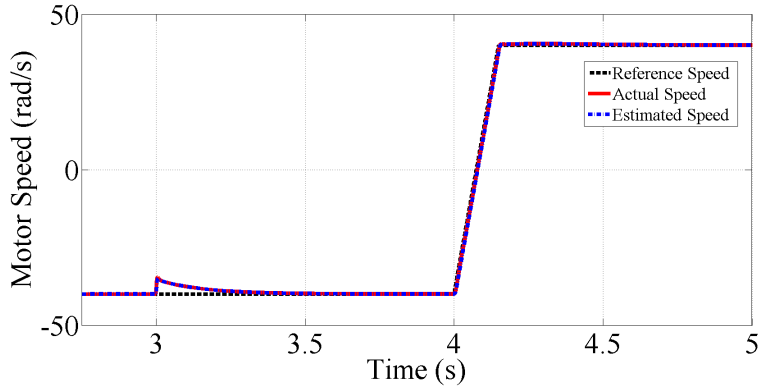

(b)

Figure 4.33: Speed estimation performance from -40 rad/s to +40 rad/s speed transition with 60% rated load disturbance. 4.33(a) PI-MRAS. 4.33(b) FLC-MRAS.

step rated load torque applied at $t = 3s$. Fig.4.30, Fig.4.31 and Fig.4.32 illustrate motor speed regulation, speed estimation & tracking errors and speed tuning signal respectively under speed transition from positive to negative speed with 60% step rated load disturbance.

Motor speed transition from negative to positive with 60% rated load disturbance at $t = 3s$

For this case a reference speed is applied from -50 rad/sec to 50 rad/sec with 60% step rated load torque applied at $t = 3s$. It is noticeable that in case of FLC-MRAS that the motor actual speed follow the applied reference speed much better

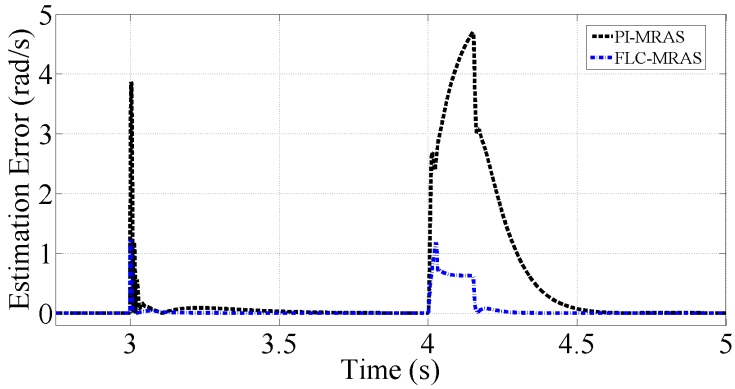

(a)

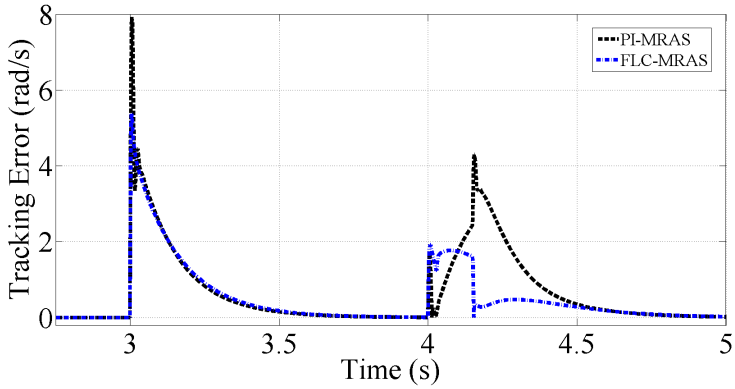

(b)

Figure 4.34: Absolute error of estimation speed and tracking speed during -40 rad/s to +40 rad/s speed transition. 4.34(a) Speed estimation error. 4.34(b) Speed tracking error.

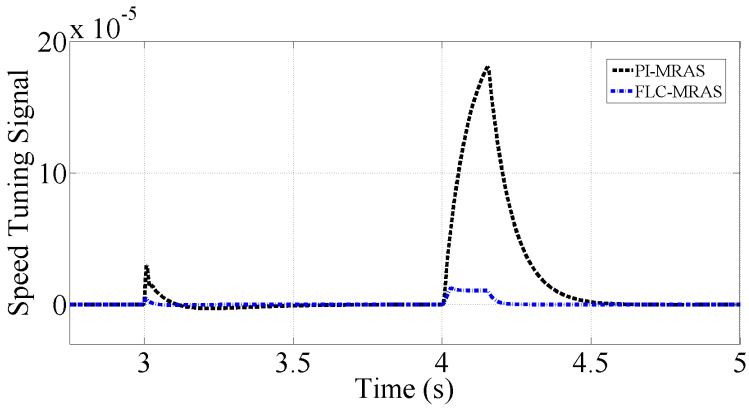

Figure 4.35: Speed tuning signal during negative to positive speed transition.

and tracked quickly at the speed change mode. Fig.4.33, Fig.4.34 and Fig.4.35 show motor speed regulation response, speed estimation & tracking errors and speed tuning signal respectively under speed transition from negative to positive speed with 60% step rated load disturbance.

4.6 Conclusion

This chapter presents a novel fuzzy logic control based rotor flux model reference adaptive system speed observer. This new speed observer replaces the fixed gain PI controller which is usually used in conventional rotor flux MRAS observer. In this observer, two differences are used at the same time, reference and estimated rotor fluxes like conventional observer as well as reference and estimated torques in order to improve the speed estimation specifically in load torque disturbance condition which is the most important feature during vehicle sensorless operation due to uncertain load disturbance condition. The proposed scheme uses two inputs and one output Mamdani-type FL controller with triangular shape membership function which works in a nonlinear optimization mode. Seven different fuzzy sets are used for both inputs and one output. However, the fuzzy inference system is defined by using AND logical operator by using IF Then expression. In both FLC-MRAS and PI-MRAS observer, parameters are tuned in such a way which provide similar steady state performance. Different simulation cases are designed with respect to the vehicle operation such as load disturbance rejection capability, quick acceleration, un smooth road condition and different speed transition with load torque. All simulations have been carried out by using indirect vector control induction motor drive system. In all simulation cases the performance of proposed FLC-MRAS is compared to the PI-MRAS observer. The proposed scheme shows better transient performance as well as better load torque disturbance rejection capability as compare to the PI-MRAS and found a suitable solution for speed sensorless IM drive for EVs.

Chapter 5

Sensorless Induction Motor Drive Control Using Sliding Mode based Speed Observer

5.1 Introduction

APPLICATION of PI-controller is very common in different industrial control system. Since, these controllers have simple structure relatively and can produce a satisfactory performance over a wide range of operation. Most of the MRAS based speed observer schemes presented in the literature have used the fixed gain PI-controller to minimize the speed tuning signal or error signal so as to get the estimated rotor speed. However, in different industrial electric drive applications, system electrical and mechanical parameters are hardly constant throughout the operation [3]. Moreover, there is a load torque disturbance, which also effects the performance. For instance, the amount of inertia in case of vehicle operation or in subway drive vary with passenger load apart from the other aerodynamic effects. similarly, in case of robotic arm drive, the amount of inertia is dependent on the length of arm and the load it carries. On the other hand, in case

of rolling mill drive, the load torque applied on the rolling mill suddenly changes when the metal slab is introduced within the rolls.

However, the control performance of drive is influenced by uncertainties which are composed of unpredictable variations in the machine parameters, external load torque disturbances, unmodellded non-linear dynamics, operating condition such as temperature variation as well as the inverter nonlinearities [94], these fixed gain PI-controller may not be able to provide the required performance. However, lots of research have been done in order to control the performance of motor drive including non-linear control, optimal control, variable structure system control, adaptive control and neural control [132, 133], [134].

Therefore, it is important to consider other types of adaptation mechanism in order to minimise the speed tuning signal or error signal to obtain the accurate speed estimation. Presently, sliding mode (SM) observers have been presented for the estimation of induction machine parameters such as speed, rotor fluxes and rotor time constant [96], [135], [136], [137]. Several SM strategies have been proposed to control the operation of IM drive [94], [138], [139]. The SM control based electric drive offers several advantages including better performance with unmodelled dynamics, less sensitivity against the machine parameter variations, external load disturbance rejection capability, fast dynamics response, a stable control system and easy hardware/software implementation [95], [140], [136], [141], [142]. However, due to discontinuous nature, it has some drawbacks in electric drive, which is high frequency oscillations as chattering characteristic. This chattering characteristic creates some unwanted effects that are torque pulsation and current harmonics [139], [143]. In the last few years this chattering problem has become a focus of researchers [144], [145], [146].

This chapter presents a novel adaptation scheme to replace the classical fixed gain PI controller used in rotor flux model reference adaptive system speed estimator. The proposed speed observer is based on SM theory. This speed estimation adaptation law is derived using Lyapunov theory to ensure the estimation stability as

well as fast error dynamics. For speed estimation performance comparison, different simulation tests are carried out with respect to the vehicle operation as mentioned in the previous chapter and compare with the PI-MRAS speed observer by using indirect vector control IM drive. All simulation results show the better performance of the proposed observer at different speed driving profiles under load disturbance conditions

5.2 Principle of Sliding Mode Control System

Sliding mode control has received much attention of researchers in the last few decades because of its fast dynamic response and system robustness. SMC is a variable control structure strategy which is basically an adaptive control that produces robust performance of drive under system parameter variations and load disturbance condition [3], [147], [148]. This is a non-linear control method and can be applied on both linear and non-linear systems. In SMC, as the name implies the drive system response is forced to tract or slide on to the predefined trajectory or reference surface in a phase plane by using a switching control law, irrespective to the system's parameter variations or load disturbance [3], [95], [149]. The control DSP determines the deviation of actual trajectory from the reference trajectory and the corresponding deviation is track through the switching strategy.

The main part of MSC is to define a suitable switching control law in order to drive the state trajectory onto a switching surface and maintains this trajectory sliding on this surface for all subsequent time [150]. The sliding mode comprises of a reaching phase where the state trajectory is driven to the surface $s = 0$ and reaches this in a finite time, followed by a sliding phase where it slides on the switching surface to an equilibrium point as shown in Fig.5.1 [94], [68]. These states x_1 and x_2 are usually error function and its derivative and in this case the equilibrium point is $(0, 0)$. On the basis of Lyapunov theory, a control law is defines which ensures the motion of the state trajectory towards the sliding surface [150]. It can be achieved

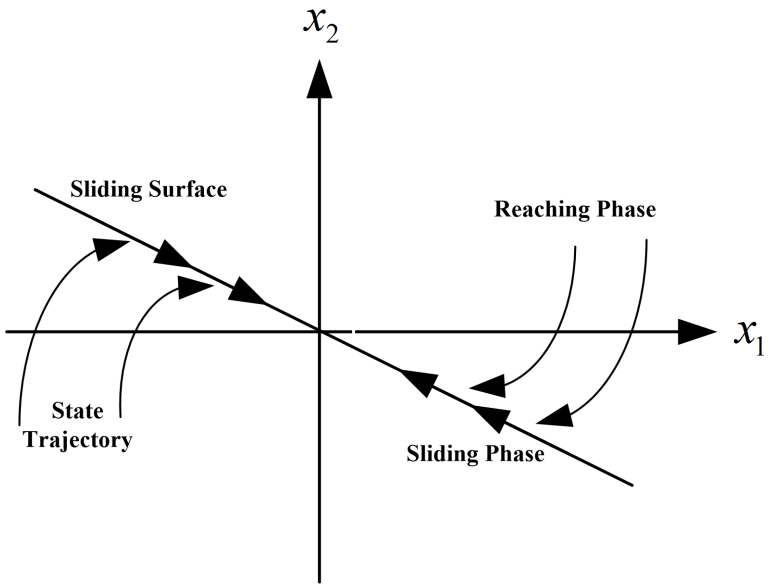

Figure 5.1: The sliding mode control principle

by choosing a hitting control gain in order to maintain the derivative of Lyapunov function always negative definite [151].

5.3 Proposed Sliding Mode based Rotor Flux-MRAS Speed Estimator

In the proposed rotor flux error based SMC-MRAS speed observer, two differences are used at the same time. The first difference is in between the two different rotor fluxes, which is between reference value of rotor fluxes (ψ_{rD}, ψ_{rQ}) from voltage model and estimated value of rotor fluxes ($\hat{\psi}_{rD}, \hat{\psi}_{rQ}$) from current model as shown in Fig.4.5 of conventional PI-controller based rotor flux MRAS speed observer. In addition,in the new proposed scheme, the second difference is taken between reference electromagnetic torque T_e by using reference rotor fluxes and estimated value of electromagnetic torque $\hat{T}_e$ by means of estimated rotor fluxes so as

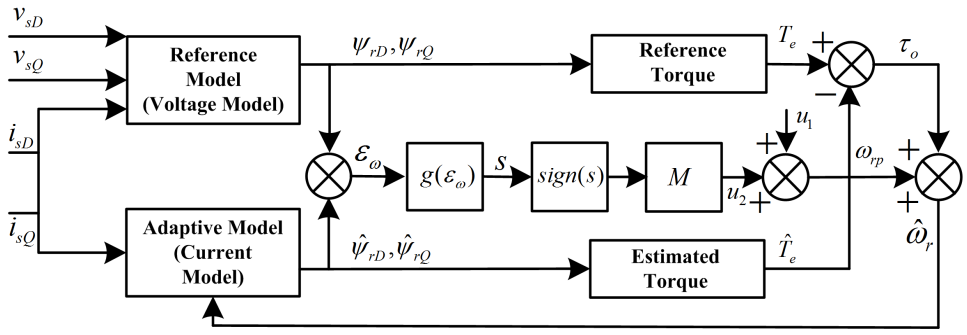

Figure 5.2: Block diagram of proposed rotor flux SMC-MRAS speed observer

to improve the speed estimation of observer specifically in transient region of operation and load disturbance condition [131]. The basic block diagram of proposed rotor flux SMC-MRAS speed observer is shown in Fig. 5.2.

Both reference rotor flux components (ψ_{rD}, ψ_{rQ}) defined into the stationary reference frame and generated from the monitored stator voltage and current component, can be expressed as

$$\begin{aligned} p\psi_{rD} &= \tfrac{L_r}{L_m}\left(v_{sD} - R_s i_{sD} - \sigma L_s p i_{sD}\right) \\ p\psi_{rQ} &= \tfrac{L_r}{L_m}\left(v_{sQ} - R_s i_{sQ} - \sigma L_s p i_{sQ}\right) \end{aligned} \tag{5.3.1}$$

In order to achieve both estimated components of rotor fluxes $(\hat{\psi}_{rD}, \hat{\psi}_{rQ})$, the adaptive or adjustable model is used which is usually presented by the current model where the rotor voltage equation presents in terms of rotor speed and rotor current defined into the stationary reference frame. Both estimated values of rotor flux components expressed in terms of stator current and estimated rotor speed $(\hat{\omega}_r)$ can be written as

$$\begin{aligned} p\hat{\psi}_{rD} &= \tfrac{L_m}{T_r} i_{sD} - \tfrac{1}{T_r}\hat{\psi}_{rD} - \hat{\omega}_r \hat{\psi}_{rQ} \\ p\hat{\psi}_{rQ} &= \tfrac{L_m}{T_r} i_{sQ} - \tfrac{1}{T_r}\hat{\psi}_{rQ} + \hat{\omega}_r \hat{\psi}_{rD} \end{aligned} \tag{5.3.2}$$

The estimated rotor speed is generated from the adaptation mechanism in such a way so that the error between both rotor fluxes can be minimized in order to get the

better rotor speed estimation. This error or speed tuning signal can be written as

$$\varepsilon_\omega = \psi_{rQ}\hat{\psi}_{rD} - \psi_{rD}\hat{\psi}_{rQ} \tag{5.3.3}$$

In order to generate the estimated value of rotor speed in conventional rotor flux MRAS, this speed tuning signal is minimized through the constant gain PI-controller. However, the proposed speed estimation scheme replaces the PI-controller to the sliding mode based controller. Rotor speed estimation adaptation law for SMC based scheme is obtained based on the Lyapunov theory in order to ensure the stability and fast error dynamics [129]. By means of speed tuning signal defined in (5.3.3), the sliding surface s can be chosen as [129].

$$s = \varepsilon_\omega + \int k\varepsilon_\omega dt, \qquad k > 0 \tag{5.3.4}$$

In such a way that the error dynamics at the sliding surface $s = 0$ will be forced to exponentially decay to zero. The system reaches the sliding surface when

$$\dot{s} = \dot{\varepsilon}_\omega + k\varepsilon_\omega = 0 \tag{5.3.5}$$

Now the error dynamics can be defined by

$$\dot{\varepsilon}_\omega = -k\varepsilon_\omega \tag{5.3.6}$$

The SMC law can be defined by using the Lyapunov theory as well as defining the Lyapunov function candidate [151] as

$$v = \frac{1}{2}s^2 \tag{5.3.7}$$

According to the Lyapunov theory, if the function defined above $\dot{v}$ is negative definite, this condition will ensure that the state trajectory will be driven and attracted toward the sliding surface s, and once reached , it will remain sliding on it until the origin is reached asymptotically [151]. The time derivative of the Lyapunov function defined in (5.3.7) can be written as

$$\dot{v} = s\dot{s} = s(\dot{\varepsilon}_\omega + k\varepsilon_\omega) \tag{5.3.8}$$

Differentiating the speed tuning signal in (5.3.3)

$$\dot{\varepsilon}_\omega = \dot{\psi}_{rQ}\hat{\psi}_{rD} + \psi_{rQ}\dot{\hat{\psi}}_{rD} - \dot{\psi}_{rD}\hat{\psi}_{rQ} - \psi_{rD}\dot{\hat{\psi}}_{rQ} \tag{5.3.9}$$

Substituting the estimated rotor flux components from (5.3.2)

$$\begin{aligned}\dot{\varepsilon}_\omega = \dot{\psi}_{rQ}\hat{\psi}_{rD} - \dot{\psi}_{rD}\hat{\psi}_{rQ} + \frac{L_m}{T_r}i_{sD}\psi_{rQ} - \frac{1}{T_r}\hat{\psi}_{rD}\psi_{rQ} \\ - \frac{L_m}{T_r}i_{sQ}\psi_{rD} + \frac{1}{T_r}\hat{\psi}_{rQ}\psi_{rD} - \hat{\omega}_r(\psi_{rQ}\hat{\psi}_{rQ} + \psi_{rD}\hat{\psi}_{rD})\end{aligned} \tag{5.3.10}$$

By considering

$$\begin{aligned}A_1 = \dot{\psi}_{rQ}\hat{\psi}_{rD} - \dot{\psi}_{rD}\hat{\psi}_{rQ} + \frac{L_m}{T_r}i_{sD}\psi_{rQ} - \frac{1}{T_r}\hat{\psi}_{rD}\psi_{rQ} \\ - \frac{L_m}{T_r}i_{sQ}\psi_{rD} + \frac{1}{T_r}\hat{\psi}_{rQ}\psi_{rD}\end{aligned} \tag{5.3.11}$$

$$A_2 = \psi_{rQ}\hat{\psi}_{rQ} + \psi_{rD}\hat{\psi}_{rD} \tag{5.3.12}$$

(5.3.10) can be written in the simplified form as

$$\dot{\varepsilon}_\omega = A_1 - \hat{\omega}_r A_2 \tag{5.3.13}$$

Now (5.3.5) can be written as

$$\dot{s} = A_1 + k\varepsilon_\omega - \hat{\omega}_r A_2 \tag{5.3.14}$$

By substituting (5.3.13) into (5.3.8) yields

$$\dot{v} = s(A_1 + k\varepsilon_\omega - \hat{\omega}_r A_2) \tag{5.3.15}$$

The above defined derivative is negative definite if

$$(A_1 + k\varepsilon_\omega - \hat{\omega}_r A_2)\begin{cases} < 0, & \text{for } s > 0 \\ = 0, & \text{for } s = 0 \\ > 0, & \text{for } s < 0 \end{cases} \tag{5.3.16}$$

This can be ensured if

$$\hat{\omega}_r = \frac{A_1 + k\varepsilon_\omega}{A_2} + (M)\, sign\,(s)\,, \qquad M > 0 \tag{5.3.17}$$

where the sign function is defined as

$$sign(s) = \begin{cases} -1, & \text{for } s < 0 \\ +1, & \text{for } s > 0 \end{cases} \tag{5.3.18}$$

Here, equation (5.3.17) defines the switching law of the SMC and can be expressed in general form as

$$\hat{\omega}_r = u_1 + u_2 \tag{5.3.19}$$

where u_1 represents the equivalent control that actually defines the control action which keeps the state trajectory on the sliding surface. u_2 is the switching control that depends on the sign of the switching surface, and M is the hitting control gain which makes (5.3.8) a negative definite [151]. No design criteria is used to assign the value of M, however the value should be selected to make the manifold $s = 0$ in (5.3.4) [151], [96]. However, the control law defined in (5.3.17) will ensure the existence of the switching surface s in (5.3.4), and when the error function ε_ω reaches the sliding surface , the system dynamics will be governed by (5.3.6), which is always stable [140].

The expression for the equivalent control and switching control function can be expressed as

$$u_1 = \frac{A_1 + k\varepsilon_\omega}{A_2} \tag{5.3.20}$$

$$u_2 = (M)\, sign\,(s)\,, \qquad M > 0 \tag{5.3.21}$$

In the equivalent control u_1 expression, the function A_2 in the denominator may cause some problems in the estimation performance of the proposed scheme if its value approaches to zero. This problem can be avoided by magnetizing the machine before starting up and by adding a very small value to the A_2. In the proposed rotor flux SMC-MRAS, the speed component in (5.3.19) can be expressed as a pre-processed rotor speed component as

$$\omega_{rp} = u_1 + u_2 \tag{5.3.22}$$

In the second loop reference and estimated torque differences are used at the same time in order to improve the speed estimation performance of observer. According to the motor motion equation it can be written as

$$T_e - T_l = J\frac{d\omega_r}{dt} + f\omega_r \tag{5.3.23}$$

The motor electromagnetic torque can be expressed as

$$T_e = \frac{PL_m}{L_r}(i_{sQ}\psi_{rD} - i_{sD}\psi_{rQ}) \tag{5.3.24}$$

In case of unknown load torque and viscous coefficient f then (5.3.23) can be written as

$$T_e - T = J\frac{d\omega_r}{dt} \tag{5.3.25}$$

where, $T = T_l + f\omega_r$

By means of reference fluxes (ψ_{rD}, ψ_{rQ}), the reference electromagnetic torque can be written as

$$T_e = \frac{PL_m}{L_r}(i_{sQ}\psi_{rD} - i_{sD}\psi_{rQ}) \tag{5.3.26}$$

Now the expression for estimated electromagnetic torque can be written with the help of estimated rotor fluxes ($\hat{\psi}_{rD}, \hat{\psi}_{rQ}$)

$$\hat{T}_e = \frac{PL_m}{L_r}(i_{sQ}\hat{\psi}_{rD} - i_{sD}\hat{\psi}_{rQ}) \tag{5.3.27}$$

The motion expression presented in (5.3.23) explains the mechanical dynamic part of an electric motor. This equation clearly explains that the variation in a load torque results in the variation of motor speed and this variation or change will continue until the steady state condition appears or motor electromagnetic torque becomes equal to the load torque.

On behalf of the same principle, a variation in an estimated torque results in the variation or change in estimated speed of motor and this change or variation will continue until the steady state condition appears or estimated torque becomes equal to the motor electromagnetic torque. With the help of motor mechanical equation

(5.3.23), the electromagnetic torque and the motor speed can be written in their estimated expression as

$$\hat{T}_e - T_l = J\frac{d\hat{\omega}_r}{dt} + f\hat{\omega}_r \tag{5.3.28}$$

By subtracting the (5.3.28) from (5.3.23), the following expression can be obtained

$$\tau_o = T_e - \hat{T}_e = J\frac{d(\omega_r - \hat{\omega}_r)}{dt} + f(\omega_r - \hat{\omega}_r) \tag{5.3.29}$$

Finally, rotor estimated speed can be written as

$$\hat{\omega}_r = \omega_{rp} + \tau_o \tag{5.3.30}$$

The expression presented in (5.3.29) reveals the purpose of utilization of this second torque loop, because the difference between both torques estimated and reference appears when the rate of change in estimated speed appears from the reference speed under transient or load disturbance condition. In order to improve the observer speed estimation performance under load disturbance or robustness against the load variation, this torque difference is added in the conventional rotor flux loop.

5.4 Simulation Results and Analysis

In this section the operational performance analysis and comparison of both PI-MRAS and SMC-MRAS are presented. Different simulations tests are performed by using different speed and torque profiles which are usually required in vehicle operation. In all tests, different speed levels and percentages of rated load torque are used to examine the operational performance of both observers. An indirect vector control method is implemented to control the operation of IM traction drive.

Simulation results presented in this section show the satisfactory speed estimation performance and the proposed SMC-MRAS observer structure is verified through different simulation tests. For this purpose, a 4-pole and 200 watt induction machine is used, whereas the detail of induction machine parameters are already

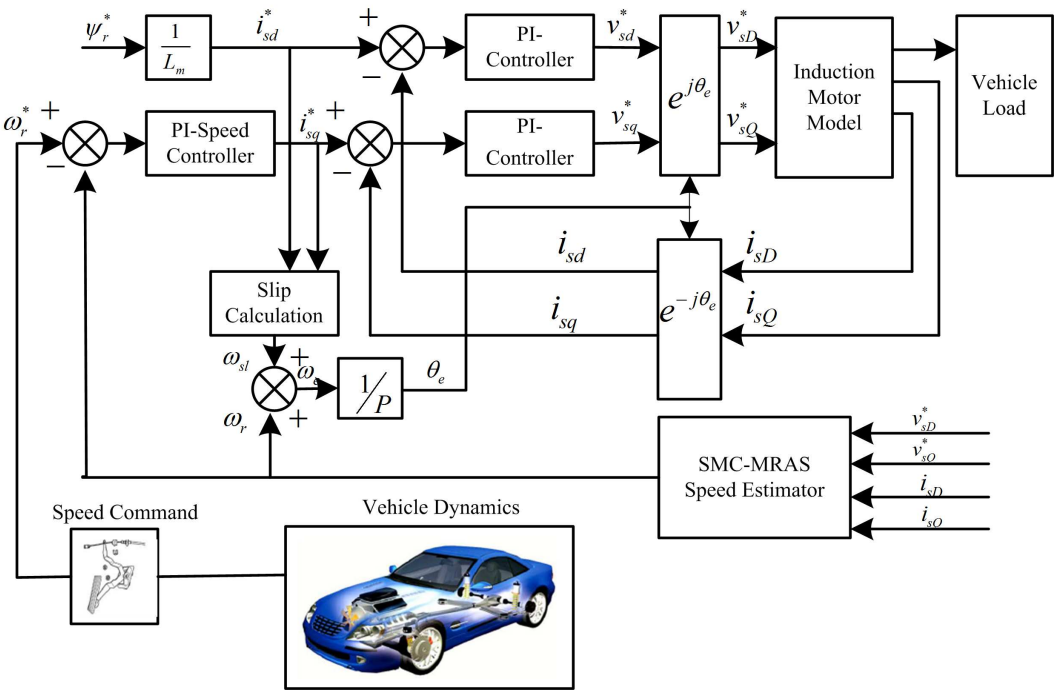

Figure 5.3: Block diagram of speed sensorless indirect vector control of induction motor traction drive by using SMC-MRAS speed estimator

given in Table 4.2. Induction machine is modelled using two axis theory or $d-q$ axis theory as discussed in chapter 3.

By using simulink library blocks in Matlab-Simulink environment, a speed sensorless indirect vector control method based-IM traction drive system is developed. Induction machine $d-q$ model is directly fed through the reference voltages, therefore, an ideal inverter operation as well as pulse width modulator are considered in all simulations. In both PI-MRAS and SMC-MRAS, reference model is solved using pure integration and there is no drift and initial condition issues are considered in the simulation tests. It should be noted that in order to compare the operational performance difference between both observers, the PI controller gains used in the vector control blocks are the same during all simulations. Fig. 5.3 illustrates the basic block diagram of SMC-MRAS speed sensorless indirect vector control of induction motor traction drive system.

Understanding of operational performance effectiveness of the proposed speed observer as compare to the PI-based MRAS, different tests are designed with respect to the observer application specifically which are important in EV operation. During the vehicle operation, it is important to follow the speed limits, avoid collisions and to start, accelerate, decelerate and stop when it is required. Vehicle speed operation is adjusted by two main controls, the first one is accelerator, which controls the driving torque or operational twisting force, and the second one is brake, which adjusts the load torque. These both controls are important for vehicle safe operation, and vehicle driver has to maintain a required speed operation even in the condition of load torque variation, during different operating circumstances such as an uphill, downhill or strong wind conditions. In all these tests, observer speed regulation response, speed tracking error, speed estimation error, convergence of speed tuning signal under different load conditions etc are considered for performance comparison. The following tests are presented in this section and performance is compared with the PI-MRAS.

5.4.1 Load disturbance rejection capability of observer at different rated load torque

This test is performed to understand the load disturbance rejection capability of the proposed SMC-MRAS speed observer. During the test, different values of rated load torque are used at different speed levels during the motor operation. In this test, it is desired to get the SMC-speed observer response close to the actual motor speed under different load torque conditions. However, this is one of the most important tests for proposed observer performance analysis. Since, during the vehicle operation, applied load torque is very uncertain due to different road conditions and aerodynamic effects which continuously change the net load torque effect on the traction drive. The performance of proposed observer is compared with the PI-MRAS speed observer.

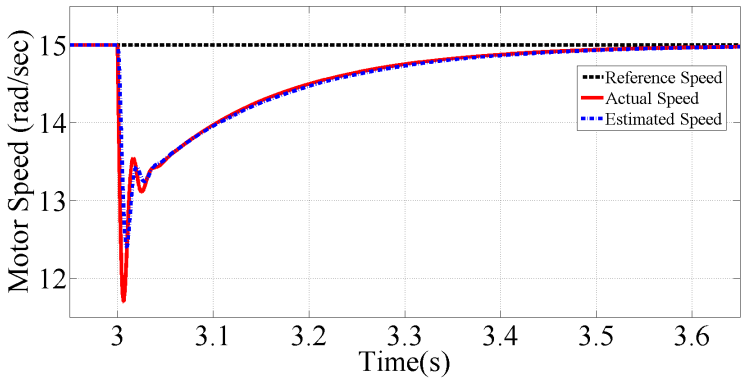

(a)

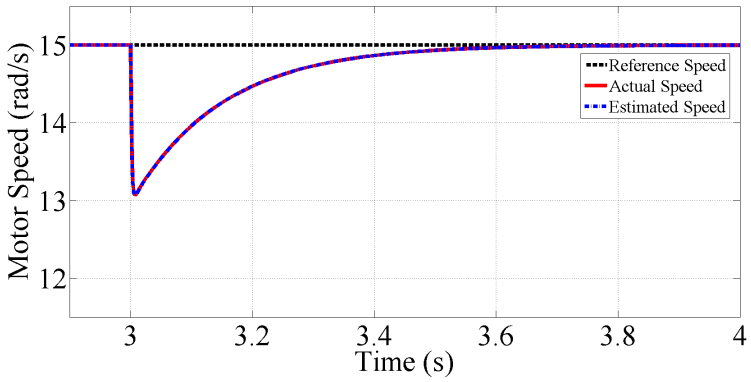

(b)

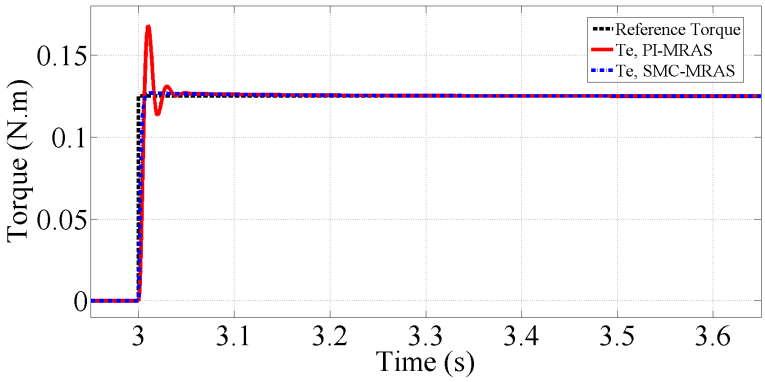

(c)

Figure 5.4: Speed estimation performance of Observer for 25% rated load disturbance rejection capability at 15 rad/sec motor speed. 5.4(a) PI-MRAS. 5.4(b) SMC-MRAS 5.4(c) Motor electromagnetic torque T_e response.

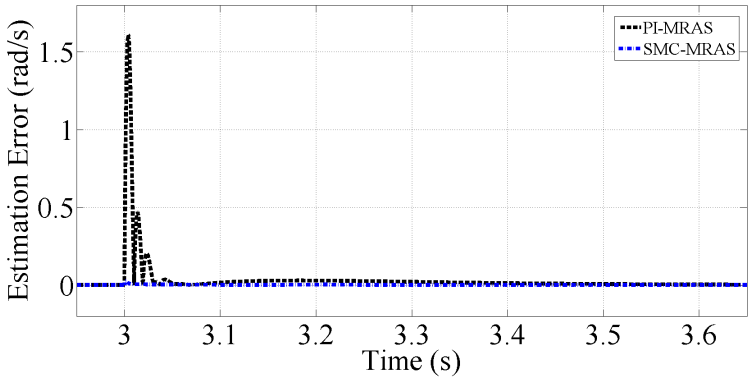

(a)

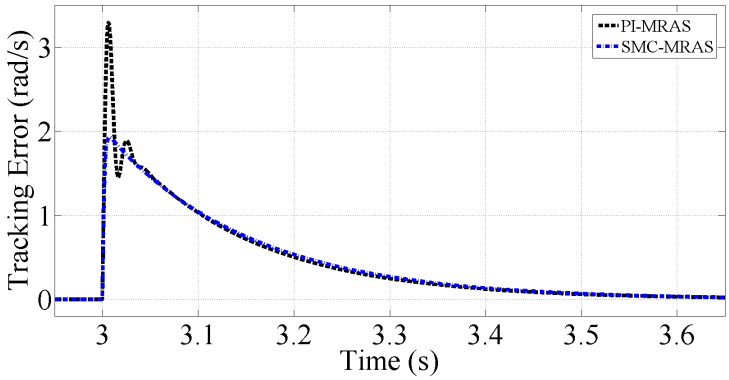

(b)

Figure 5.5: Absolute error of estimation speed and tracking speed at 15 rad/sec with 25% rated load disturbance at $t = 3s$. 5.5(a) Speed estimation error. 5.5(b) Speed tracking error.

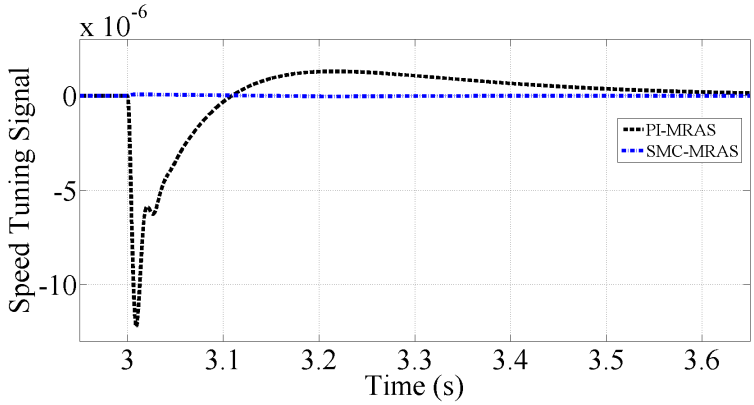

Figure 5.6: Speed tuning signal for 25% rated load disturbance at 15 rad/sec motor speed.

Load disturbance rejection capability of observer at 15 rad/sec motor speed with applied 25% rated load disturbance:

In this test induction motor is operated at command speed 15 rad/sec so as to analyse the performance of observer, whereas 25% rated step load torque is applied at $t = 3s$. Proposed speed observer performance is analysed in terms of speed regulation response, speed estimation error, speed tracking error and speed tuning or error signal. Simulation results show better load disturbance rejection capability of proposed SMC-MRAS over PI-MRAS scheme. In case of PI-MRAS 22% and 5.98% tracking error and estimations error are obtained respectively while in case of SMC-MRAS 12.84% and 0.33% tracking error and estimations error are achieved respectively. However, the relative tracking and estimation errors are 9.16% and 5.65% respectively.The transient response or dynamic response of the proposed scheme is faster and show better error dynamics than the conventional PI based scheme. Optimal speed tuning or error signal is obtained in the proposed scheme with fast convergence to zero in the transient state. Fig.5.4 shows the speed regulation response and motor electromagnetic torque response by using both SMC-MRAS and PI-MRAS schemes. Whereas, Fig.5.5 illustrates the speed estimation error along with speed tracking error and Fig.5.6 speed tuning or error signal response after load torque disturbance.

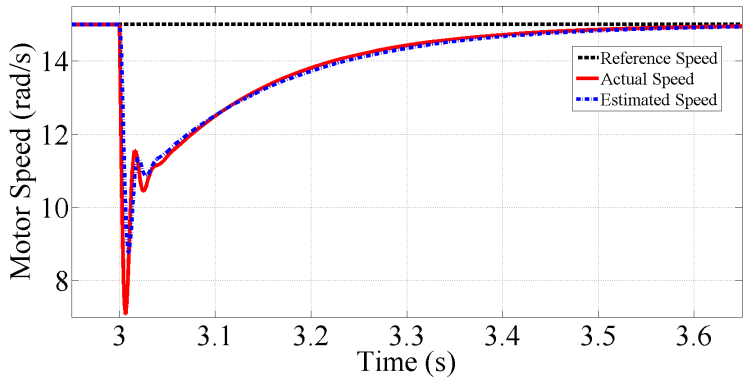

(a)

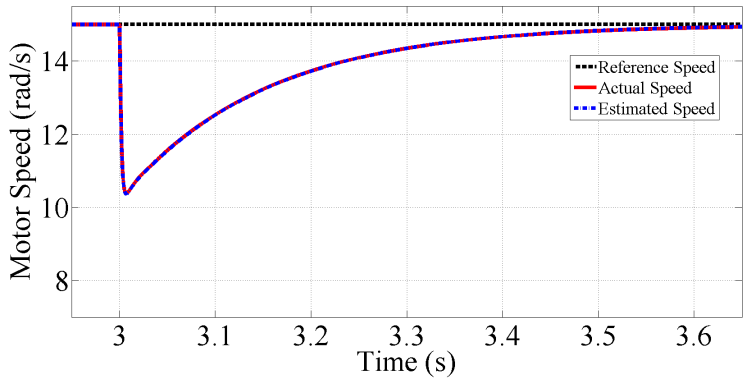

(b)

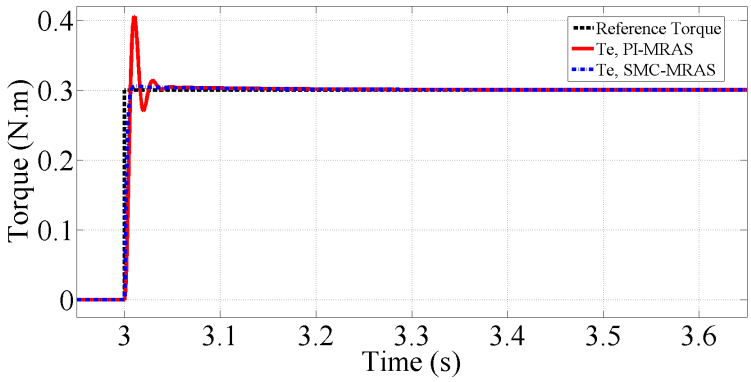

(c)

Figure 5.7: Speed estimation performance of Observer for 60% rated load disturbance rejection capability at 15 rad/sec motor speed. 5.7(a) PI-MRAS. 5.7(b) SMC-MRAS 5.7(c) Motor electromagnetic torque T_e response.

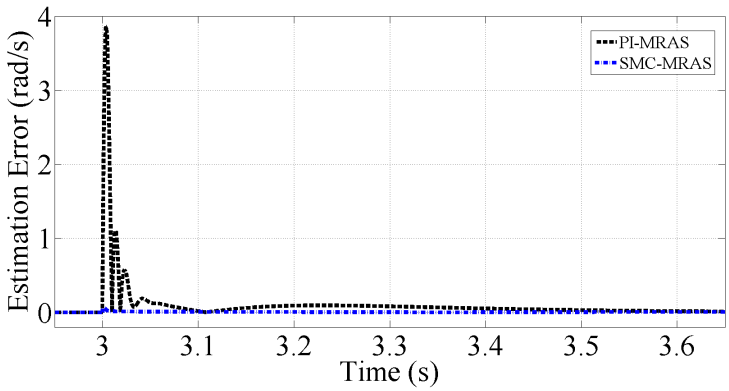

(a)

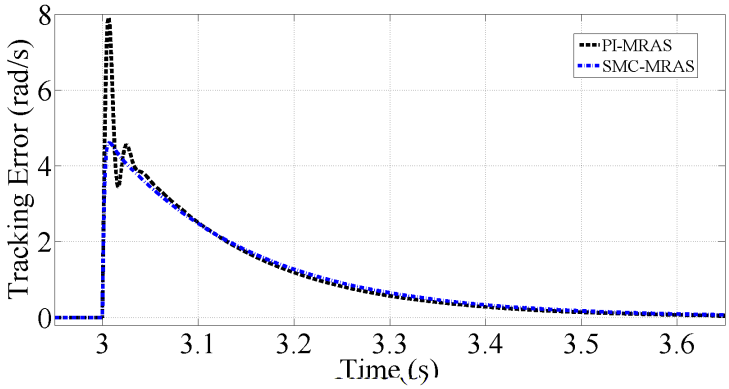

(b)

Figure 5.8: Absolute error of estimation speed and tracking speed at 15 rad/sec with 60% rated load disturbance at $t = 3s$. 5.8(a) Speed estimation error. 5.8(b) Speed tracking error.

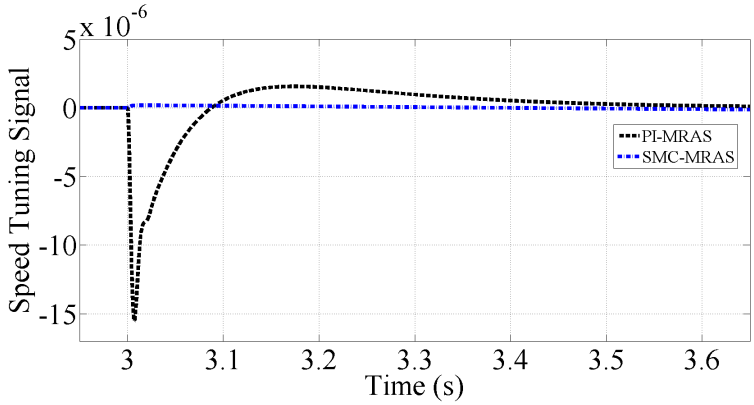

Figure 5.9: Speed tuning signal for 60% rated load disturbance at 15 rad/sec motor speed.

Load disturbance rejection capability of observer at 15 rad/sec motor speed with applied 60% rated load disturbance:

The proposed observer load disturbance rejection capability test is also performed at 15 rad/sec motor speed with applied 60% rated load torque disturbance at $t = 3s$. Even at higher applied rated load torque, the proposed algorithm provides much smaller values of speed estimation and tracking error and better performance as compare to PI based scheme is obtained. In case of PI-MRAS 52.79% and 24.98% tracking error and estimations error are obtained respectively when the load disturbance is applied at $t = 3s$ while in case of SMC-MRAS 30.75% and around 1% tracking error and estimations error are achieved respectively. However, the relative tracking and estimation errors are 22.04% and 23% respectively. Fig.5.7, Fig.5.8 and Fig.5.9 show the speed regulation response, speed estimation & tracking error and speed tuning signal at 15 rad/sec motor speed with applied 60% rated load disturbance.

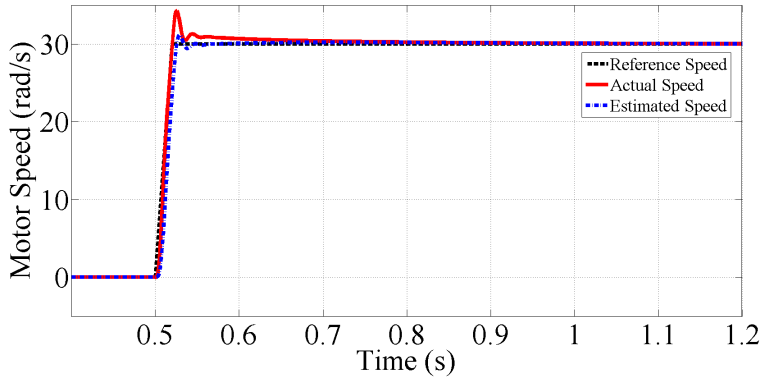

(a)

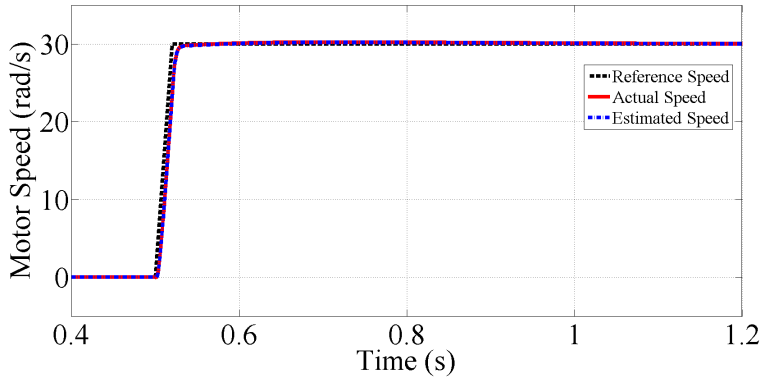

(b)

Figure 5.10: Speed estimation performance of Observer during quick speed change from zero speed level to 30 rad/sec motor speed. 5.10(a) PI-MRAS. 5.10(b) SMC-MRAS.

5.4.2 Quick acceleration or sudden speed change performance of observer

This test is performed to understand the quick acceleration and quick speed change performance of the proposed SMC-MRAS observer. This test is required to analyse the performance of vehicle at cruising and in start operation with quick speed change or quick acceleration mode. The motor speed response should be as close as to the reference speed and in the similar way the speed estimation of observer should be closer to the actual motor speed.

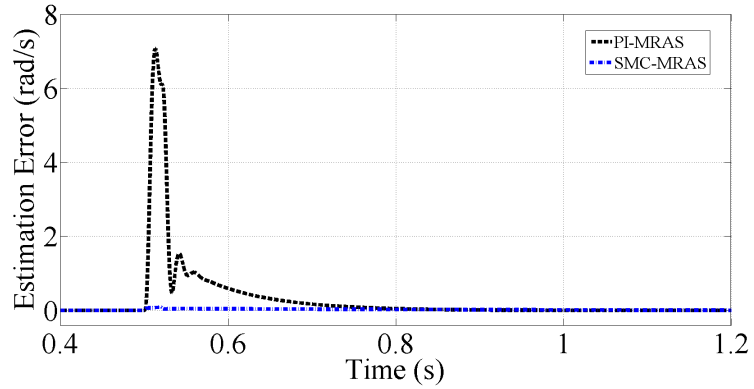

(a)

Figure 5.11: Absolute error of estimation speed during quick speed change at $t = 0.5s$.

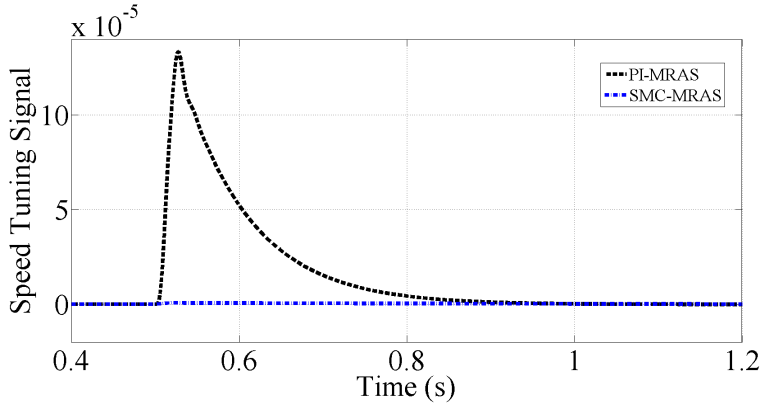

Figure 5.12: Speed tuning signal for quick speed change of 30 rad/sec motor speed.

For this test a quick speed change is applied from zero to 30 rad/sec at $t = 0.5s$. In the proposed SMC-MRAS scheme, the motor actual speed is less deviated from the reference speed and provides fast transient response with minimal speed estimation error over PI-MRAS. Fig.5.10, Fig.5.11 and Fig.5.12 illustrate the speed regulation response, absolute speed estimation error and speed tuning signal during sudden speed change point.

5.4.3 Observer performance during Un-smooth road condition or with time varying load disturbance

This test is performed to understand the performance of proposed SMC-MRAS observer under time varying load torque disturbance condition. It is clearly understood that the whole motoring operation or in different driving conditions, it is impossible for traction drive to face a fixed kind of load torque. Because the net vehicle load torque changes with road conditions and different aerodynamic effects. It is important that the proposed observer should be able to provide a satisfactory performance during time varying load condition.

Performance of the proposed SMC-MRAS observer is measured with 40 rad/sec command speed at 20% rated load torque. For un-smooth road condition, a saw-tooth shape from 20% to 50% rated load torque is applied between $t = 2.5s$ and $t = 4s$ which provides first linearly increase and sudden load torque drop. Similar performance is obtained in steady state before $t = 2.5s$ but during the transient mode the speed regulation performance of proposed SMC-MRAS observer is much improved with minimal speed estimation and tracking error as shown in Fig.5.13 and Fig.5.14. Achieved optimal speed tuning signal during this un-smooth road condition is shown in Fig.5.15.

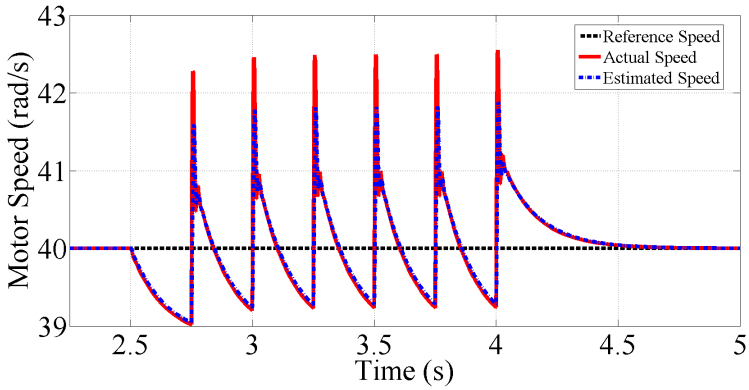

(a)

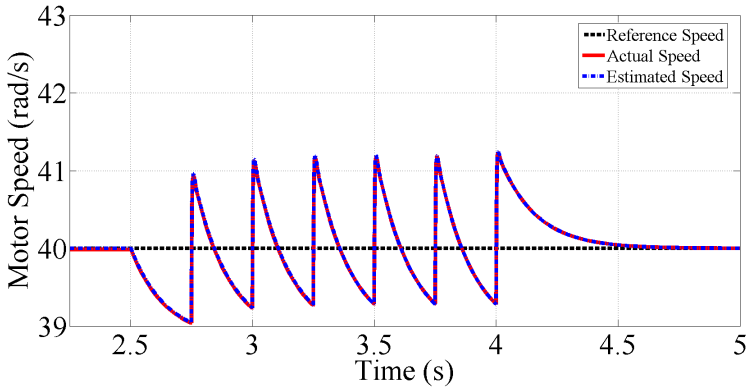

(b)

Figure 5.13: Speed estimation performance of Observer during un-smooth road condition at 40 rad/sec motor speed. 5.13(a) PI-MRAS. 5.13(b) SMC-MRAS.

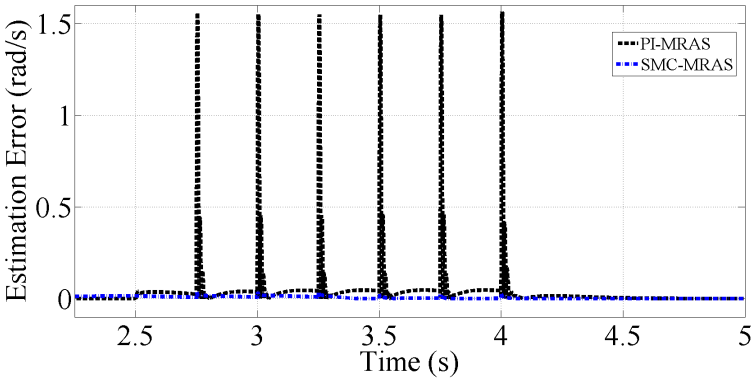

(a)

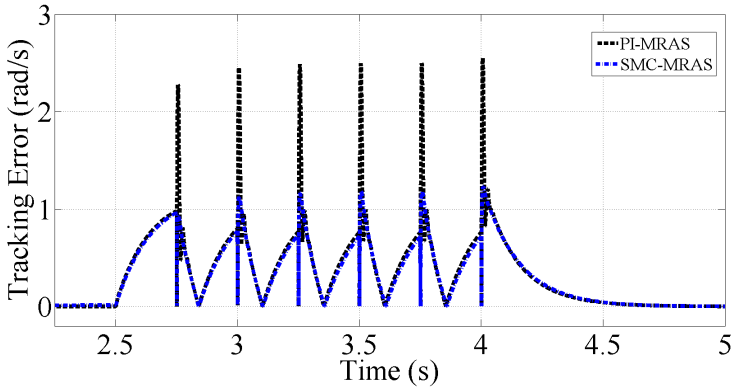

(b)

Figure 5.14: Absolute error of estimation speed and tracking speed during un-smooth road condition. 5.14(a) Speed estimation error. 5.14(b) Speed tracking error.

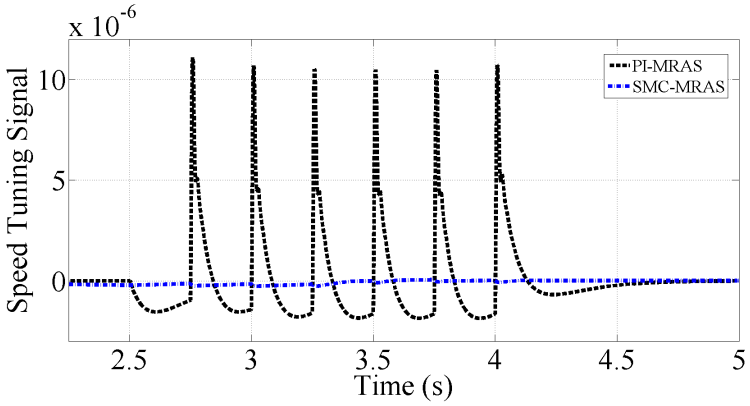

Figure 5.15: Speed tuning signal during un-smooth road condition.

5.4.4 Motor speed transition from positive to negative and vice versa at different load disturbance conditions

This test is performed to analyse the operational performance of proposed SMC-MRAS speed observer when different speed change appears under certain vehicle load torque conditions. In vehicle operation, this speed change could happen in any quadrant of the following mode of operation as shown in Fig. 4.26. In this test different speed commands from high level positive to low positive speed and motor speed transition from positive speed to negative and vice versa conditions are used. In all cases the proposed SMC-MRAS provides the improved speed regulation response with minimal speed estimation, tracking error and tuning signal under different load conditions.

Motor speed transition from high to low positive speed with 60% rated load disturbance:

In this test a command speed is applied from 40 rad/sec to 10 rad/sec with 60% rated load torque applied at $t = 3s$. Fig.5.16, Fig.5.17 and Fig.5.18 show the motor speed regulation, speed estimation & tracking errors and speed tuning signal respectively under speed transition from high to low positive speed with 60% rated load disturbance.

Motor speed transition from positive to negative with 60% rated load disturbance at $t = 3s$:

For this test a reference speed is applied from 50 rad/sec to -50 rad/sec with 60% step rated load torque applied at $t = 3s$. Fig.5.19, Fig.5.20 and Fig.5.21 present the motor speed regulation response, speed estimation & tracking errors and speed tuning signal respectively under speed transition from positive to negative speed command with 60% rated load disturbance condition.

Motor speed transition from negative to positive with 60% rated load disturbance at $t = 3s$:

In this case a reference speed is applied from -50 rad/sec to 50 rad/sec with 60%

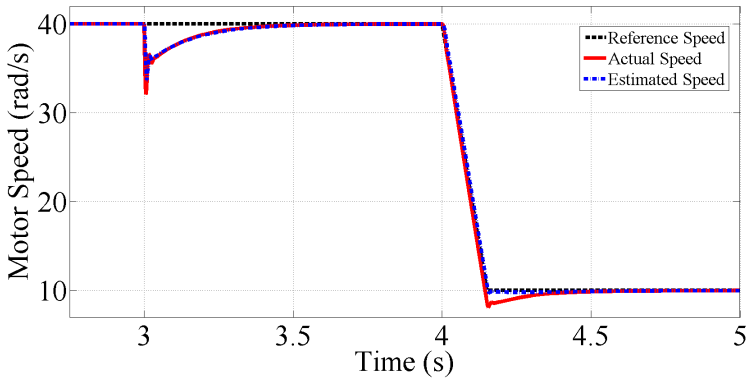

(a)

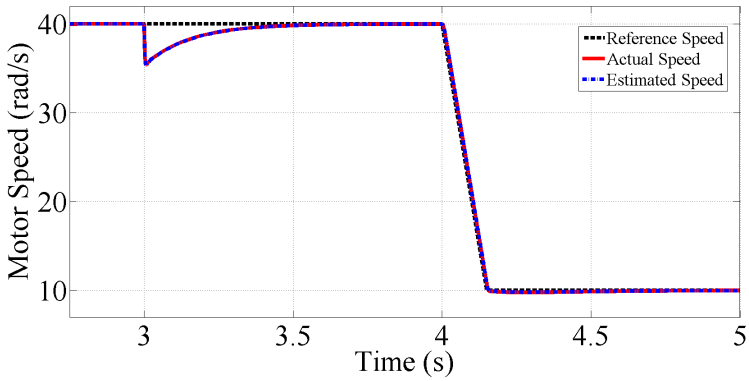

(b)

Figure 5.16: Speed estimation performance from 40 rad/s to 10 rad/s speed transition with 60% rated load disturbance. 5.16(a) PI-MRAS. 5.16(b) SMC-MRAS.

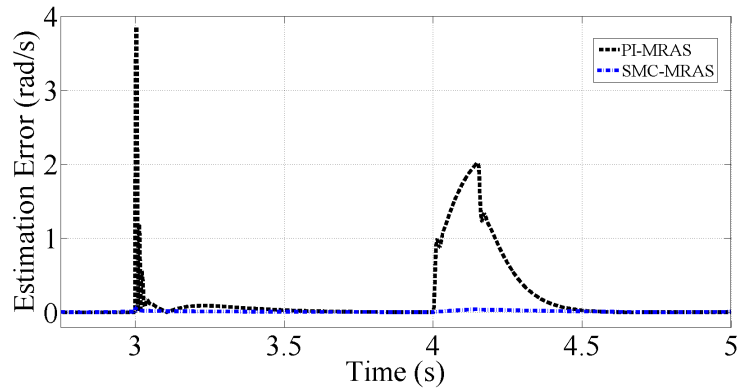

(a)

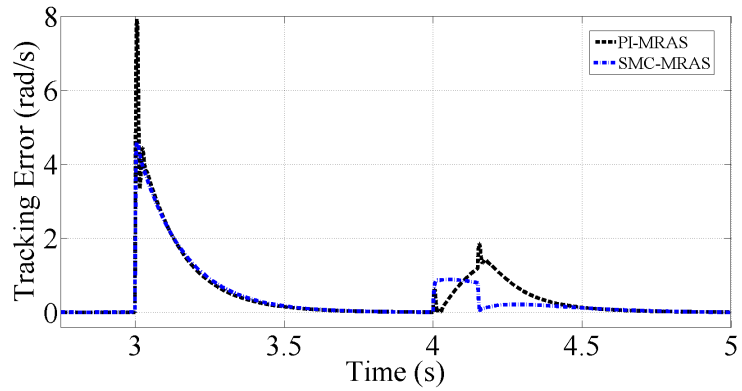

(b)

Figure 5.17: Absolute error of estimation speed and tracking speed during speed 40 rad/s to 10 rad/s speed transition. 5.17(a) Speed estimation error. 5.17(b) Speed tracking error.

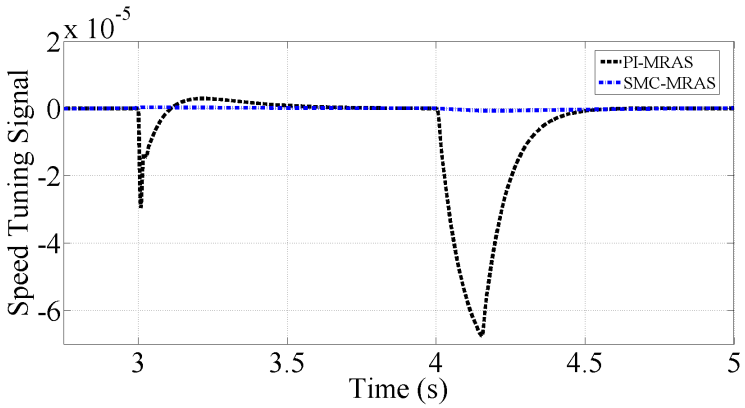

Figure 5.18: Speed tuning signal during high to low positive speed transition.

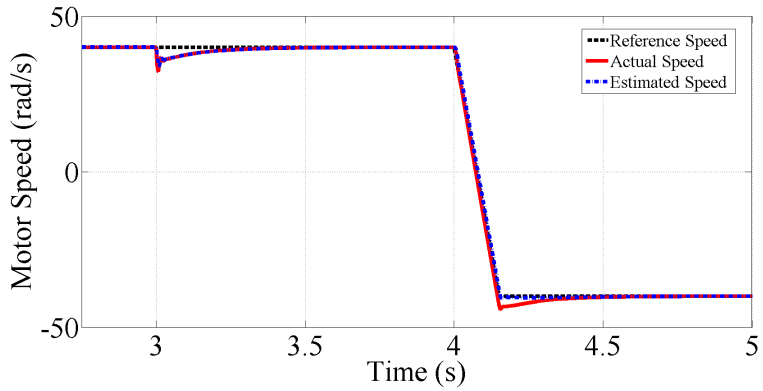

(a)

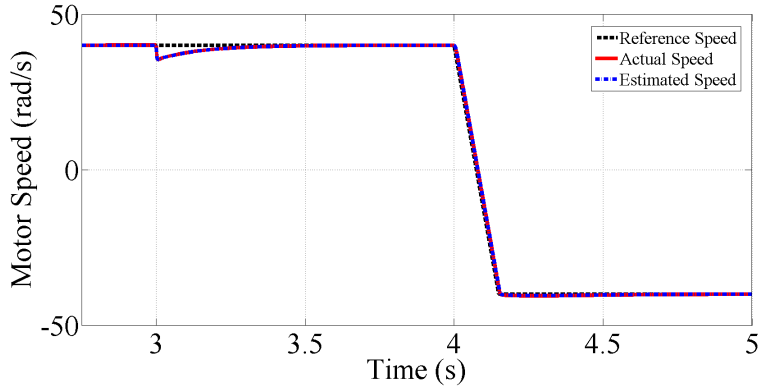

(b)

Figure 5.19: Speed estimation performance from 40 rad/s to -40 rad/s speed transition with 60% rated load disturbance at $t = 3s$. 5.19(a) PI-MRAS. 5.19(b) SMC-MRAS.

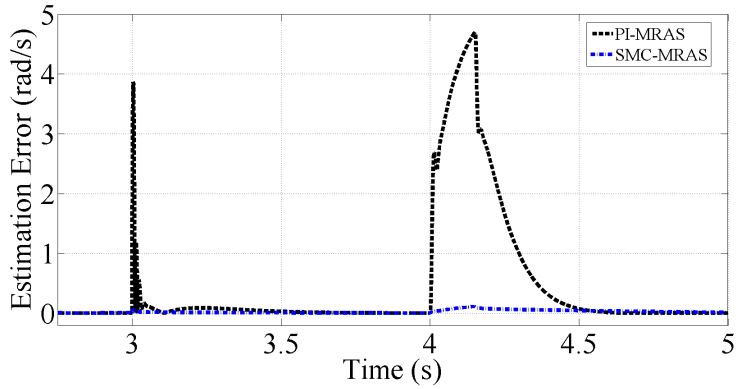

(a)

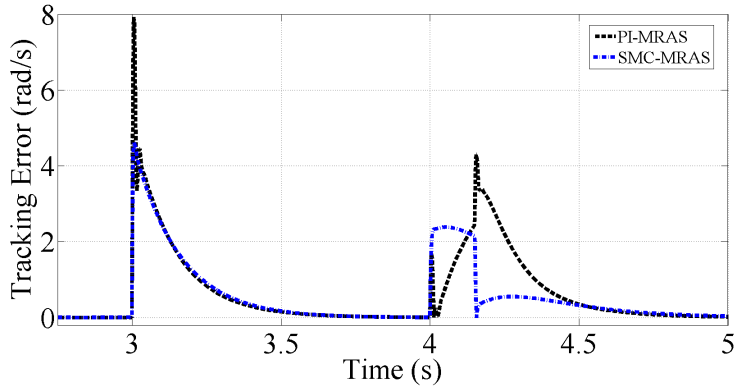

(b)

Figure 5.20: Absolute error of estimation speed and tracking speed during speed +40 rad/s to -40 rad/s speed transition. 5.20(a) Speed estimation error. 5.20(b) Speed tracking error.

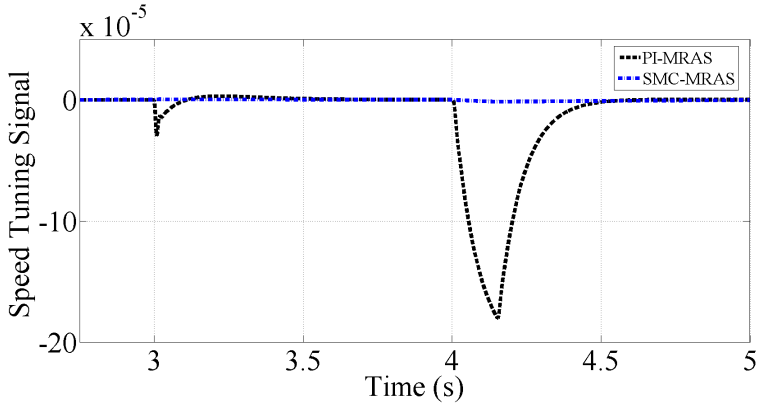

Figure 5.21: Speed tuning signal from positive to negative speed transition.

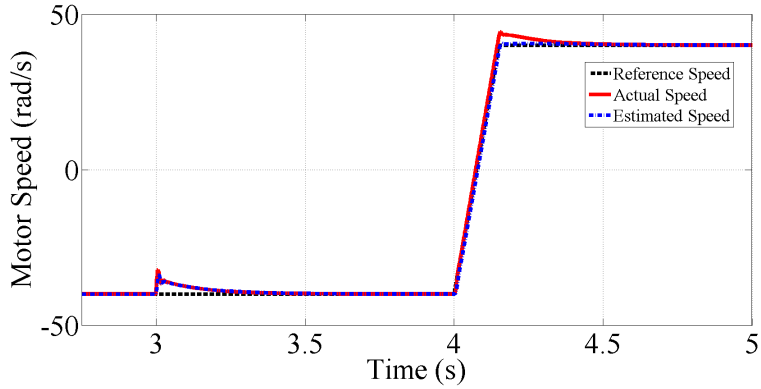

(a)

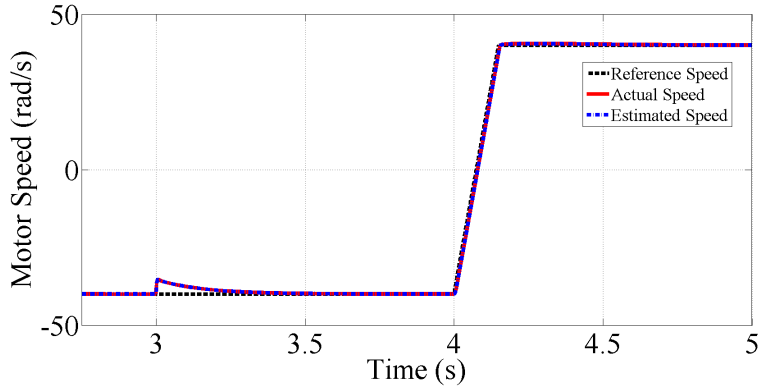

(b)

Figure 5.22: Speed estimation performance from -40 rad/s to +40 rad/s speed transition with 60% rated load disturbance at $t = 3s$. 5.22(a) PI-MRAS. 5.22(b) SMC-MRAS.

step rated load torque applied at $t = 3s$. Fig.5.22, Fig.5.23 and Fig.5.24 show the motor speed regulation performance, speed estimation & tracking errors and speed tuning signal respectively under speed transition from negative to positive speed command with 60% step rated load disturbance condition.

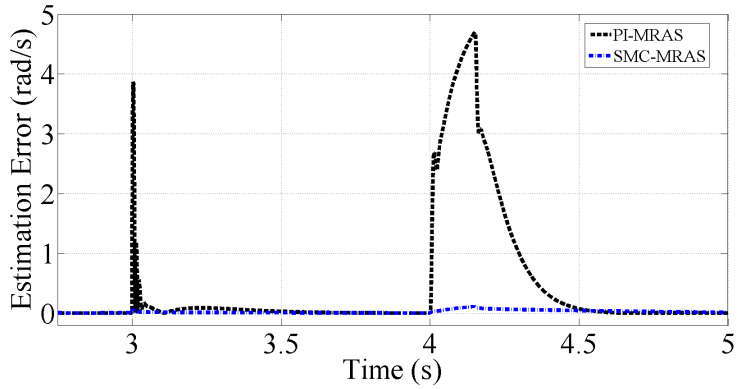

(a)

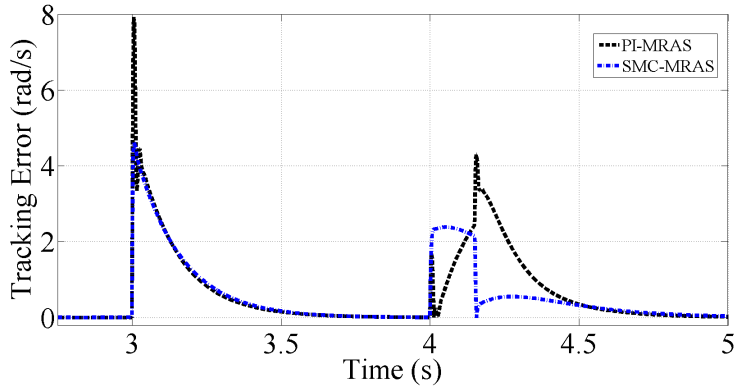

(b)

Figure 5.23: Absolute error of estimation speed and tracking speed during -40 rad/s to +40 rad/s speed transition. 5.23(a) Speed estimation error. 5.23(b) Speed tracking error.

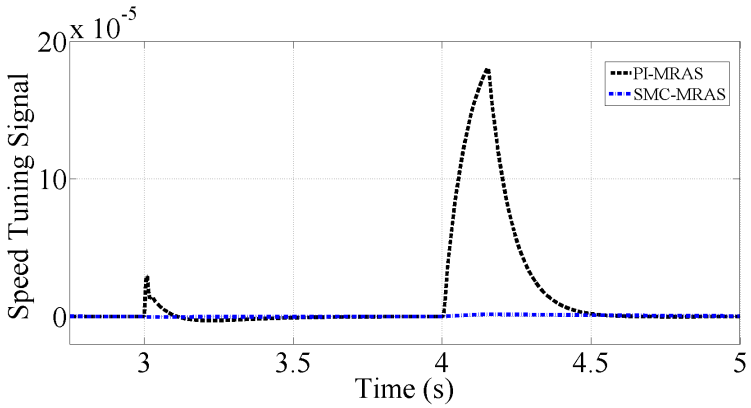

Figure 5.24: Speed tuning signal from positive to negative speed transition.

5.5 Conclusion

In this chapter a novel sliding mode control based rotor flux model reference adaptive system speed observer has been presented. This proposed observer replaces the fixed gain PI controller which is normally used in conventional rotor flux MRAS observer. This observer uses two differences at the same time, reference and estimated rotor fluxes like conventional rotor flux MRAS as well as reference and estimated electromagnetic torques in order to improve the speed estimation specifically in load torque disturbance condition, an important feature during vehicle speed sensorless operation due to uncertain load disturbance condition. This SM scheme is derived based on the Lyapunov theory to ensure the system stability as well as fast error dynamics. Switching surface or sliding surface is defined with the help of speed tuning signal in the designed SMC. However, the motion stability of state trajectories are ensured by using the Lyapunov function candidate. Different simulation cases are designed with respect to the vehicle operation and applied by using indirect vector control induction motor drive. In all simulation cases the performance of proposed SMC-MRAS is compared to the PI-MRAS observer. The proposed scheme shows much better transient performance, fast error dynamics as well as better load torque disturbance rejection capability and presents a good solution for speed sensorless IM traction drive.

Chapter 6

Experimental Validation and Analysis

6.1 Introduction

THE DSP-based electric-drives system is used in order to perform practical testing and the real time implementation of the proposed speed observer schemes. DSP-based electric-drives system used for the experimental purpose, has four major components. The following four major components include : 1) Motor coupling system, 2) Power Electronics Drive Board, 3) DSP based DS1104 R& D controller card and CP 1104 I/O board and 4) MATLAB Simulink and Control-desk. A 200W induction machine experimental platform along with a dSPACE DS1104 controller board is used to validate the proposed schemes. Induction motor parameters and ratings used for the experiments have already mentioned in Table.4.2. The architecture or schematic diagram of experimental system is shown in Fig. 6.1 [6] whereas Fig. 6.2 illustrates the real time implementation of the hardware setup.

In the following section, introduction and the role & operation of four components listed above in the DSP-based electric-drives system will be discussed briefly.

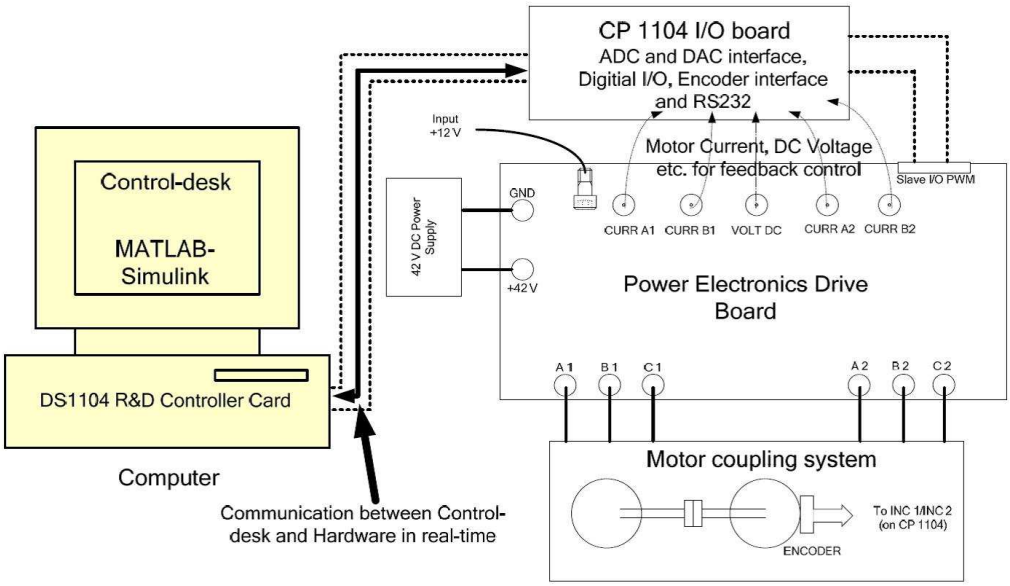

Figure 6.1: Schematic diagram of DSP-based electric drive experimental system [6]

The communication among these four components are discussed and how these units work together while controlling the speed and torque of the motor. Then the experimental performance of PI-MRAS observer and the estimation performance of proposed both schemes FLC-MRAS & SMC-MRAS will be presented by using different speed driving profiles and load torques.

6.2 The Experimental System

The DSP-based electric-drives system has following four major components.

6.2.1 Motor coupling system

This system consists of the motor that needs to be characterized or controlled and in this case induction motor is used. By means of mechanical coupling arrangement, two different motors can be coupled to each other. The motor under test (MUT) or whose speed and torque characteristics need to be controlled, could be

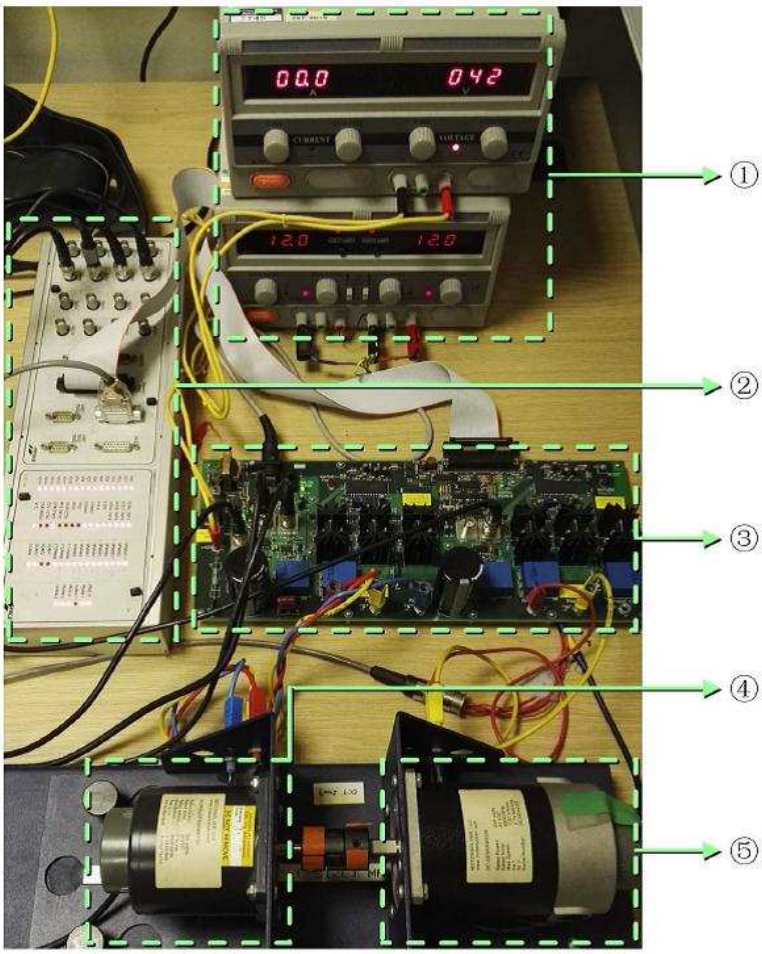

① DC power supply
② dSPACE CLP1104 control panel
③ MOSFET based power electronics board
④ Controlled target induction motor
⑤ Load DC motor

Figure 6.2: Real time DSP-based induction motor drive experimental system

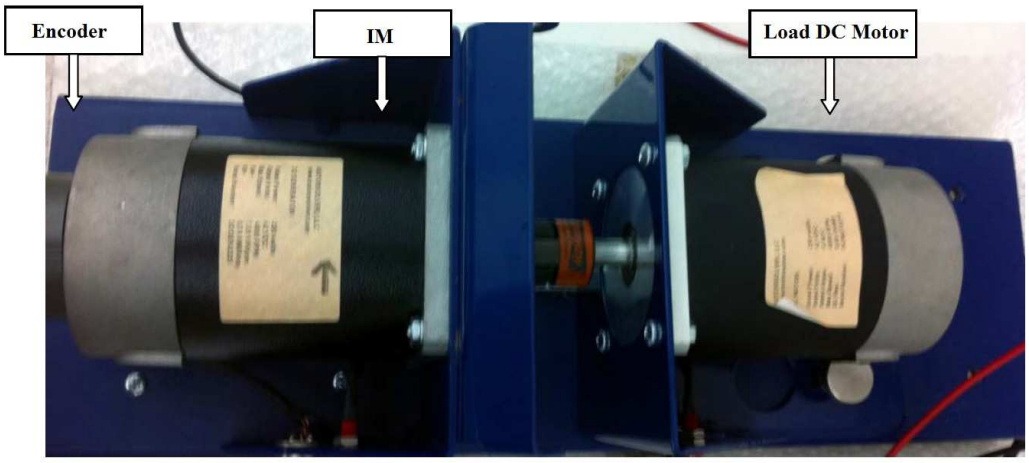

Figure 6.3: Motor Coupling System showing Induction Motor, Load DC Motor and Encoder

either a DC motor or a Three-phase induction motor or a Three-phase Permanent-Magnet AC (PMAC) motor. In the experiment, a DC load motor is connected to the shaft of IM to provide a load torque condition. The DC motor is connected in the separately excited configuration in order to control the speed and torque control of motor separately. In order to measure the speed of MUT, an encoder is mounted on the machine. This speed information can be used for close loop feedback speed-control of the motor. The motor is operated by the controlled pulse-width-modulated (PWM) voltage to run at controlled speed or torque. The generated PWM voltage from the Power Electronics Drive Board which will be explained in the next section, is connected to the motor coupling unit as shown in Fig 6.3.

6.2.2 Power Electronics Drive Board

This power electronic board is capable of generating two independent PWM voltage sources (A1B1C1 and A2B2C2) from a constant 42-volt DC source. Since, there are two independent three phase PWM inverters, hence two different machines coupled in the motor coupling system can be controlled independently for indepen-

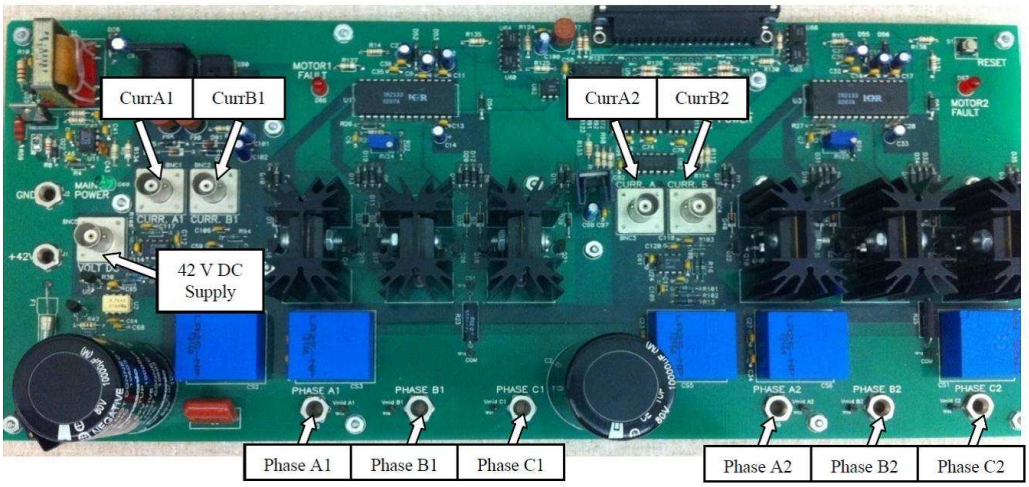

Figure 6.4: Power electronic drive board with indicated key labels

dent control of motor operation at the same time. Fig. 6.4 shows the power electronic drive board used for the experimental purpose. This controller board also provides the motor phase currents, dc-bus voltage etc in order to control the motor for a required speed or torque operation. This electronic board uses several digital control signals so as to generate the controlled PWM voltage source. These control signals indicate the magnitude and phase of the PWM voltage source. These controlled signals are generated by the DS1104 R& D Controller board that is installed inside the computer.

6.2.3 DS1104 R & D controller Board and CP 1104 I/O board

This DS1104 controller board takes some actions in order to produce the digital control signals. These actions are taken on the basis of executed programme in this board by means of MATLAB-Simulink real-time interface. This board monitors the input of motor such as motor current, speed and voltage etc with the help of CP1104 I/O board as shown in Fig. 6.5 in each sampling time. This board generates the controlled digital signals according to the inputs and the variables need to be

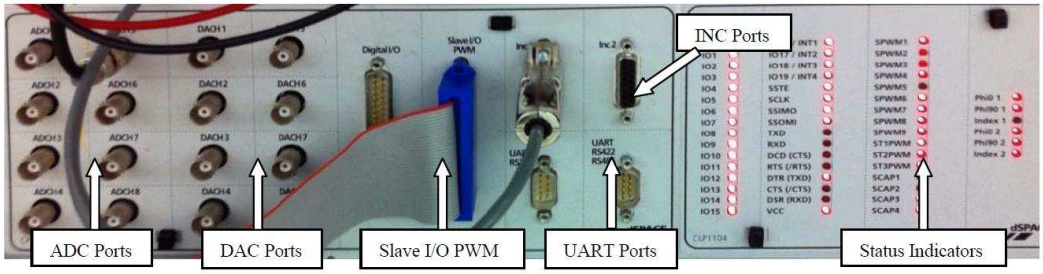

Figure 8: CP 1104 Board

Figure 6.5: CP1104 I/O board

controlled such as motor speed and torque. CP1104 I/O board is an input-output interface board which provides the interface between power electronic drive board and DS1104 controller board installed inside the computer. This interface board receives different analog signals from the power electronic board such as motor current and DC-voltage etc to its ADC port and speed signal from the mounted encoder to the INC port for the DS1104 controller board. Similarly, the controlled digital signals are forwarded to the power electronic converter board through the same CP1104 board.

6.2.4 MATLAB Simulink and Control-desk

Matlab-Simulink software is used to generate the model-based design such as in our case speed sensorless indirect vector control of IM drive by using proposed MRAS speed observers. All I/O ports of the CP1104 interface board can be accessed through the Simulink library browser. After building the Simulink control-system (pressing CTRL+B) by using real-time option, it implements the whole designed system inside DS1104 board, i.e. the control system that was earlier in software (Matlab-Simulink) gets converted into a real-time system on hardware (DS1104). Simulink generates a code file when you build (CTRL+B) the control system. This file provides the access to the variables of control-system (like reference speed, gain, tuning the controller etc) to separate software called Control-desk. In this software a

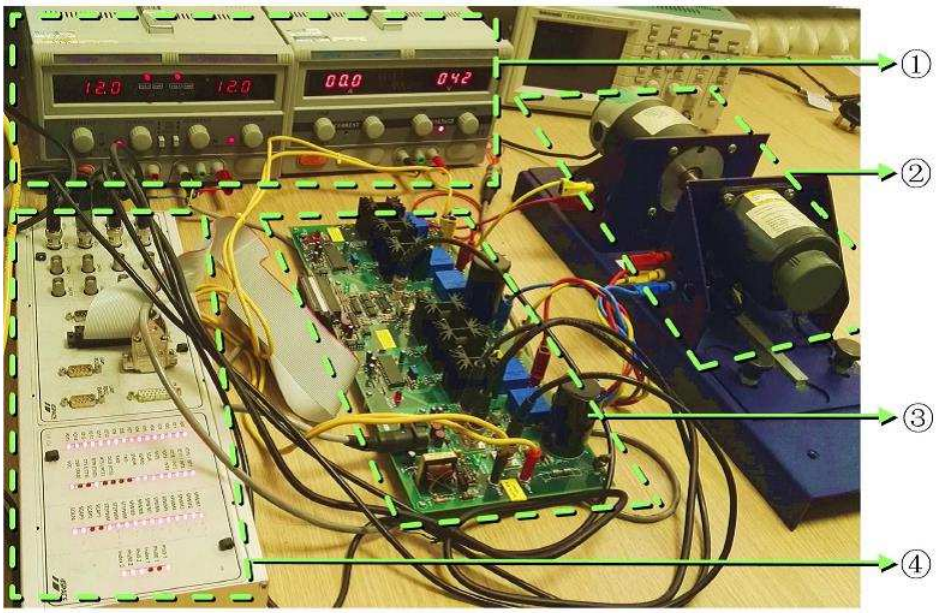

Figure 6.6: Experimental setup of IM sensorless electric drive system

control panel can change the variables of control-system in real time to communicate with DS1104 and hence change the reference quantities such as the speed or torque of the motor.

6.3 Experimental Results

Different experimental tests were performed in order to compare the operational performance of PI-MRAS, FLC-MRAS and SMC-MRAS. In all tests, indirect vector control induction motor drive system with same PI controller settings was used. During the experiments, a three phase 200W four poles IM from Motorsolver company was used whereas the IM parameters and ratings are mentioned in Table. 4.2. The electric drive system was used with 42V DC power electronic converter and DS1104 controller board. Fig. 6.6 shows the practical implementation of sensorless

IM electric drive system.

In order to implement MRAS schemes, it is important to cascade a low cut-off frequency, high pass filter at the output stage of MRAS voltage model to remove integrator drift and any initial condition problem. The cut-off frequency should be taken as minimum as possible in order to remove the possible DC component. Therefore, for this purpose 1.5 HZ frequency was selected.

However, in FLC-MRAS simulations, FL controller tool box was used from Matlab-Simulink to designe the speed observer. But in order to implement FLC in real time through the dSPACE card and simulink, a two dimensional look-up table was created from the Matlab toolbox for the practical implementation of observer. The saturation limits for the input saturation blocks were 0.1 and -0.1. The following section will present some comprehensive designed tests performance. The drive was operated at different speed profiles with fixed and time varying load torque conditions. Fig. 6.7 illustrates different operation conditions of EVs. The gain of PI controllers in PI-MRAS were kept as high as possible but avoided for noise appearance. The PI gains were taken by using trial and error method online which shown the optimal performance of the PI-MRAS speed observer experimentally. FLC gains were tuned in such a way which produced a similar steady state performance as we achieved from the PI-MRAS observer for a fair comparison and to understand the performance in the transient region. The FLC controller gains k_1, k_2 and k_3 are taken 10, 4200 and 350 respectively. The value of hitting gain was chosen 0.1 in the SMC-MRAS.

6.3.1 Performance of PI-MRAS Observer

First the performance of PI-MRAS speed observer was tested by different speed driving profiles and load torques. First test is for speed regulation response of observer at 50 rad/sec motor speed with time varying load torque. In this test 50 rad/sec reference speed was used to check the performance of observer with time

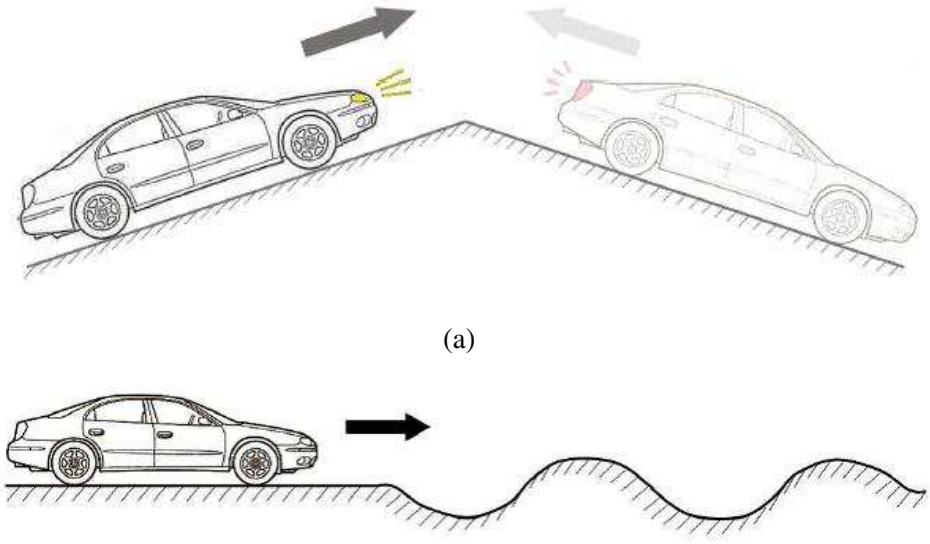

(a)

(b)

Figure 6.7: Different operation conditions of EV. 6.7(a) EV forward and reverse motoring operation condition. 6.7(b) EV constant speed with un-smooth road condition operation.

varying load torque between $t = 5s$ and $t = 10$. The applied load torque was varying between 20% to 70% rated load condition. Fig.6.8 shows the Speed regulation response of PI-MRAS observer at 60 rad/sec motor speed with time varying load torque. The next test is about the Speed regulation response of observer from positive 60 rad/sec to -60 rad/sec motor speed or motor operation in forward and reverse speed with time specified load torque. In this test around 90% rated load torque was applied for performance understanding between $t = 1s$ and $t = 15s$. Fig.6.9 shows the Speed regulation response of observer from positive 60 rad/sec to -60 rad/sec motor speed with time specified load torque. Fig. 6.10 illustrates the PI-MRAS observer speed regulation response of staircase at 80 rad/sec reference speed without load condition.

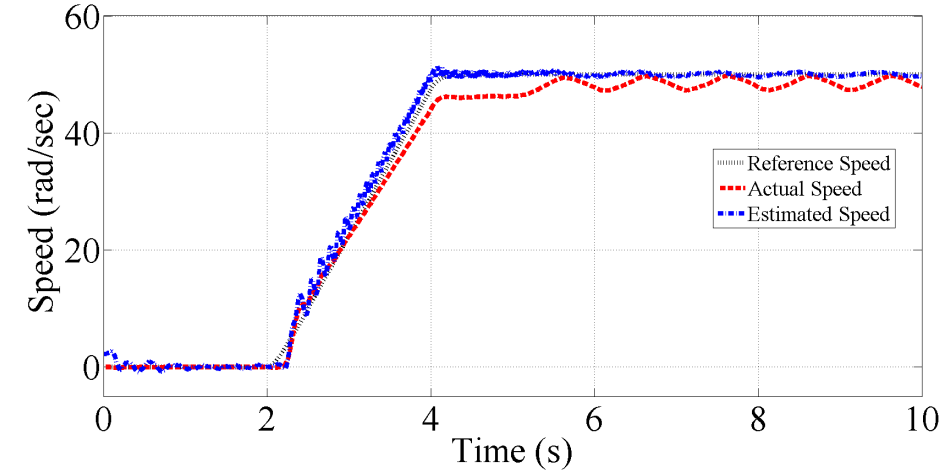

(a)

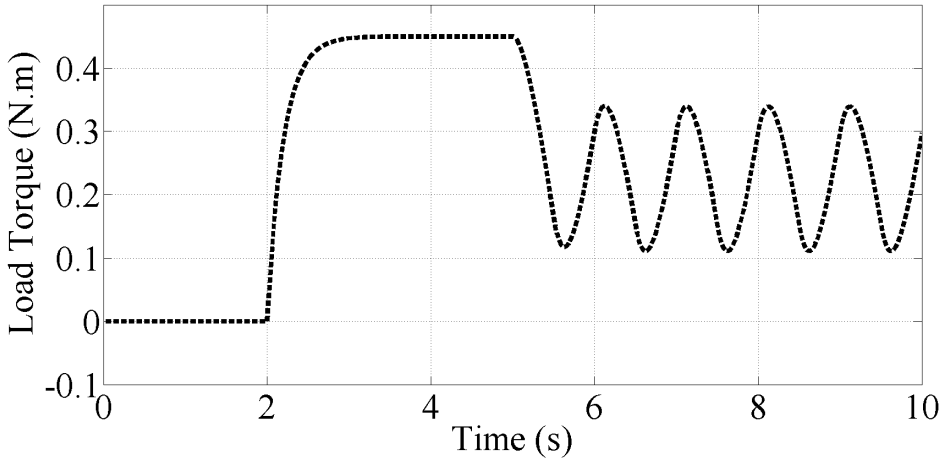

(b)

Figure 6.8: Speed regulation response of observer at 50 rad/sec motor speed with time varying load torque. 6.8(a) PI-MRAS Speed estimation response. 6.8(b) Applied load torque.

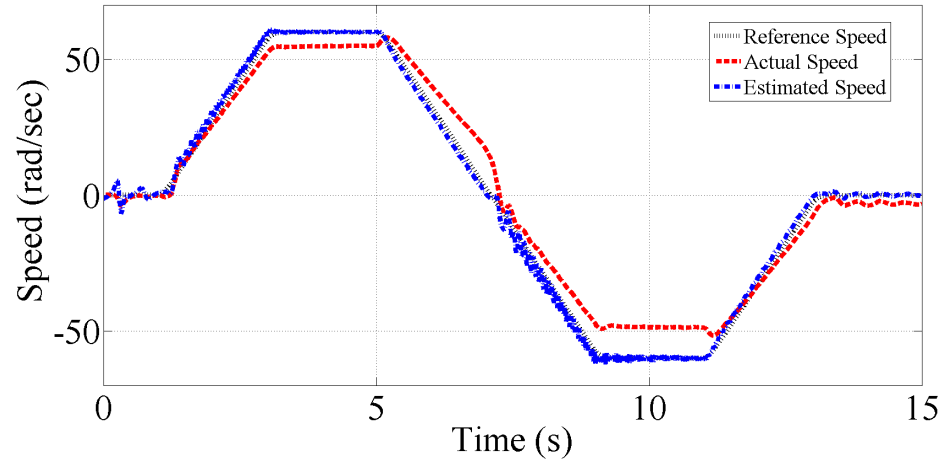

(a)

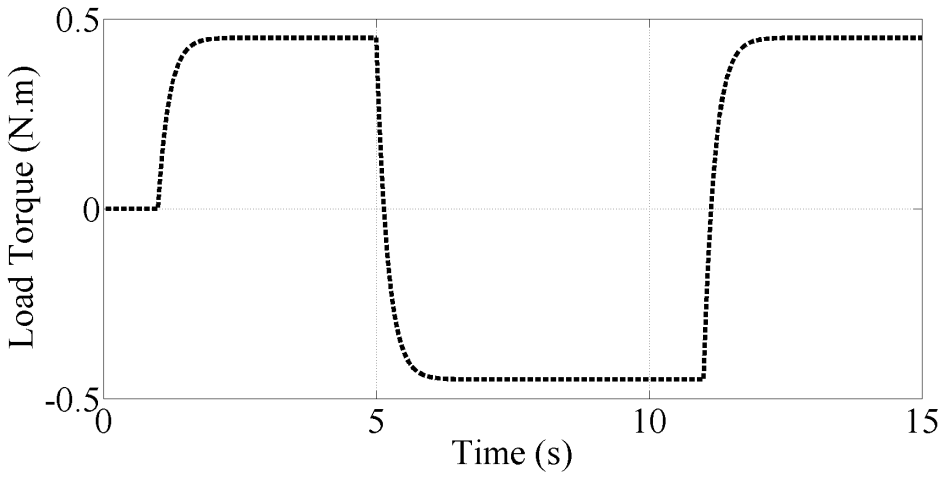

(b)

Figure 6.9: Speed regulation response of observer from +60 rad/sec to -60 rad/sec motor speed with specified load torque. 6.9(a) PI-MRAS speed regulation response. 6.9(b) Applied load torque.

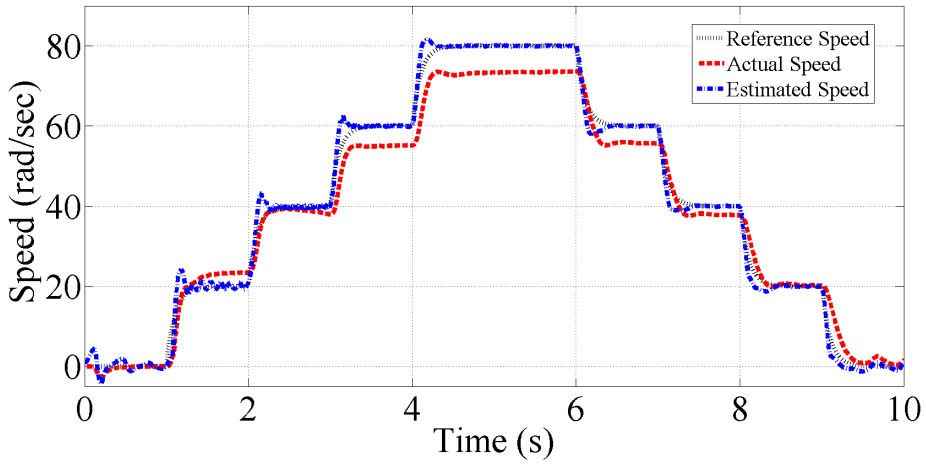

Figure 6.10: PI-MRAS observer speed regulation response of staircase at 80 rad/sec reference speed.

6.3.2 Performance of FLC-MRAS Observer

Similar kind of tests were performed in order to understand the performance of FLC-MRAS speed observer by using different speed driving profiles and load torques conditions. These tests are in the following section.

In FLC MRAS, the first test is for speed regulation response of observer by using 60 rad/sec ramp reference speed with time varying load torque. In this test 60 rad/sec reference speed was used to understand the performance of FLC observer with time varying 90% rated load torque between $t = 4s$ and $t = 9$.Fig.6.11 shows the speed regulation response of FLC-MRAS observer at 60 rad/sec motor speed with time varying load torque. The next test is for the Speed regulation response of observer from positive 60 rad/sec to -60 rad/sec motor speed with time specified load torque. In this test around 90% rated load torque was applied for performance understanding between $t = 1s$ and $t = 15s$. Fig.6.12 shows the Speed regulation response of observer from positive 60 rad/sec to -60 rad/sec motor speed with time specified load torque. Fig. 6.13 illustrates the FLC-MRAS observer speed regulation response of staircase at 80 rad/sec reference speed without load condition. However, the better speed estimation can be observes as compare to the PI-MRAS.

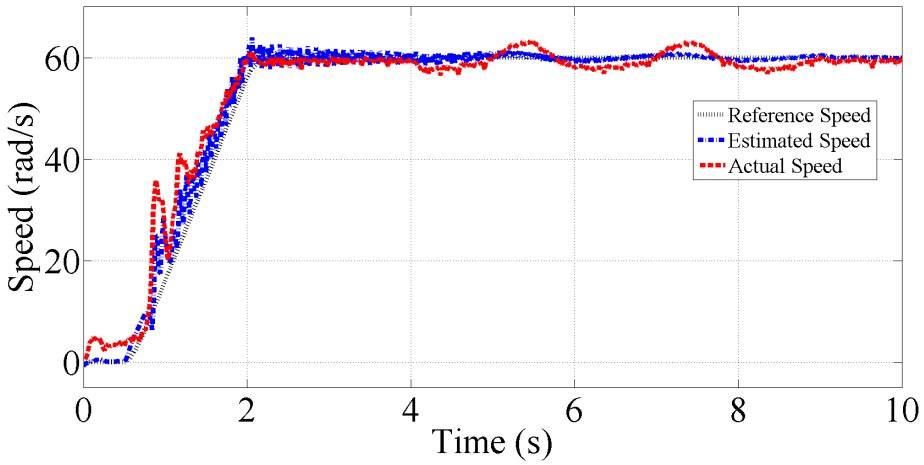

(a)

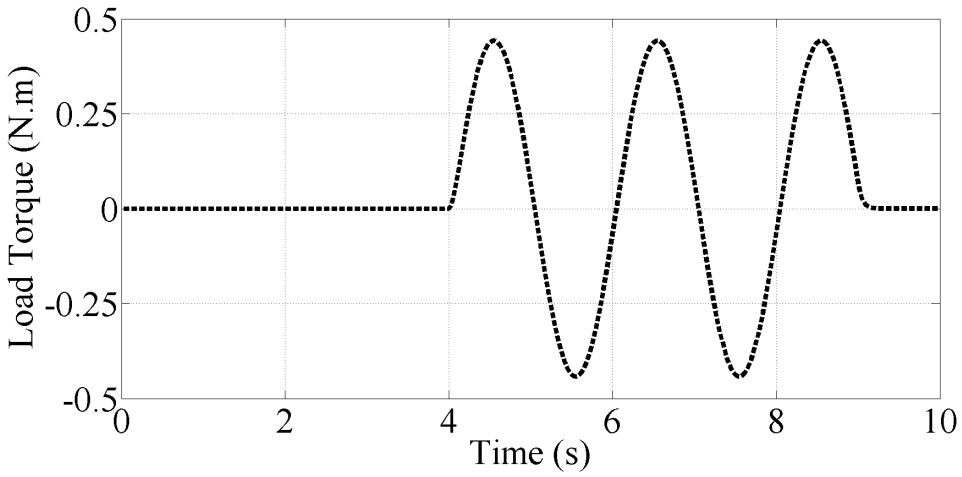

(b)

Figure 6.11: Speed regulation response of observer at 60 rad/sec motor speed with time varying load torque. 6.11(a) FLC-MRAS Speed estimation response. 6.11(b) Applied load torque.

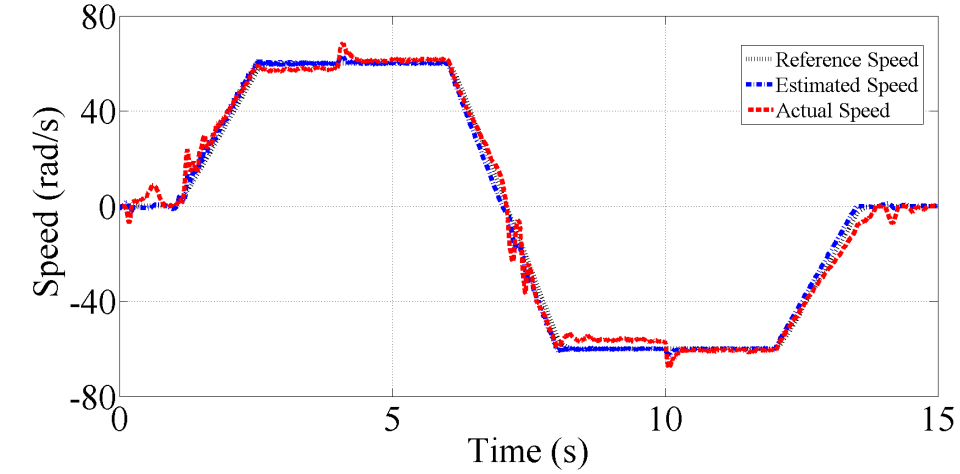

(a)

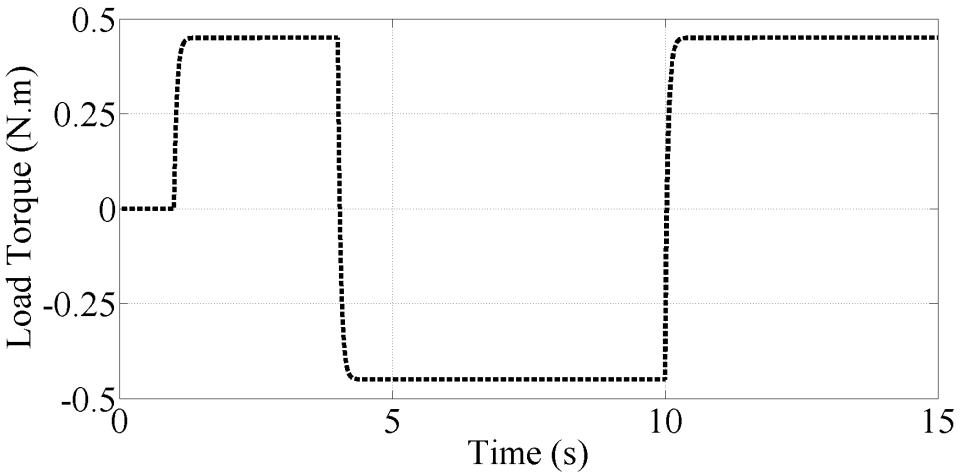

(b)

Figure 6.12: Speed regulation response of observer from +60 rad/sec to -60 rad/sec motor speed with specified load torque. 6.12(a) FLC-MRAS speed regulation response. 6.12(b) Applied load torque.

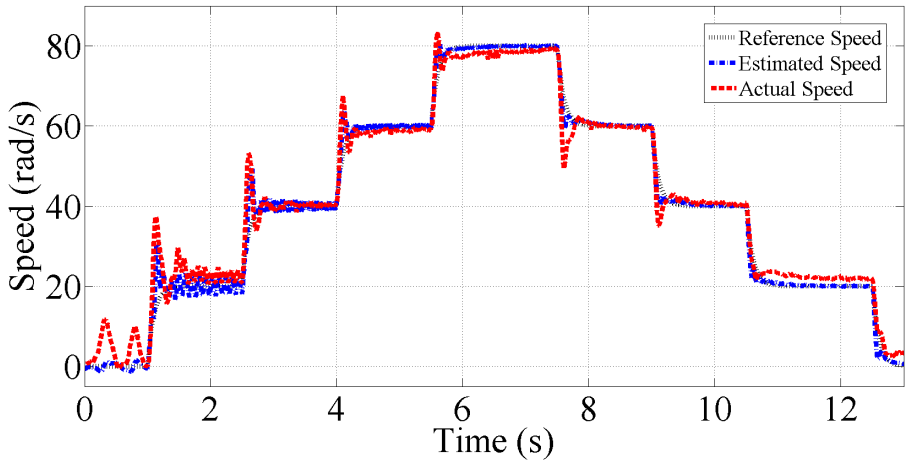

Figure 6.13: FLC-MRAS observer speed regulation response of staircase at 80 rad/sec reference speed.

6.3.3 Performance of SMC-MRAS Observer

Finally the performance of SMC-MRAS observer is tested by two different tests. In SMC MRAS, the first test is for the Speed regulation response of observer from positive 80 rad/sec to -80 rad/sec motor speed with time specified load torque. This case show the performance of observer in the case of vehicle forward motoring and reverse moting along with applied load condition at specific time. In this test around 90% rated load torque was applied for performance understanding between $t = 4.5s$ and $t = 14s$. The second test is observer speed response on staircase. This test has different small steps of quick speed change or quick acceleration operation. Fig.6.14 shows the Speed regulation response of observer from positive 80 rad/sec to -80 rad/sec motor speed with time specified load torque. Fig. 6.15 illustrates the SMC-MRAS observer speed regulation response of staircase at 80 rad/sec reference speed without load condition..

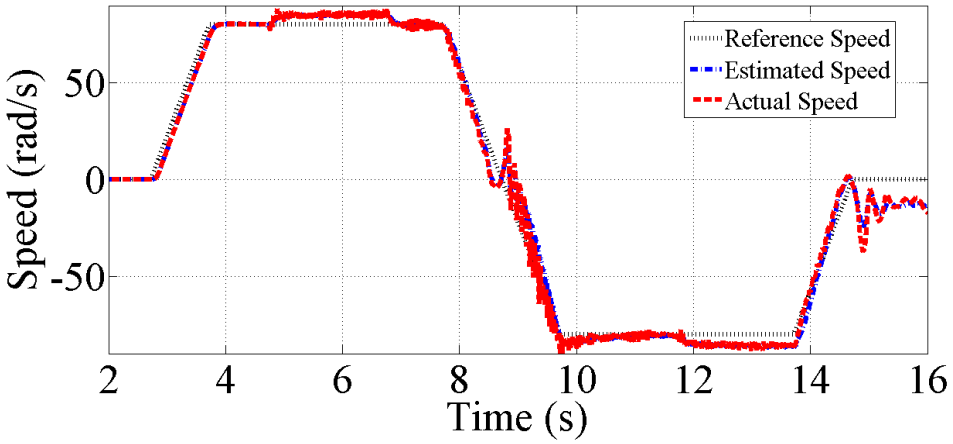

(a)

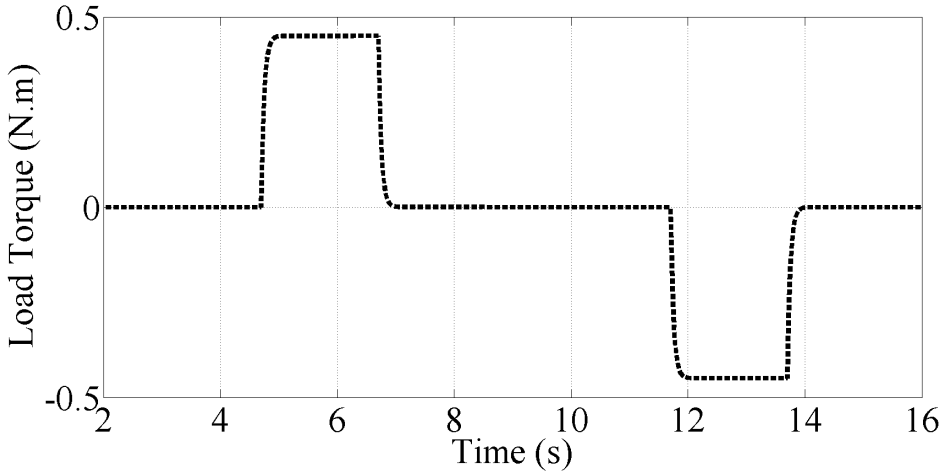

(b)

Figure 6.14: Speed regulation response of observer from +60 rad/sec to -60 rad/sec motor speed with specified load torque. 6.14(a) SMC-MRAS speed regulation response. 6.14(b) Applied load torque.

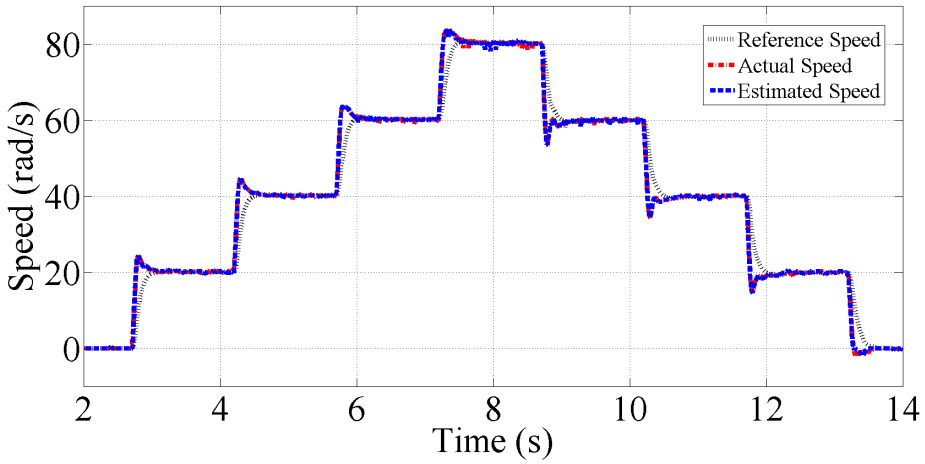

Figure 6.15: SMC-MRAS observer speed regulation response of staircase at 80 rad/sec reference speed.

6.4 Conclusion

This chapter has introduced first the DSP-based electric-drives system, used in order to perform practical testing and the real time implementation of the proposed speed observer schemes. The major components related to the hardware and software of the experimental system have been discussed. Different speed profiles and time varying load torque were used so as to compare the operational performance of PI-MRAS, FLC-MRAS and SMC-MRAS. Several comprehensive tests have been used to validate the performance and practical implementation of proposed schemes. In author's opinion, both proposed schemes FLC-MRAS and SMC-MRAS show better speed estimation and transient response as well as better load torque disturbance rejection capability as compare to the conventional PI-MRAS but SMC provides fast error dynamics or quick speed tuning signal convergence to zero under load torque disturbance condition compare with FLC-MRAS.

Chapter 7

Conclusion and Future Work

7.1 Introduction

THE research presented in this thesis has focused and proposed the application of speed sensorless IM drive control for EVs. The main objective was to investigate different strategies in order to improve the performance of speed sensorless traction drive which are based on rotor flux MRAS observer. Particular focus was given to the critical load torque disturbance conditions which are more common condition in traction drive control as well as different speed levels are used in the operation. Fuzzy logic control and sliding mode control-based rotor flux MRAS schemes have been developed and their better performance at different load disturbance conditions are shown through numerous tests. These all proposed schemes have been simulated by using Matlab-Simulink environment and experimentally validated based on dSPACE DS1104 controller board. The main purpose of this chapter is to summarise the investigations and findings of this research along with conclusions and provide different recommendations & various possibilities for future studies.

7.2 Discussion and Conclusions

As discussed in chapter 1, the application of speed sensor not only difficult to integrate into the vehicle drive train package but also fragility and susceptible to the EMI & signal distortion reduce the reliability of drive system. Therefore, the absence of speed sensor is entirely advantageous and provide cost effectiveness in the mass production of EVs if an adequate speed estimation algorithm is available to control the traction motor. These techniques are classified into two major categories; Signal injection and estimation techniques based on machine fundamental model. In this thesis, particular focus was given to the machine model based MRAS schemes where stator voltages and currents are used to estimate the motor speed and the flux linkages. However, these schemes do not provide better speed estimation performance at low speed levels and under different load torque disturbance. However, speed control at low speed and different load torque disturbance are more important specifically motor in wheel drive train configuration of EV where motor shaft is directly connected to the wheel rim to control the speed and torque.

In this research particular focus was given to MRAS based speed observers due to their simple structure and low computational effort as compare to other estimation techniques. All issues associated with these speed observers such as machine parameter sensitivity during the operation, pure integration problems and inverter nonlinearity are discussed in detail in chapter 2. Different methods and efforts of researchers in order to avoid such problems presented in the literature review. Application of AI techniques and particularly the use of fuzzy logic control in the variable speed drive was also discussed.

Chapter 3 presented the mathematical modelling of vehicle dynamics, which provides the understanding of different acting forces on the vehicle during the slope surface operation and required tractive force from the traction motor to operate the vehicle. Understanding of two axes theory or $d-q$ axes and coordinate transformations from three phase to two phase and between different reference frames have

been discussed. Induction machine dynamic model by using two axes theory in stationary and synchronously rotating reference frame were presented. The principles of vector control were also illustrated with the help of machine model equations defined into the synchronous reference frame. The machine dynamic equations have been used to formulate the rotor flux based MRAS speed observer, the most common speed estimation strategy used for sensorless control of motor. Design of reference model, adaptive model and adaptation mechanism of MRAS observer by using machine equations have also been presented.

In the conventional rotor flux based MRAS observer, usually a fixed gain PI controller is used to minimize the speed tuning signal and to estimate the rotor speed. However, due to the continuous variation in motor parameters and different load disturbance operating conditions, fixed gain PI-controller may not be able to provide a satisfactory performance. Therefore, chapter 5 proposed a novel fuzzy logic control based rotor flux model reference adaptive system speed observer. Which replaces the fixed gain PI controller used in the conventional MRAS. Both inputs and one output Mamdani-type FL controller was used to minimise the speed tuning signal.

In the proposed FLC-MRAS observer, two differences were used at the same time, reference and estimated rotor fluxes like conventional observer as well as reference and estimated torques with the help of rotor fluxes in order to improve the speed estimation specifically in load torque disturbance condition which is the most important feature during vehicle sensorless operation due to uncertain load disturbance condition.

Several simulation cases were designed for the implementation of vehicle operation such as load disturbance rejection capability, vehicle quick acceleration mode, operation of vehicle on un-smooth road condition and different speed transitions with load torque. All simulations were performed on Matlab-Simulink platform by using indirect vector control induction motor drive system. Simulation performance of the proposed FLC-MRAS was compared to the PI-MRAS observer. The proposed scheme has shown better transient performance as well as better load torque

disturbance rejection capability and provided a good solution for effective speed sensorless IM traction drive.

A novel sliding mode control based rotor flux model reference adaptive system speed observer was presented in chapter 5. The proposed SMC-MRAS observer replaces the fixed gain PI controller used in conventional rotor flux MRAS observer. Two differences were used at the same time, reference and estimated rotor fluxes as well as reference and estimated torques in order to improve the speed estimation in load torque disturbance condition. This SMC-MRAS scheme is derived based on the Lyapunov theory to ensure the system stability as well as fast error dynamics. Similar simulation cases designed in chapter 4 were perfromed by using indirect vector control induction motor drive system on Matlab-Simulink platform. Simulation performance of the proposed SMC-MRAS was compared to the PI-MRAS observer. The proposed algorithm have shown much better transient performance, fast error dynamics as well as better load torque disturbance rejection capability.

The DSP-based electric-drives system was utilized in order to perform practical testing and the real time implementation of the proposed speed observer schemes. Operational connectivity of all major components related to the hardware and software of the experimental system were also discussed in chapter 6. Different speed profiles and time varying load torque conditions were used in order to compare the operational performance of PI-MRAS, FLC-MRAS and SMC-MRAS. Comprehensive tests have been used to validate the performance and practical implementation of proposed schemes. Both proposed schemes FLC-MRAS and SMC-MRAS show better speed estimation and transient response as well as better load torque disturbance rejection capability.

In conclusion, this thesis has proposed two novel speed observers FLC-MRAS and SMC-MRAS. Proposed schemes have been simulated on Matlab-Simulink platform and experimentally validated for real time implementation. The operational performance of both schemes have been compared with the conventional PI-MRAS. For comparison purpose, several simulations and experimental tests with respect to

EV application were performed. Both proposed schemes were found better in speed estimation, transient response as well as better in load torque disturbance condition and provide a suitable application of speed sensorless IM drive control for EVs. This speed sensorless not only improves the operational performance of traction drive, but also the elimination of speed sensor provides the cost effectiveness in the mass production of EVs and AEVs in order to commercialise for the next generation.

7.3 Recommendations for Future Work

In the last few years, Artificial Intelligence based techniques are getting more and more attention of researchers in different fields including variable speed drive control. In present, the development of fast processing DSPs and advanced power electronic switching devices have brought the implementation of these computation intensive tools easily in different motion control applications. Some suggested future work activities are as follows.

- Rotor flux MRAS speed estimator is very dependent on machine parameters variation such as stator and rotor resistances during the operation and deteriorates the rotor speed estimation. An online parameter estimation and adaptation strategy can be implemented in the proposed schemes so as to improve the speed estimation performance under different circumstances.

- Apart from the proposed strategies, other optimization algorithms can be considered for speed tuning signal or error signal minimization. Therefore, it will be interesting point to investigate a new strategy and conduct a study work to replace the conventional fixed gain PI-controller for optimization purpose.

- Presently, lots of researchers are working on fuzzy-sliding mode control methods so it can also be implemented in the proposed schemes.

- Considering the current application focus on AI techniques in sensorless control, other AI tools like ANN and GA may be applied for performance improvement.

- The proposed speed sensorless traction drive not only provides the reliability and performance improvement in the drive system but also offers cost effectiveness in the mass production of EVs. Detail of cost analysis may also be included in this research work for EV manufacturing companies.

References

[1] M. Ehsani, Y. Gao, and A. Emadi, *Modern electric, hybrid electric, and fuel cell vehicles: fundamentals, theory, and design*. CRC press, 2009.

[2] www.globalspec.com/newsletter accessed in June 2016.

[3] K. B. Bimal, "Modern power electronics and ac drives," 2002.

[4] www.mathworks.com accessed in December 2016.

[5] M. Barnes, *Practical variable speed drives and power electronics*. Newnes, 2003.

[6] *DSP Based Electric Drives Laboratory, User Manual, Department of Electrical and Computer Engineering, University of Minnesota, August, 2011.*

[7] C. Chan, A. Bouscayrol, and K. Chen, "Electric, hybrid, and fuel-cell vehicles: Architectures and modeling," *IEEE Transactions on Vehicular Technology*, vol. 59, no. 2, pp. 589–598, Feb 2010.

[8] M. Ehsani, K. Rahman, and H. Toliyat, "Propulsion system design of electric and hybrid vehicles," *IEEE Transactions on Industrial Electronics*, vol. 44, no. 1, pp. 19–27, Feb 1997.

[9] B. Bilgin and A. Emadi, "Electric motors in electrified transportation: A step toward achieving a sustainable and highly efficient transportation system," *IEEE Power Electronics Magazine*, vol. 1, no. 2, pp. 10–17, June 2014.

[10] C. Chan, "The state of the art of electric, hybrid, and fuel cell vehicles," *IEEE Proceedings*, vol. 95, no. 4, pp. 704–718, April 2007.

[11] M. Zeraoulia, M. Benbouzid, and D. Diallo, "Electric motor drive selection issues for HEV propulsion systems: A comparative study," *IEEE Transactions on Vehicular Technology*, vol. 55, no. 6, pp. 1756–1764, Nov 2006.

[12] J. Finch and D. Giaouris, "Controlled AC electrical drives," *IEEE Transactions on Industrial Electronics*, vol. 55, no. 2, pp. 481–491, Feb 2008.

[13] J. Holtz, "Sensorless control of induction motor drives," *IEEE Proceedings*, vol. 90, no. 8, pp. 1359–1394, Aug 2002.

[14] C. Chan, "The state of the art of electric and hybrid vehicles," *IEEE Proceedings*, vol. 90, no. 2, pp. 247–275, Feb 2002.

[15] I. Husain, *Electric and hybrid vehicles: design fundamentals*. CRC press, 2011.

[16] S. Soylu, "Electric vehicles-the benefits and barriers," *Rijeka, Croatia: Intech Open Access Publisher*, 2011.

[17] C. Chan and Y. Wong, "Electric vehicles charge forward," *IEEE Power and Energy Magazine*, vol. 2, no. 6, pp. 24–33, Nov 2004.

[18] K. Chau, C. Chan, and K. Chau, *Modern electric vehicle technology*. Oxford science publications, 2001.

[19] C. Chan, "An overview of electric vehicle technology," *IEEE Proceedings*, vol. 81, no. 9, pp. 1202–1213, Sep 1993.

[20] J. de Santiago, H. Bernhoff, B. Ekergard, S. Eriksson, S. Ferhatovic, R. Waters, and M. Leijon, "Electrical motor drivelines in commercial all-electric vehicles: A review," *IEEE Transactions on Vehicular Technology*, vol. 61, no. 2, pp. 475–484, Feb 2012.

[21] L. Chang, "Comparison of ac drives for electric vehicles-a report on experts' opinion survey," *Magazine IEEE Aerospace and Electronic Systems*, vol. 9, no. 8, pp. 7–11, Aug 1994.

[22] C. Lungoci, M. Georgescu, and M. Calin, "Electrical motor types for vehicle propulsion," in *13th International Conference on Optimization of Electrical and Electronic Equipment , Brasov, Romania*, May 2012, pp. 635–640.

[23] S. Rind, Y. Ren, and L. Jiang, "Traction motors and speed estimation techniques for sensorless control of electric vehicles: A review," in *49th International Universities Power Engineering Conference (UPEC), Cluj-Napoca, Romania*, Sept 2014, pp. 1–6.

[24] P. Vas, *Sensorless vector and direct torque control*. Oxford Univversity Press, 1998.

[25] H. Abu-Rub, A. Iqbal, and J. Guzinski, *High performance control of ac drives with MATLAB/Simulink models*. John Wiley & Sons, 2012.

[26] W. Leonhard, "Controlled ac drives, a successful transition from ideas to industrial practice," *Control Engineering Practice*, vol. 4, no. 7, pp. 897–908, 1996.

[27] G. Pellegrino, A. Vagati, B. Boazzo, and P. Guglielmi, "Comparison of induction and PM synchronous motor drives for EV application including design examples," *IEEE Transactions on Industry Applications*, vol. 48, no. 6, pp. 2322–2332, Nov 2012.

[28] K. Rajashekara, "Present status and future trends in electric vehicle propulsion technologies," *IEEE Journal of Emerging and Selected Topics in Power Electronics,*, vol. 1, no. 1, pp. 3–10, March 2013.

[29] M. Ehsani, Y. Gao, and J. Miller, "Hybrid electric vehicles: Architecture and motor drives," *IEEE Proceedings*, vol. 95, no. 4, pp. 719–728, April 2007.

[30] X. He and J. Hodgson, "Modeling and simulation for hybrid electric vehicles. ii. simulation," *IEEE Transactions on Intelligent Transportation Systems*, vol. 3, no. 4, pp. 244–251, Dec 2002.

[31] X. Nian, F. Peng, and H. Zhang, "Regenerative braking system of electric vehicle driven by brushless DC motor," *IEEE Transactions on Industrial Electronics*, vol. 61, no. 10, pp. 5798–5808, Oct 2014.

[32] T. Jahns, "Motion control with permanent-magnet ac machines," *IEEE Proceedings*, vol. 82, no. 8, pp. 1241–1252, Aug 1994.

[33] T. Miller and R. Rabinovici, "Back-EMF waveforms and core losses in brushless DC motors," *IEE Electric Power Applications*, vol. 141, no. 3, pp. 144–154, May 1994.

[34] A. Emadi, *Handbook of automotive power electronics and motor drives*. CRC press, 2005.

[35] T. Jahns and V. Blasko, "Recent advances in power electronics technology for industrial and traction machine drives," *IEEE Proceedings*, vol. 89, no. 6, pp. 963–975, Jun 2001.

[36] K. Kiyota, H. Sugimoto, and A. Chiba, "Comparing electric motors: An analysis using four standard driving schedules," *IEEE Industry Applications Magazine*, vol. 20, no. 4, pp. 12–20, July 2014.

[37] B. Fahimi, A. Emadi, and R. Sepe, "A switched reluctance machine-based starter/alternator for more electric cars," *IEEE Transactions on Energy Conversion*, vol. 19, no. 1, pp. 116–124, March 2004.

[38] K. Rahman and S. Schulz, "Design of high-efficiency and high-torque-density switched reluctance motor for vehicle propulsion," *IEEE Transactions on Industry Applications*, vol. 38, no. 6, pp. 1500–1507, Nov 2002.

[39] S. Ramamurthy, J. Balda, and T. Ericsen, "Sizing a switched reluctance motor for electric vehicles," in *IEEE Industry Applications Conference, Rome, Italy*, vol. 1, 2000, pp. 71–78 vol.1.

[40] Z. Zhu and D. Howe, "Electrical machines and drives for electric, hybrid, and fuel cell vehicles," *IEEE Proceedings*, vol. 95, no. 4, pp. 746–765, April 2007.

[41] Z. Rahman, M. Ehsani, and K. Butler, "An investigation of electric motor drive characteristics for EV and HEV propulsion systems," SAE Technical Paper, Tech. Rep., 2000.

[42] J. R. Heredia, F. P. Hidalgo, and J. L. D. Paz, "Sensorless control of induction motors by artificial neural networks," *IEEE Transactions on Industrial Electronics*, vol. 48, no. 5, pp. 1038–1040, Oct 2001.

[43] J. M. Miller, *Propulsion systems for hybrid vehicles*. IET, 2004, vol. 45.

[44] W. Leonhard, *Control of Electrical Drives*. Springer-Verlag, 1996.

[45] P. Vas, *Artificial-intelligence-based electrical machines and drives: application of fuzzy, neural, fuzzy-neural, and genetic-algorithm-based techniques*. Oxford University Press New York, 1999, vol. 45.

[46] J. Holtz, "Sensorless control of induction machines ; with or without signal injection?" *IEEE Transactions on Industrial Electronics*, vol. 53, no. 1, pp. 7–30, Feb 2005.

[47] G. Buja and M. Kazmierkowski, "Direct torque control of PWM inverter-fed ac motors - a survey," *IEEE Transactions on Industrial Electronics*, vol. 51, no. 4, pp. 744–757, Aug 2004.

[48] H.-u. Rehman and L. Xu, "Alternative energy vehicles drive system: Control,

flux and torque estimation, and efficiency optimization," *IEEE Transactions on Vehicular Technology*, vol. 60, no. 8, pp. 3625–3634, 2011.

[49] J. Holtz and J. Quan, "Drift and parameter compensated flux estimator for persistent zero stator frequency operation of sensorless controlled induction motors," in *37th IAS Annual Meeting Industry Applications Conference, Pittsburgh, PA, USA*, vol. 3, Oct 2002, pp. 1687–1694 vol.3.

[50] K. M. Rahman, N. R. Patel, T. G. Ward, J. M. Nagashima, F. Caricchi, and F. Crescimbini, "Application of direct-drive wheel motor for fuel cell electric and hybrid electric vehicle propulsion system," *IEEE Transactions on Industry Applications*, vol. 42, no. 5, pp. 1185–1192, 2006.

[51] K. Ohyama, G. Asher, and M. Sumner, "Comparative analysis of experimental performance and stability of sensorless induction motor drives," *IEEE Transactions on Industrial Electronics*, vol. 53, no. 1, pp. 178–186, Feb 2005.

[52] Y. Hu, X. Song, W. Cao, and B. Ji, "New SR drive with integrated charging capacity for plug-in hybrid electric vehicles (PHEVs)," *IEEE Transactions on Industrial Electronics*, vol. 61, no. 10, pp. 5722–5731, 2014.

[53] K. Kim and A. G. Parlos, "Induction motor fault diagnosis based on neuropredictors and wavelet signal processing," *IEEE/ASME Transactions on mechatronics*, vol. 7, no. 2, pp. 201–219, 2002.

[54] H. J. Van de Straete, J. De Schutter, and R. Belmans, "An efficient procedure for checking performance limits in servo drive selection and optimization," *IEEE/ASME transactions on mechatronics*, vol. 4, no. 4, pp. 378–386, 1999.

[55] R. Marino, S. Peresada, and P. Valigi, "Adaptive input-output linearizing control of induction motors," *IEEE Transactions on Automatic control*, vol. 38, no. 2, pp. 208–221, 1993.

[56] Y. Liu, J. Zhao, R. Wang, and C. Huang, "Performance improvement of induction motor current controllers in field-weakening region for electric vehicles," *IEEE Transactions on Power Electronics*, vol. 28, no. 5, pp. 2468–2482, 2013.

[57] A. Emadi, Y. J. Lee, and K. Rajashekara, "Power electronics and motor drives in electric, hybrid electric, and plug-in hybrid electric vehicles," *IEEE Transactions on industrial electronics*, vol. 55, no. 6, pp. 2237–2245, 2008.

[58] A. C. Lima-Filho, R. D. Gomes, M. O. Adissi, T. A. B. da Silva, F. A. Belo, and M. A. Spohn, "Embedded system integrated into a wireless sensor network for online dynamic torque and efficiency monitoring in induction motors," *IEEE/ASME Transactions on Mechatronics*, vol. 17, no. 3, pp. 404–414, 2012.

[59] K. Rajashekara, "Present status and future trends in electric vehicle propulsion technologies," *IEEE Journal of Emerging and Selected Topics in Power Electronics*, vol. 1, no. 1, pp. 3–10, 2013.

[60] K. Rajashekara, A. Kawamura, and K. Matsuse, *Sensorless control of AC motor drives: speed and position sensorless operation*. IEEE press New York, 1996.

[61] H. A. Toliyat, E. Levi, and M. Raina, "A review of RFO induction motor parameter estimation techniques," *IEEE Transactions on Energy Conversion*, vol. 18, no. 2, pp. 271–283, June 2003.

[62] I. Vicente, M. Brown, A. Renfrew, A. Endemano, and X. Garin, "Stable MRAS-based sensorless scheme design strategy for high power traction drives," in *4th IET Conference on Power Electronics, Machines and Drives, PEMD, York, UK*, April 2008, pp. 562–567.

[63] C. Silva and R. Araya, "Sensorless vector control of induction machine with low speed capability using MRAS with drift and inverter nonlinearities compensation," in *The International Conference on Computer as a Tool, EUROCON, Warsaw, Poland*, Sept 2007, pp. 1922–1928.

[64] S. F. Tie and C. W. Tan, "A review of energy sources and energy management system in electric vehicles," *Renewable and Sustainable Energy Reviews*, vol. 20, pp. 82–102, 2013.

[65] T. D. Batzel and K. Y. Lee, "Electric propulsion with sensorless permanent magnet synchronous motor: implementation and performance," *IEEE Transactions on Energy Conversion*, vol. 20, no. 3, pp. 575–583, 2005.

[66] Y. Fan, L. Zhang, J. Huang, and X. Han, "Design, analysis, and sensorless control of a self-decelerating permanent-magnet in-wheel motor," *IEEE Transactions on Industrial Electronics*, vol. 61, no. 10, pp. 5788–5797, 2014.

[67] J. CatalaiLopez, L. Romeral, A. Arias, and E. Aldabas, "Novel fuzzy adaptive sensorless induction motor drive," *IEEE Transactions on Industrial Electronics*, vol. 53, no. 4, p. Cata2006, June 2006.

[68] S. M. Gadoue, "Artificial-intelligence-applied to speed sensorless induction motor drives," Ph.D. dissertation, Newcastle University, January, 2009.

[69] M. Zerbo, A. Ba-Razzouk, and P. Sicard, "Open-loop speed estimators design for online induction machine synchronous speed tracking," in *IEEE International Conference on Electric Machines and Drives, San Antonio, TX, USA*, May 2005, pp. 1089–1094.

[70] K. J. Astrom, "Adaptive control around 1960," *Control Systems, IEEE*, vol. 16, no. 3, pp. 44–49, 1996.

[71] Y. D.Landau, *Adaptive Control: The Model Reference Approach*. Marcel Dekker INC, 1979.

[72] Z. Tan, Y. Li, and Z. Ji, "Speed sensorless DTC and parameter estimation of induction motor based on a full-order MRAS method," in *The Third International Power Electronics and Motion Control Conference Proceedings, IPEMC , Beijing, China*, vol. 3, 2000, pp. 1202–1206 vol.3.

[73] R.-J. Wai and K.-M. Lin, "Robust decoupled control of direct field-oriented induction motor drive," *IEEE Transactions on Industrial Electronics*, vol. 52, no. 3, pp. 837–854, June 2005.

[74] Q. Yang, Y. Xue, S. X. Yang, Q. Li, R. Li, and M. Q. H. Meng, "An embedded structure of model reference adaptive system," in *10th International Conference on Control, Automation, Robotics and Vision, ICARCV, Hanoi, Vietnam*, Dec 2008, pp. 256–261.

[75] C. Schauder, "Adaptive speed identification for vector control of induction motors without rotational transducers," *IEEE Transactions on Industry Applications*, vol. 28, no. 5, pp. 1054–1061, Sep 1992.

[76] F.-Z. Peng and T. Fukao, "Robust speed identification for speed-sensorless vector control of induction motors," *IEEE Transactions on Industry Applications*, vol. 30, no. 5, pp. 1234–1240, Sep 1994.

[77] T. Orlowska-Kowalska and M. Dybkowski, "Stator-current-based MRAS estimator for a wide range speed-sensorless induction-motor drive," *IEEE Transactions on Industrial Electronics*, vol. 57, no. 4, pp. 1296–1308, April 2010.

[78] S. Tamai, H. Sugimoto, and M. Yano, "Speed sensorless vector control of induction motor applied model reference adaptive system," in *Proceedings IEEE/IA Ann. Mtg. Conf*, 1985, pp. 613–620.

[79] S. Tami, H. Sugimoto, and Y. Masao, "Speed sensorless vector control of

induction motor with model reference adaptive system," in *IEEE/IAS. Annu. Meeting*, 1987, pp. 189–195.

[80] J. Soltani, "Simultaneous speed and rotor time constant identification of an induction motor drive based on the model reference adaptive system combined with a fuzzy resistance estimator," in *International Conference on Power Electronic Drives and Energy Systems for Industrial Growth, Proceedings, Perth, WA, Australia*, vol. 2. IEEE, 1998, pp. 739–744.

[81] K. Ohyama, G. Asher, and M. Sumner, "Comparative experimental assessment for high-performance sensorless induction motor drives," in *Proceedings of the IEEE International Symposium on Industrial Electronics, ISIE', Bled, Slovenia*, vol. 1. IEEE, 1999, pp. 386–391.

[82] F.-Z. Peng and T. Fukao, "Robust speed identification for speed-sensorless vector control of induction motors," *IEEE Transactions on Industry Applications*, vol. 30, no. 5, pp. 1234–1240, 1994.

[83] M. N. Gayathri, S. Himavathi, and R. Sankaran, "Performance enhancement of vector controlled drive with rotor flux based mras rotor resistance estimator," in *International Conference on Computer Communication and Informatics (ICCCI), Coimbatore, India*. IEEE, 2012, pp. 1–6.

[84] J.-F. Stumper and R. Kennel, "Field-oriented control of a speed-sensorless induction motor for the complete speed range using a nonlinear observer," in *Symposium on Sensorless Control for Electrical Drives (SLED), Birmingham, UK*. IEEE, 2011, pp. 107–113.

[85] F.-J. Lin and H.-M. Su, "A high-performance induction motor drive with online rotor time-constant estimation," *IEEE Transactions on Energy Conversion*, vol. 12, no. 4, pp. 297–303, 1997.

[86] J. Li, H. Ren, Q. Huang, and Y. Zhong, "A novel on-line MRAS rotor resistance identification method insensitive to stator resistance for vector control systems of induction machines," in *IEEE International Symposium on Industrial Electronics (ISIE), Bari, Italy*. IEEE, 2010, pp. 591–595.

[87] D. P. Marcetic, I. R. Krcmar, M. A. Gecic, and P. R. Matic, "Discrete rotor flux and speed estimators for high-speed shaft-sensorless im drives," *IEEE Transactions on Industrial Electronics*, vol. 61, no. 6, pp. 3099–3108, 2014.

[88] M. Rashed and A. Stronach, "A stable back-EMF MRAS-based sensorless low-speed induction motor drive insensitive to stator resistance variation," in *IEE Proceedings Electric Power Applications*, vol. 151, no. 6. IET, 2004, pp. 685–693.

[89] R. Blasco-Gimenez, G. Asher, M. Sumner, and K. Bradley, "Dynamic performance limitations for MRAS based sensorless induction motor drives. i. stability analysis for the closed loop drive," in *IEE Proceedings-Electric Power Applications*, vol. 143, no. 2. IET, 1996, pp. 113–122.

[90] S. Maiti, C. Chakraborty, Y. Hori, and M. C. Ta, "Model reference adaptive controller-based rotor resistance and speed estimation techniques for vector controlled induction motor drive utilizing reactive power," *IEEE Transactions on Industrial Electronics*, vol. 55, no. 2, pp. 594–601, 2008.

[91] M. Tsuji, S. Chen, K. Izumi, and E. Yamada, "A sensorless vector control system for induction motors using q-axis flux with stator resistance identification," *IEEE Transactions on Industrial Electronics*, vol. 48, no. 1, pp. 185–194, 2001.

[92] Z. Wu, D. Zhi, and J. Ying, "Research on speed estimation algorithm for induction motor drive," in *The 4th International Power Electronics and Mo-*

tion Control Conference, IPEMC , Xi'an, China, vol. 3. IEEE, 2004, pp. 1387–1392.

[93] H.-u. Rehman, A. Derdiyok, M. K. Guven, and L. Xu, "A new current model flux observer for wide speed range sensorless control of an induction machine," *IEEE Transactions on Power Electronics*, vol. 17, no. 6, pp. 1041–1048, 2002.

[94] O. Barambones, A. Garrido, and F. Maseda, "Integral sliding-mode controller for induction motor based on field-oriented control theory," *IET Control Theory & Applications*, vol. 1, no. 3, pp. 786–794, 2007.

[95] V. I. Utkin, "Sliding mode control design principles and applications to electric drives," *IEEE Transactions on Industrial Electronics*, vol. 40, no. 1, pp. 23–36, 1993.

[96] M. Comanescu and L. Xu, "Sliding-mode MRAS speed estimators for sensorless vector control of induction machine," *IEEE Transactions on Industrial Electronics*, vol. 53, no. 1, pp. 146–153, 2006.

[97] Z. Yan, C. Jin, and V. I. Utkin, "Sensorless sliding-mode control of induction motors," *IEEE Transactions on Industrial Electronics*, vol. 47, no. 6, pp. 1286–1297, 2000.

[98] M. Hinkkanen, "Analysis and design of full-order flux observers for sensorless induction motors," *IEEE Transactions on Industrial Electronics*, vol. 51, no. 5, pp. 1033–1040, 2004.

[99] T. Du, P. Vas, and F. Stronach, "Design and application of extended observers for joint state and parameter estimation in high-performance AC drives," in *IEE Proceedings-Electric Power Applications*, vol. 142, no. 2. IET, 1995, pp. 71–78.

[100] M. Barut, S. Bogosyan, and M. Gokasan, "Speed-sensorless estimation for induction motors using extended kalman filters," *IEEE Transactions on Industrial Electronics*, vol. 54, no. 1, pp. 272–280, 2007.

[101] K. Shi, T. Chan, Y. Wong, and S. Ho, "Speed estimation of an induction motor drive using an optimized extended kalman filter," *IEEE Transactions on Industrial Electronics*, vol. 49, no. 1, pp. 124–133, 2002.

[102] G. J. Armstrong, D. J. Atkinson, and P. P. Acarnle, "A comparison of estimation techniques for sensorless vector controlled induction motor drives," in *International Conference on Power Electronics and Drive Systems, Proceedings, Singapore*, vol. 1. IEEE, 1997, pp. 110–116.

[103] G. Wang, H. Hofmann, and A. El-Antably, "Speed-sensorless torque control of induction machine based on carrier signal injection and smooth-air-gap induction machine model," *IEEE Transactions on Energy Conversion*, vol. 21, no. 3, pp. 699–707, Sept 2006.

[104] S. Morimoto, M. Sanada, and Y. Takeda, "Mechanical sensorless drives of IPMSM with online parameter identification," *IEEE Transactions on Industry Applications*, vol. 42, no. 5, pp. 1241–1248, 2006.

[105] N. Bianchi and S. Bolognani, "Influence of rotor geometry of an IPM motor on sensorless control feasibility," *IEEE Transactions on Industry Applications*, vol. 43, no. 1, pp. 87–96, 2007.

[106] J. Campbell and M. Sumner, "Practical sensorless induction motor drive employing an artificial neural network for online parameter adaptation," in *IEE Proceedings-Electric Power Applications*, vol. 149, no. 4. IET, 2002, pp. 255–260.

[107] V. Vasi, S. N. Vukosavic, and E. Levi, "A stator resistance estimation scheme

for speed sensorless rotor flux oriented induction motor drives," *IEEE Transactions on Energy Conversion,*, vol. 18, no. 4, pp. 476–483, 2003.

[108] L. Zhen and L. Xu, "Sensorless field orientation control of induction machines based on a mutual MRAS scheme," *IEEE Transactions on Industrial Electronics*, vol. 45, no. 5, pp. 824–831, 1998.

[109] V. Vasic and S. Vukosavic, "Robust MRAS-based algorithm for stator resistance and rotor speed identification," *IEEE Power Engineering Review*, vol. 21, no. 11, pp. 39–41, 2001.

[110] Y. A. Kwon and D. W. Jin, "A novel MRAS based speed sensorless control of induction motor," in *The 25th Annual Conference of the IEEE Industrial Electronics Society, IECON Proceedings, San Jose, CA, USA*, vol. 2. IEEE, 1999, pp. 933–938.

[111] B. Karanayil, M. F. Rahman, and C. Grantham, "An implementation of a programmable cascaded low-pass filter for a rotor flux synthesizer for an induction motor drive," *IEEE Transactions on Power Electronics*, vol. 19, no. 2, pp. 257–263, 2004.

[112] M. Hinkkanen and J. Luomi, "Modified integrator for voltage model flux estimation of induction motors," in *The 27th Annual Conference of the IEEE Industrial Electronics Society, IECON, Denver, CO, USA*, vol. 2. IEEE, 2001, pp. 1339–1343.

[113] Q. Gao, C. Spiteri, G. Asher, and M. Sumner, "Sensorless speed operation of cage induction motor using zero drift feedback integration with MRAS observer," in *European Conference on Power Electronics and Applications, Dresden, Germany*. IEEE, 2005, pp. 9–pp.

[114] C. Lascu, I. Boldea, and F. Blaabjerg, "A modified direct torque control for

induction motor sensorless drive," *IEEE Transactions on Industry Applications*, vol. 36, no. 1, pp. 122–130, 2000.

[115] M. Shiref, "Investigation into pi controller output ripple in MRAS based electrical drives," 2013.

[116] J. Holtz and J. Quan, "Sensorless vector control of induction motors at very low speed using a nonlinear inverter model and parameter identification," *IEEE Transactions on Industry Applications*, vol. 38, no. 4, pp. 1087–1095, 2002.

[117] T.-F. Chan and K. Shi, *Applied intelligent control of induction motor drives*. John Wiley & Sons, 2011.

[118] B. K. Bose, "Neural network applications in power electronics and motor drives an introduction and perspective," *IEEE Transactions on Industrial Electronics*, vol. 54, no. 1, pp. 14–33, 2007.

[119] M. Cirrincione, M. Pucci, G. Cirrincione, and G.-A. Capolino, "Sensorless control of induction machines by a new neural algorithm: The tls exin neuron," *IEEE Transactions on Industrial Electronics*, vol. 54, no. 1, pp. 127–149, 2007.

[120] B. Karanayil, M. F. Rahman, and C. Grantham, "Online stator and rotor resistance estimation scheme using artificial neural networks for vector controlled speed sensorless induction motor drive," *IEEE transactions on Industrial Electronics*, vol. 54, no. 1, pp. 167–176, 2007.

[121] M. Cirstea, A. Dinu, M. McCormick, and J. G. Khor, *Neural and fuzzy logic control of drives and power systems*. Newnes, 2002.

[122] S. Buyamin and J. Finch, "Comparative study on optimising the EKF for speed estimation of an induction motor using simulated annealing and genetic

algorithm," in *IEEE International Electric Machines & Drives Conference, IEMDC, Jounieh, Lebanon*, vol. 2. IEEE, 2007, pp. 1689–1694.

[123] Y.-C. Luo and C.-C. Lin, "Fuzzy MRAS based speed estimation for sensorless stator field oriented controlled induction motor drive," in *International Symposium on Computer Communication Control and Automation (3CA), Tainan, Taiwan*, vol. 2. IEEE, 2010, pp. 152–155.

[124] Y. Bensalem and M. N. Abdelkrim, "A sensorless neural model reference adaptive control for induction motor drives," in *3rd International Conference on Signals, Circuits and Systems (SCS), Medenine, Tunisia*. IEEE, 2009, pp. 1–6.

[125] S. Mir, M. E. Elbuluk, and D. S. Zinger, "PI and fuzzy estimators for tuning the stator resistance in direct torque control of induction machines," *IEEE Transactions on Power Electronics*, vol. 13, no. 2, pp. 279–287, 1998.

[126] C.-J. Chen and T.-C. Chen, "Speed sensorless of an induction motor using self-tuning fuzzy identification," in *Second International Conference on Innovative Computing, Information and Control, ICICIC, Kumamoto, Japan*. IEEE, 2007, pp. 398–398.

[127] K.-Y. Lian and C.-Y. Hung, "Sensorless control for induction motors via fuzzy observer design," in *IEEE International Symposium on Industrial Electronics, Montreal, Que., Canada*, vol. 3. IEEE, 2006, pp. 2140–2145.

[128] L. James and L. John, "Electric vehicle technology explained," 2003.

[129] S. M. Gadoue, D. Giaouris, and J. W. Finch, "Mras sensorless vector control of an induction motor using new sliding-mode and fuzzy-logic adaptation mechanisms," *IEEE Transactions on Energy Conversion*, vol. 25, no. 2, pp. 394–402, 2010.

[130] L. Reznik, *Fuzzy controllers handbook: how to design them, how they work*. Newnes, 1997.

[131] I. Benlaloui, S. Drid, L. Chrifi-Alaoui, and M. Ouriagli, "Implementation of a new MRAS speed sensorless vector control of induction machine," *IEEE Transactions on Energy Conversion*, vol. 30, no. 2, pp. 588–595, 2015.

[132] F.-J. Lin and C.-M. Liaw, "Control of indirect field-oriented induction motor drives considering the effects of dead-time and parameter variations," *IEEE Transactions on industrial electronics*, vol. 40, no. 5, pp. 486–495, 1993.

[133] R. Ortega, C. Canudas, and S. I. Seleme, "Nonlinear control of induction motors: Torque tracking with unknown load disturbance," *IEEE Transactions on Automatic Control*, vol. 38, no. 11, pp. 1675–1680, 1993.

[134] V. Utkin, J. Guldner, and J. Shi, *Sliding mode control in electro-mechanical systems*. CRC press, 2009, vol. 34.

[135] B. Bose, "Sliding mode control of induction motor," in *IEEE/IAS conference record*, 1985, pp. 479–486.

[136] E. Y. Ho and P. C. Sen, "A microcontroller-based induction motor drive system using variable structure strategy with decoupling," *IEEE Transactions on Industrial Electronics*, vol. 37, no. 3, pp. 227–235, 1990.

[137] Y. Zhao, W. Qiao, and L. Wu, "An adaptive quasi-sliding-mode rotor position observer-based sensorless control for interior permanent magnet synchronous machines," *IEEE Transactions on Power Electronics*, vol. 28, no. 12, pp. 5618–5629, 2013.

[138] F.-J. Lin, W.-D. Chou, and P.-K. Huang, "Adaptive sliding-mode controller based on real-time genetic algorithm for induction motor servo drive," *IEE Proceedings-Electric Power Applications*, vol. 150, no. 1, pp. 1–13, 2003.

[139] F. Barrero, A. Gonzalez, A. Torralba, E. Galvan, and L. G. Franquelo, "Speed control of induction motors using a novel fuzzy sliding-mode structure," *IEEE Transactions on Fuzzy Systems*, vol. 10, no. 3, pp. 375–383, 2002.

[140] K.-K. Shyu and H.-J. Shieh, "A new switching surface sliding-mode speed control for induction motor drive systems," *IEEE Transactions on Power Electronics*, vol. 11, no. 4, pp. 660–667, 1996.

[141] F.-J. Lin, S.-L. Chiu, and K.-K. Shyu, "Novel sliding mode controller for synchronous motor drive," *IEEE Transactions on Aerospace and Electronic Systems*, vol. 34, no. 2, pp. 532–542, 1998.

[142] A. Saghafinia, H. W. Ping, M. N. Uddin, and K. S. Gaeid, "Adaptive fuzzy sliding-mode control into chattering-free im drive," *IEEE Transactions on Industry Applications*, vol. 51, no. 1, pp. 692–701, 2015.

[143] J. Zhang, P. Shi, and Y. Xia, "Robust adaptive sliding-mode control for fuzzy systems with mismatched uncertainties," *IEEE Transactions on Fuzzy Systems*, vol. 18, no. 4, pp. 700–711, 2010.

[144] T. Orlowska-Kowalska, M. Kaminski, and K. Szabat, "Implementation of a sliding-mode controller with an integral function and fuzzy gain value for the electrical drive with an elastic joint," *IEEE Transactions on Industrial Electronics*, vol. 57, no. 4, pp. 1309–1317, 2010.

[145] R. Pupadubsin, N. Chayopitak, D. G. Taylor, N. Nulek, S. Kachapornkul, P. Jitkreeyarn, P. Somsiri, and K. Tungpimolrut, "Adaptive integral sliding-mode position control of a coupled-phase linear variable reluctance motor for high-precision applications," *IEEE Transactions on Industry Applications*, vol. 48, no. 4, pp. 1353–1363, 2012.

[146] A. J. Garrido, I. Garrido, M. Amundarain, M. Alberdi, and M. De la Sen,

"Sliding-mode control of wave power generation plants," *IEEE Transactions on Industry Applications*, vol. 48, no. 6, pp. 2372–2381, 2012.

[147] R. Datta and V. Ranganathan, "A method of tracking the peak power points for a variable speed wind energy conversion system," *IEEE Transactions on Energy Conversion*, vol. 18, no. 1, pp. 163–168, 2003.

[148] K. Vrdoljak, N. Perić, and I. Petrović, "Sliding mode based load-frequency control in power systems," *Electric Power Systems Research*, vol. 80, no. 5, pp. 514–527, 2010.

[149] B. Bandyopadhyay, F. Deepak, and K.-S. Kim, *Sliding mode control using novel sliding surfaces*. Springer, 2009, vol. 392.

[150] W.S.Levine, *The Control Handbook, Boca Raton,FL.* CRC Press, 1996.

[151] J.-C. Lo and Y.-H. Kuo, "Decoupled fuzzy sliding-mode control," *IEEE Transactions on Fuzzy systems*, vol. 6, no. 3, pp. 426–435, 1998.